NUCLEAR ENGINEERING

MASSACHUSETTS INSTITUTE
OF TECHNOLOGY

ANALYSIS OF FORCED CONVECTION DEGRADED CORE COOLING IN LIGHT WATER REACTORS

by

S. M. Mohammed and M. S. Kazimi

August 1981

DEPARTMENT OF NUCLEAR ENGINEERING
MASSACHUSETTS INSTITUTE OF TECHNOLOGY
Cambridge, Massachusetts 02139

ANALYSIS OF FORCED CONVECTION DEGRADED CORE COOLING IN LIGHT WATER REACTORS

by

S. M. Mohammed and M. S. Kazimi

August 1981

Work Performed with Support from E.G. & G. Idaho, Inc.

ABSTRACT

The literature on heat transfer and hydrodynamics of forced convection cooling of particle beds is reviewed. The information is used to assess the characteristics of in-situ cooling of a degraded LWR reactor core under conditions representative of severe accidents.

It is found that while adequate information exists on the behavior of particulate beds of uniform size particles, considerable uncertainty remains about the behavior of beds of nonuniform particle sizes. Important areas that need further investigation for LWR safety analysis include the pressure drop as a function of flow rate in beds of mixed size particles, self-pumping capability, boiling heat transfer and dryout as a function of flow rate and bed characteristics.

In analyzing the forced convection cooling in a degraded LWR core, it is found that the pressure head required to force the flow through a totally degraded core is one to two orders of magnitude higher than the case of intact core geometry. If, for example, the temperature rise across the core is to be 20 °C, the minimum water coolant superficial velocity required to remove the decay heat (conservatively taken as 2% of the initial total power) is 0.075 m/sec. At such a velocity the pressure drop in the initial intact core is only 70 Pa. In a totally degraded core, consisting of particles with a mean diameter equal 1 mm, the pressure drop is about 110,000 Pa. Even with these conservative assumptions, the pressure head is within the capability of the main reactor pumps. Furthermore, at such coolant velocity only particles with diameter smaller than

80 μm will be swept out by the flow. The sensitivity of the hydraulic characteristics to the allowed coolant temperature rise is also investigated.

ACKNOWLEDGEMENTS

Support for this Project provided by EG&G Idaho, Inc. is greatly appreciated.

We are also grateful to Ms. Gail Jacobson for her patience and help in the preparation of this typed manuscript.

This report is based on a thesis submitted by the first author as part of the requirements of an M.S. degree in Nuclear Engineering at M.I.T.

TABLE OF CONTENTS

LIST OF FIGURES

LIST OF TABLES

NOMENCLATURE

$\bar{a}$ = mean specific surface (L^{-1})

A_B = bed cross sectional area (L^2)

A_f = fuel cross sectional area (L^2)

A_T = total flow area

Ar = Archimedis number = $\left(\frac{D_p^3 g}{\nu^2}\right)\left(\frac{\Delta T \beta}{T}\right)$

C_p = specific heat at constant pressure $\left(\frac{L^2}{t^2 \theta}\right)$

d_c = core equivalent diameter (L)

$\bar{d}_p$ = particle mean diameter (L)

d_t = bed diameter (L)

D = diffusion coefficient $\frac{L^2}{t}$

D_c = column diameter (L)

D_p = particle diameter (L)

D_T = bed diameter

Fe = Fedorov number used in Ref. [111]

Fr_{pm} = modified Froud number in Ref. [115]

$$= (D_p g/U_f)^{1/2} \times \left[\frac{\rho_p - \rho_f}{\rho_f} (1-\varepsilon)^2\right]^{1/2}$$

g = acceleration due to gravity $\left(\frac{L}{t^2}\right)$

G = mass velocity $\left(\frac{M}{L^2 t}\right)$

h_p = particle heat transfer coefficient $\left(\frac{M}{t}\right)\theta$

h_{fg} = enthalpy of vaporization $\left(\frac{L^2}{t^2}\right)$

J_h = heat transfer factor = $\left(\frac{h}{c_p G}\right) Pr^2$

Nomenclature (continued)

$(J_h)_{fp}$ = heat transfer factor used in Ref. [115]

k_f = thermal conductivity of fluid $\left(\frac{ML}{t^3\theta}\right)$

k_p = thermal conductivity of solids $\left(\frac{ML}{t^3\theta}\right)$

k_w = thermal conductivity of water $\left(\frac{ML}{t^3\theta}\right)$

K = Darcy permeability

K_{eff} = effective thermal conductivity $\left(\frac{ML}{t^3\theta}\right)$

K_{er} = thermal conductivity in radial direction $\left(\frac{ML}{t^3\theta}\right)$

K_{ob} = overall bed conductivity $\left(\frac{ML}{t^3\theta}\right)$

L = remaining intact fuel rod length used in Eq. (A.1) (L)

L_B = bed height (L)

$(L_B)_{mf}$ = bed height at minimum fluidization velcoity (L)

L_o = core active height (L)

$\dot{m}$ = mass flow rate $(\frac{M}{t})$

$\dot{m}_o$ = initial mass flow rate in core $(\frac{M}{t})$

M = sweepout rate constant

N_f = number of fuel rods

Nu_p = particle Nusselt number = $\left(\frac{hd_p}{k_f}\right)$

P = pressure $\left(\frac{M}{Lt^2}\right)$

ΔP = pressure drop (M/Lt^2)

Nomenclature (continued)

Pe = Peclet number = $\left(\frac{Ud_p}{D}\right)$

Pr = Prandtl number = $(\mu_f c_p/k_f)$

q''' = volumetric heat generation (M/Lt^3)

q_b''' = bed volumetric heat generation rate (M/Lt^3)

q_d = dryout heat flux (M/t^3)

q_D = decay heat (ML^2/t^3)

Ra = Rayleigh number = $\rho_f g\beta LK/\mu\alpha)$ $(q_b H^2/K_B)$

Re_p = particle Reynolds number = $(d_p U\rho_f/\mu_f)$

Re_{mf} = Reynolds number at mimimum fluidization velocity = $(d_p U_{mf}\rho_f/\mu_f)$

Re_t = Reynolds number at particle terminal velocity = $(\rho_f U_t d_p/\mu_f)$

St = Stanton number = $(h/c_p G)$

t = time, a fundamental dimension (t)

T = temperature (θ)

U = superficial velocity (L/t)

U_t = particle terminal velocity (L/t)

U_{mf} = superficial minimum fluidization velocity (L/t)

V_b = bed volume (L^3)

V_o = initial core volume (L^3)

x_i = fraction of material in size interval i

α = factor in Eq. (2), or diffusivity in Eq. (33)

β = factor in Eq. (2), or linear thermal expansion in Eq. (33) (θ^{-1})

ε = void fraction of the bed

ε_d = void fraction for dense packed bed

ε_ℓ = void fraction for loose packed bed

Nomenclature (continued)

ε_{mf} = void fraction at minimum fluidization conditions

θ = temperature, a fundamental dimension (θ)

μ_f = density of fluid (M/L^3)

ρ_s = density of solid (M/L^3)

ρ_v = density of vapor (M/L^3)

ρ_ℓ = density of liquid (M/L^3)

ϕ_s = sphericity

ν_ℓ = kinematic viscosity of liquid (L^2/t)

ν_v = kinematic viscosity of vapor (L^2/t)

σ = surface tension (M/t^2)

ξ = ratio of channelling length to particle diameter

ψ = particle specific surface area (L^{-1})

CHAPTER 1
INTRODUCTION

1.1 Research Objectives

The objective of this work is to review the state of knowledge of the heat transfer and the hydrodynamics of a particle bed and assess the applicability of this information to in-situ cooling of a degraded reactor core in the forced convection mode. The work is aimed primarily at conditions representative of what may be expected under Light Water Reactor (LWR) severe accidents. However the information, in general, has been originated either in the chemical industry or in Liquid Metal Fast Breeder Reactor (LMFBR) safety research.

1.2 Insight into Problem

The accident at the Three Mile Island has promoted numerous investigations of the safety aspects of nuclear power plants. As a result of the sequence of events at TMI, class 9 accidents, in which the events are classified as highly improbable, gained increased attention in analysis of safety of the plants.

In one scenario, the loss of coolant, may result in partial uncovering of the core and subsequent heat up and damage of fuel elements. When molten core materials encounter liquid coolant, freezing and fragmentation normally occur. The frozen particles may settle on horizontal surfaces such as spacer grids forming the so-called debris or rubblized bed. The fuel in these debris beds will be heated by radioactive decay of retained fission products.

Previous work on particle bed coolability assumed the presence of an overlying layer of coolant and that heat removal is governed by natural

convection and boiling providing there is an adequate heat sink or coolant source to maintain the overlying coolant pool. The hazard level which should be assigned to the resulting post-accident condition depends on the extent to which natural cooling of the debris may be relied upon. For sufficiently high decay power, the liquid from the overlying pool cannot penetrate the particle bed swiftly enough to offset the vaporization. In this case, portions of the bed dry out and begin heating to above the coolant boiling point. Thus, even if there is a maintained coolant pool overlying a particle bed, it is still possible under certain conditions to have structural failure or particle remelt. However, one alternative method to avoid bed dryout and assure particle coolability would be to force liquid coolant upward through the bottom of the particulate bed.

Determination of the minimum flow rate necessary to prevent bed dryout requires the understanding and the evaluation of the modes of heat transfer and the controlling mechanisms as the coolant is forced through the rubblized bed. The configuration and the geometry of the bed play an important part in the manner in which heat is transferred from the particles to the coolant. Depending on the pressure drop, the bed may exist in a fixed or fluidized state. High rates of heat transfer exist in the bed when the fuel particles fluidize due to the mixing caused by the motion of particles in the coolant.

Considerable experimental effort has been reported on the characteristics of debris beds that may result from a hypothetical LMFBR accident. Most of the investigations focused on the problem of thermal behavior and dryout of particulate beds when present in a coolant pool. Attention was not paid to the potential of forced flow cooling until recently. However,

information on particle-to-fluid heat transfer under single phase forced flow is available from research conducted in the chemical industry. Packed and fluidized particulate beds have been the subject of many investigations in that field for a variety of applications. It is not clear, at the present time, as to what extent this information can be applied to the analysis of degraded LWR cores, since the conditions may differ considerably from those investigated in the chemical engineering area.

It is the aim of the present work to try to utilize such information, where valid, in assessing the coolability of degraded LWR core, and to identify areas of further research needs.

CHAPTER 2

REVIEW OF SOME PHENOMENA ASSOCIATED WITH LWR ACCIDENT

2.1 Accident Initiation

A hypothetical accident in a pressurized light water reactor (PWR) may be initiated by events resulting in loss-of-water inventory from inadequate normal system makeup, a small pipe break, or through a safety/relief valve (SRV). The latter category includes events that might result in reactor isolation with SRV actuation, complicated by a stuck-open relief valve (SRV) such as occurred at the Three Mile Island, TMI plant [1]. It also includes the case of a SRV opening inadvertantly and remaining open. The loss of water inventory will result in progressive uncovery of the core and a consequence heat-up of the top region of the fuel elements. Fuel rods may burst and zircaloy cladding will embrittle by oxidation and conversion into zirconium oxide; "liquified fuel" (UO_2 dissolved in either molten zircaloy metal or eutectic liquid formed between zircaloy metal and its oxide) will also be formed and may flow down between oxidized cladding shells and freeze upon reaching a lower temperature at a lower level. However, if the reactor coolant pumps are turned on, the embrittled cladding will be thermally shocked by the influx of coolant (whether steam or water) shattering it, producing a "rubble" or "debris" bed of cladding fragments, zircaloy oxide shells, fuel pellets and liquified fuel, supported by fuel rod stubs and unmelted grid spacers.

Another event that may lead to the fragmentation and dispersal of fuel is the result of the violent mixing of hot molten fuel with cold liquid coolant at high pressure and temperature, known as fuel-coolant interaction

(MFCI). The RIA-ST-4 experiment recently conducted at EG&G [2] under conditions that are more conservative than what may be expected for LWR reactivity transients produced extensive fuel fragmentation. The fragmentation of the molten fuel debris may have been caused by the violent release of dissolved gases and entrapped water vapor from within the molten drops [3], or by a film boiling collapse mechanism [4] or both. The particle size distributions obtained during the RIA-ST-4 experiment and the high power excursion tests performed in the (CDC) facility at the Idaho National Engineering Laboratory are shown in Fig. 1.

2.2 Potential of Core Inadequate Cooling

In a reactor accident, the ultimate coolability of the core materials is of prime importance. If the heat from decaying fission products cannot be adequately removed, heating of the core material will occur with possible fuel melt and damage of the surrounding structure. In an intact core, decay heat can be removed by natural circulation if there is adequate coolant available and an ultimate heat sink. However, in a damaged core, flow paths may be restricted and heat removal made more difficult. Heat removal is particularly difficult if the core material is in a particle bed. As discussed in the previous section, particle beds can form either by thermal fracturing of intact core before melt or by quenching of molten core materials. In either event, flow within the particle bed may be sufficiently restricted to prevent adequate heat removal. If the debris bed is not sufficiently cooled, it would melt through the vessel bottom and form a molten pool [5]. After breaching the pressure vessel, the molten mass interacts with the concrete base mat. If water is available it may lead to solid bed debris formation. Heat transfer through the concrete

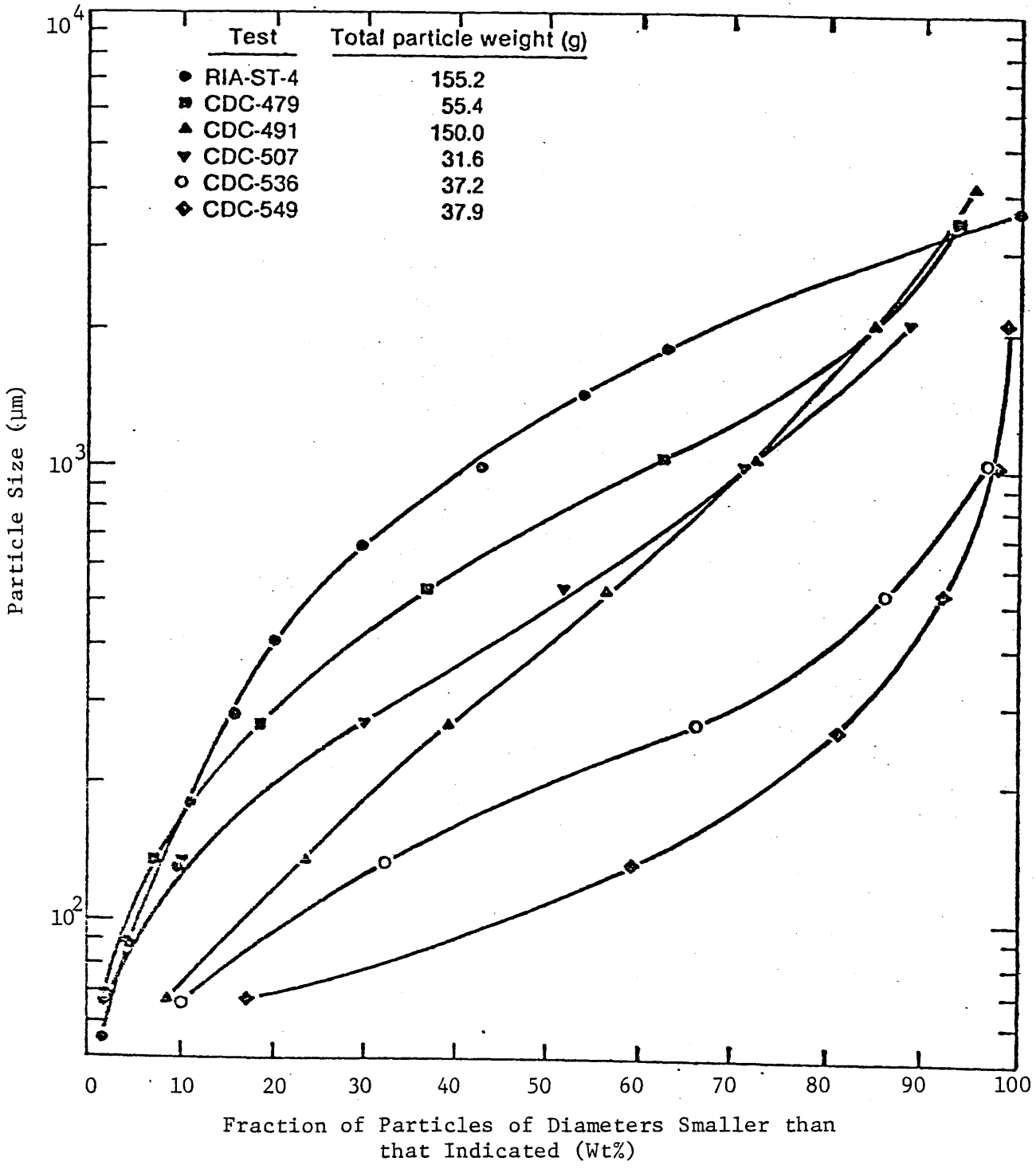

Figure 1: Results of Simulated Experiments to Predict Particle Size Distribution Expected in LWR Severe Accidents [2]

is by conduction, but convection may be the principal mechanism within the bed molten mass. The upper surface of the latter can be cooled by radiation and convection to the overlying structure.

2.3 Core Debris Behavior and Cooling

As discussed in the previous section, insufficient cooling of particulate bed will result in heat up and remelt of particles with subsequent damage of core supporting structure. However, the possibility of achieving coolable geometry depends primarily on the manner in which heat is transferred from the particles to the surrounding coolant.

In the absence of forced flow, if the bed is submerged in a coolant pool with an adequate coolant source to prevent boil-off, and if the decay power is sufficiently low, all decay heat produced can be removed by the boiling process. In this case, the bed will remain at the boiling temperature of the coolant and the supporting structure will remain intact. For sufficiently high decay powers, though, the liquid from the overlying pool cannot penetrate the particle bed swiftly enough to offset the vaporization. In this case, portions of the bed will dry out and begin heating to above the coolant boiling point. Because of the low thermal conductivity of dry particle beds, only a small dry zone is needed to reach a temperature sufficient to remelt the particles or weaken the supporting structure. Thus, even if there is a maintained coolant pool overlying a particle bed, it is still possible to have particle melt or failure of the supporting structure if the bed drys out.

Forced flow cooling is another important aspect of achieving particle coolability, however, up to the present time there is no supporting experimental evidence to address some of the important issues such as

burnout as a function of flow rate and particle geometry , self-pumping capability and pressure drop as a function of flow rate and quality. Therefore, experimental data on through-flow with heating is essential in assessing the capability of debris bed cooling. In a later section of this report a theoretical investigation in the area of single phase forced flow through a degraded LWR core is pursued with regard to the hydrodynamics and heat transfer.

CHAPTER 3
HYDRODYNAMICS OF FLUID FLOW IN POROUS MEDIA

3.1 Background

There exists now extensive literature on the flow of homogeneous fluids through porous materials. Most of the early work in this area was concerned with the flow of liquids at sufficiently low Reynolds numbers so that the linear Darcy law could be used to describe the flow process. Interest then turned to the flow of gases through porous materials and again the linear Darcy law was usually used to describe the flow, with compressibility taken into account when necessary by employing the perfect gas law and assuming isothermal conditions. When a fluid flows through a porous medium, the velocity of a fluid element changes rapidly from point to point, both in direction and magnitude, along the tortuous flow path. Hence, if the flow is dominated by viscous effects, then the relation between applied pressure and flow velocity will be linear and Darcy's law will hold. However, if inertial effects in fluid acceleration and deceleration and direction change are significant, then that relation between pressure and flow will be non-linear and Darcy's law will not be valid. Hence, Darcy's law will only hold for the "seepage flow" regime which is laminar flow without significant inertia effects.

Many investigations have been directed towards finding the range of Reynolds number for which Darcy's law is valid. That the representation by Reynolds number was chosen originally is due to the assumption of an analogy between flow in tubes and in porous media. Capillary models of porous media, which represent the media as composed of a bundle of small capillary tubes, have been widely used. Most familiar is the

transition from laminar flow to turbulent flow in circular pipes at a critical Reynolds number of approximately 2,000. This critical Reynolds number for flow transition in straight tubes is not really applicable to porous media due to the extensive curvature and tortuosity of the flow paths. The critical Reynolds number for straight tubes is not directly comparable for curved tubes. In fact, it has been shown that the critical Reynolds number is strongly dependent on curvature. The linear Hagen-Poisenville [6.7] solution for flow in straight tubes also neglects inertia terms which would be important. Both of these conditions are analogous to porous media. Sheidegger [8] reports that values of the critical Reynolds number for transition between linear laminar flow and flow where inertia terms are important range from about 0.1 to 75. This large uncertainty is principally due to the difficulty in accurately describing the correct characteristic hydraulic diameter for porous media in the reynolds number expression. Due to separate viscous and inertial regimes in laminar flow, there are three semi-distinct regimes for flow through porous media. For Reynolds numbers of about 1 or smaller, the flow is linear laminar as described by the Darcy equation in which the pressure drop and flow or velocity are related by:

$$\frac{\Delta P}{L_B} = \frac{1}{K} \mu U \qquad (1)$$

ΔP, L_B, K and U are the bed pressure drop, length, Darcy permeability, and superficial velocity, respectively, and μ the fluid viscosity. For Reynolds numbers of order 1 through order 1000, the flow is still laminar but is inertia-dominated and the pressuer drop and flow velocity

are non-linearily related according to a square law. The third flow regime for Reynolds number higher than 1000, the flow is considered fully turbulent.

The description of flow outside the Darcy regime started with an equation postulated by Reynolds [8] where the pressure drop is equivalent to a sum of two terms, such as

$$\frac{\Delta P}{L_B} = \alpha\mu U + \beta\rho U^2 \qquad (2)$$

with factors α and β functions of the media geometry and conditions, and ρ the fluid density. The first term represents viscous losses and is essentially the Darcy equation. The second term represents kinetic energy losses due to flow acceleration in magnitude and direction. The basic form of this equation will not change for fully turbulent flow since the kinetic energy losses due to inertia terms are of the same type as in the non-linear laminar flow regime.

Various expressions such as those due to Karman and Kozeny [9], have been developed to relate the coefficients α and β to the media characteristics such as porosity and specific surface area. For example, the reciprocal of α is the classical Darcy permeability K. However, the various investigations have not produced consistent results over a wide range of packing geometries. The scatter of data has been attributed to the influence of packing, shape, orientation, voidage, and entrance effects [10].

The most useful approach to correlating momentum transfer data over the whole range of flow conditions appears to be that of Ergun [11] who

proposed a semi-theoretical equation which makes allowance for the mean hydraulic radius of the flow capillaries and for the effect of voidage. This equation has been fitted with moderate accuracy to the data of several workers. The Ergun equation is given as

$$\frac{\Delta P}{L_B} = 150 \frac{(1-\varepsilon)^2}{\varepsilon^3} \frac{\mu U}{(\phi_s \bar{d}_p)^2} + 1.75 \frac{(1-\varepsilon)}{\varepsilon^3} \frac{\rho_f U^2}{\phi_s \bar{d}_p} \tag{3}$$

The relative importance of each term is decided by two statistical constants characteristic of the tortuosity of the flow passages. At low Reynolds numbers the Ergun equation reduces to the Karman-Kozeny equation and at high Reynolds numbers to the Blake equation.

$$\frac{\Delta P}{L_B} = 150 \frac{(1-\varepsilon)^2}{\varepsilon^3} \frac{\mu U}{(\phi_s \bar{d}_p)^2} \qquad Re_p = \frac{d_p \rho_f U}{\mu} < 20 \tag{4}$$

and

$$\frac{\Delta P}{L_B} = 1.75 \frac{(1-\varepsilon)}{\varepsilon^3} \frac{\rho_f U^2}{\phi_s \bar{d}_p} \qquad Re_p > 1000 \tag{5}$$

In the intermediate region both terms must be used.

For randomly packed beds the Ergun correlation is expected to represent the data within ±25% [12], however, it is not expected to extend to non-randomly packed beds, to beds of solids of abnormal void content, or to highly porous beds. Handley and Heggs [13] showed that the Ergun equation may be fitted accurately to data obtained from beds covering a large range of packing shapes and orientation, they also showed that

Ergun tortuosity constants strongly influence the convective heat transfer mechanisms within the bed. They correlated their experimental data in a linear Ergun manner covering a wide range of packing shapes and orientation with materials having equivalent diameter range from 1.3 - 10.4 mm. Their correlation is of the form:

$$\frac{\Delta P}{L_B} = 386 \frac{(1-\varepsilon)^2}{\varepsilon^3} \mu \frac{U}{\overline{d}_p^2} + 1.24 \frac{(1-\varepsilon)}{\varepsilon^3} \rho_f \frac{U^2}{\overline{d}_p} \tag{6}$$

The pressure drop in beds of mixed size particles follows any of the above correlations for single size particle with $\overline{d}_p$ representing the mean particle diameter of a mixture of different sized particles defined as:

$$\overline{d}_p = \frac{6}{\phi_s \overline{a}} \tag{7}$$

$\overline{a}$, being the mean specific surface, (i.e., surface area per unit volume of particles only)

$$\overline{a} = \frac{6}{\phi_s} \sum^{\text{all } i} \left(\frac{x}{d_p} \right)_i \tag{8}$$

where x_i is the fraction of material in size interval i.

The voidage ε for a mixture of sizes cannot be estimated reliably; factors that must be considered include the size of the particles and the shape of the size distribution curve. For example, if the size variation is large, the small particles may fit into the voids between the large ones, thus greatly decreasing voidage.

For nonspherical particles the sphericity ϕ_s is used as a parameter defined as

$$\phi_s = \left(\frac{\text{surface of sphere}}{\text{surface of particle}}\right)_{\text{both of same volume}}$$

With this definition, $\phi_s = 1$ for spheres, and $0 < \phi_s < 1$ for all other particle shapes. Table 1 lists calculated sphericities of different solids [12].

3.2 Fluidization of Particulate Beds

If the fluid velocity through a bed of particles is gradually increased, the bed hydraulic resistance increases until the force resisting the flow is equal to the bed weight whereupon no further increase in the hydraulic resistance of the bed occurs. However, further increase in the fluid velocity leads to expansion of the bed, marking its transition to the fluidized state.

If the flow rate of fluid is increased above the minimum required to produce a fluidized bed one of two things will occur: either the bed will continue to expand so that the average distance between the particles will become greater, or the excess fluid will pass through the bed in the form of bubbles, giving rise essentially to a two-phase system. These two types of fluidization are referred to as being respectively "particulate" and "aggregate." In general, particulate fluidization occurs with liquid-solid systems, and with gas-solid systems when the particles are very fine, and then over only a limited range of velocities. Aggregate fluidization occurs with all other gas-solid systems and sometimes with

TABLE 1

Data on Sphericity ϕ_s [12]

Observer	Material	ϕ_s
Leva et al. [14]	sand	0.600, 0.861
	iron catalyst	0.578
	bituminous coal	0.625
	celite cylinders	0.861
Uchida & Fujita [15]	broken solids	0.630
Shirai [16]	sand	0.534-0.628
	silica	0.554-0.628

liquid-solid systems when the solids are of a high density.

Upon increasing the fluid velocity even more, carry-over of particles from the bed finally occurs, the fluidized bed undergoes transition to a bed entrained by a fluidizing stream. At the minimum fluidizing velocity, which marks a transition from the fixed to the fluidized state, it might be expected that flow relations for the fixed bed would be applicable to the fluidized bed. At the other limit, if a bed is fully expanded so that its voidage approaches unity, it consists effectively of single isolated particles suspended in the fluid and therefore any relation describing a fluidized bed should extrapolate to one applicable to an individual particle. At intermediate conditions, the particulate fluidized bed is hydrodynamically similar to a sedimentary suspension. In the fluidized bed the particles undergo no net movement and are supported by the upward flow of fluid, whereas in a sedimentary suspension the particles are moving continuously downwards and the only net movement of fluid is that due to the displacement of fluid by the particles as they settle.

3.2.1 Pressure Drop-Velocity Relationship in Fluidized Beds

The basic interrelationships among the fluidizing variables are shown in Fig. 2, the upper plot indicating the change in the pressure gradient as the fluid velocity changes and the bottom plot the shift in the void fraction (porosity) with fluid velocity. Logarithms of the various quantities are plotted.

Fixed-bed conditions prevail from A to C with the portion from A to B varying linearly as would be expected. The deviation from linearity between B and C is indicative of movements and rearrangements within the bed as the particles shift in order to offer the least possible area in

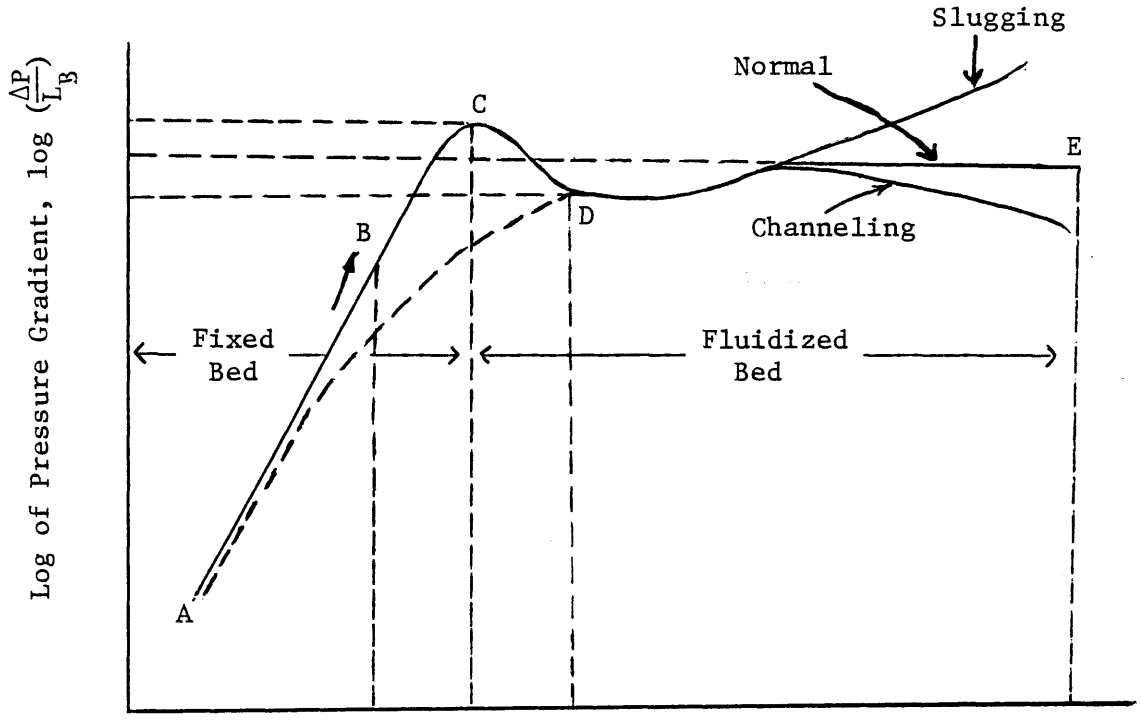

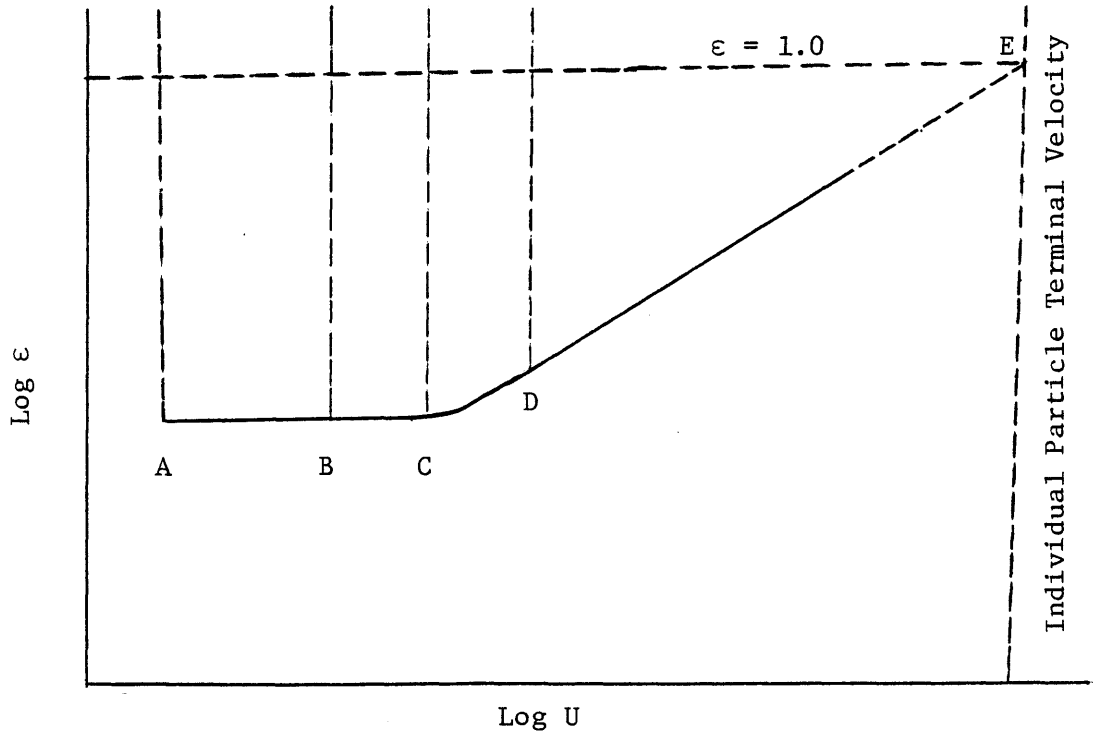

Figure 2: Typical behavior of pressure gradient and porosity of a bed as a function of the fluid superficial velocity

the direction of flow. Little, if any, change in the bed's void fraction occurs up to point C. At C fixed-bed behavior terminates, particles and clusters of particles begin to move continuously, although only a part of the bed may do so initially. A slight decrease in pressure drop often occurs as indicated between C and D as dynamic conditions develop. It apparently results as the particles separate from one another due to loosening of particle interlocking and of cohesive forces among the particles. The segment of the curve BCD is not reproduced should the fluid velocity decrease over that range; the curve diminishes, instead, approximately as shown by the dotted line. In an ideal situation, the pressure drop will rise slightly as the minimum at D is passed, but it will not exceed that indicated by point C. If there is channeling in the bed the pressure loss will not attain the value of C. In fact, the extent of the failure to recover is an indication of the channeling tendancies of the solids being fluidized.

While the pressure drop remains nearly constant once fluidization is established, bed expansion can theoretically continue until one particle remains in the space of the original bed. An upper limit for E is thus established. With liquid fluidization this greatest velocity generally corresponds closely to the particle's terminal settling velocity U_t.

3.2.2 Initiation of Fluidization

For a fluidized bed there is a minimum void condition in which the bed can exist, a minimum pressure loss for the fluid that will maintain fluidization, and a minimum fluid velocity that can produce fluidization.

(i) Minimum voids

Since there must be a discrete separation of particles for fluid flow to induce motion within particle masses, this separation sets the minimum voidage. The minimum voids for fluidization, denoted by (ε_{mf}) is apparently a characteristic of the particles. Values range from about 0.4 for spheres, to 0.8 for very irregular shapes [17]. Such a variation is to be expected since as the particles become less symmetrical, they require more space to move about without interference. The minimum void space decreases as particle size increases unless, of course, there is a decided change in shape factor or density associated with particle-size change. Theoretically, the value of ε_{mf} should be the same regardless of whether the fluid is a gas or a liquid. Actually it may be slightly higher with liquids due to inertial influence but the difference is not large.

(ii) Minimum pressure gradient

The pressure loss at the initial fluidization point (ΔP_{mf}) is readily calculated. Fluidization begins when the pressure drop equals the buoyant weight of the solid material per unit volume of bed and is given by [18]

$$(\Delta P)_{mf} = (\rho_s - \rho_f)(1 - \varepsilon_{mf})\,(L_B)_{mf}\,g \qquad (9)$$

(iii) Minimum fluidizing velocity

The minimum fluidizing velocity can be approximated by an expression for the relation between pressure drop and superficial velocity for a fixed bed when the pressure drop is equated to the buoyant weight of the particles. This does, however, necessitate a knowledge of the voidage of the bed at the minimum fluidizing velocity (ε_{mf}). This will depend on the

shape and size range of the particles.

Various attempts have been made to relate the value of ε_{mf} to a shape factor for the particle, but these have not been entirely satisfactory [19,20]. The pressure drop above the fluidized bed is given by

$$\Delta P = (\rho_s - \rho_f)(1 - \varepsilon)\, L_B\, g \tag{10}$$

If the bed expands, the product, $(1-\varepsilon)L_B$, will remain constant. Combining Eq. (3) with Eq. (9) will give a quadratic equation in U_{mf}, thus

$$\frac{1.75}{\phi_s\, \varepsilon_{mf}^3} \left(\frac{d_p U_{mf} \rho_f}{\mu}\right)^2 + \frac{150(1-\varepsilon_{mf})}{\phi_s^2\, \varepsilon_{mf}^3} \frac{d_p U_{mf} \rho_f}{\mu} = \frac{d_p^3 \rho_f (\rho_s - \rho_f) g}{\mu^2} \tag{11}$$

However, for small particles diameter (10-100 μm) and of small specific weight, Eq. (3) simplifies to Eq. (4), thus Eq. (11) gives

$$U_{mf} = \frac{(\phi_s d_p)^2}{150} \frac{\rho_s - \rho_f}{\mu} g \frac{(\varepsilon_{mf}^3)}{(1 - \varepsilon_{mf})} \qquad Re_p < 20 \tag{12}$$

For large particles Eq. (3) simplifies to Eq. (5). Thus, Eq. (11) becomes

$$U_{mf}^2 = \frac{\phi_s d_p}{1.75} \frac{\rho_s - \rho_f}{\rho_f} g\, \varepsilon_{mf}^3 \qquad Re_p > 1000 \tag{13}$$

If $\varepsilon_{mf}$and/ or ϕ_s are unknown, the following modification of these expressions can be used [22]. First it was found for a wide variety of

systems that

$$\frac{1}{\phi_s \varepsilon_{mf}^3} \cong 14 \text{ and } \frac{1-\varepsilon_{mf}}{\phi_s^2 \varepsilon_{mf}^3} \cong 11 \tag{14}$$

and when replaced in the expression above, this gives for the whole range of Reynolds numbers

$$\frac{d_p U_{mf} \rho_f}{\mu} = \left[(33.7)^2 + 0.0408 \frac{d_p^3 \rho_f (\rho_s - \rho_f) g}{\mu^2}\right]^{1/2} - 33.7 \tag{15}$$

or for small particle diameter

$$U_{mf} = \frac{d_p^2 (\rho_s - \rho_f) g}{1650 \mu} \qquad Re_p < 20 \tag{16}$$

and for large particle diameter

$$U_{mf}^2 = \frac{d_p (\rho_s - \rho_f) g}{24.5 \rho_f} \qquad Re_p > 1000 \tag{17}$$

These simplified expressions, Eq. (15) to (17), give U_{mf} in terms of the usually specified variables of densities, particle size, and fluid viscosity; and for 284 data points in a Reynolds number range of 0.001 to 4000 these expressions have been found to give predictions of U_{mf} with a standard deviation of ±34% [22]. Many alternate procedures have been proposed. These are presented by Leva [21], Wen and Yu [22], and Franz [23].

If the bed contains solid particles of various sizes (or densities), as U, the superficial velocity, increases the smallest particles are first fluidized and larger particles later. The corresponding minimum fluidizing velocities is then dependent on the size distribution or density [24].

3.3 Particulate (Liquid-Solid) Phase Expansion

Liquid-solid fluidized systems generally exhibit the characteristic of a smooth expansion of the bed as the velocity is increased from the minimum fluidizing velocity to the free-falling velocity of the particle, if the particles are uniform. Where there is a spread of particle properties, there is a marked tendency for segregation to occur within the bed [28].

A number of workers including Hancock [25], Steinour [26], Lewis et al. [27], and Richardson and Zaki [28], have suggested that the most convenient way of showing the variation of fluidizing velocity, with voidage is by means of a Log-log plot of velocity against voidage since this commonly gives a linear relation:

$$\frac{U}{U_t} = \varepsilon^n \tag{18}$$

Where (U_t) is the particle terminal velocity and (n) is a function of the flow regime and the nature of the particles. Richardson and Zaki [28] related n to the Reynolds number, based on the particle terminal velocity, U_t, as:

$$
\begin{aligned}
n &= 4.6 && 0 < Re_t = \frac{U_t d_p \rho_f}{\mu} < 0.2 \\
&= 4.4\ Re_t^{-0.33} && 0.2 < Re_t < 1 \\
&= 4.4\ Re_t^{-0.1} && 1 < Re_t < 500 \\
&= 2.4 && Re_t > 500
\end{aligned}
\tag{19}
$$

Equation (18) is applicable also for uniform nonspherical particles, but the index n has higher values than for spheres. Experimental work [28] on particles of fixed geometric forms (cubes and cylinders) and for Re_t greater than 500 has shown that the index n could be expressed in terms of the shape factor K defined by the relation

$$K = \frac{\pi}{6} \frac{d_s^3}{d_p^3} \tag{20}$$

where d_p is the diameter of the circle of the same area as the projected area of the particle when lying in its most stable position, and d_s is the diameter of the sphere with the same surface area as the particle.

The values of n for $Re > 500$ were given by

$$n = 2.7\ K^{0.16} \tag{21}$$

3.4 Particles Entrainment and Sweep-out

Core debris particles generated by the quenching of molten core debris in water are expected to settle downward into available horizontal surfaces such as a spacer grid to form particulate beds. If there is

net coolant flow, such as through the outlet plenum of a reactor vessel, then some of the particles may be swept away into the primary loop piping system instead of settling downward. The final particle locations depend strongly on the details of the flow field as well as on the particle size distribution and the physical properties of the solid and liquid phases. However, the effective parameters may be summarized according to the following general observations:

1. Sweepout is normally insignificant if the bed average size particles are fluidized with flow rates that are not significantly above the terminal velocity of the smallest or lightest particles. If the solid bed is however composed of a wide range of size components, comprising very small particles, significant sweepout of these fines may occur at fluid rates which are only slightly in excess of the terminal velocity of these smallest particles.
2. For fluid flow rates that are significantly above the terminal velocities of the particles, sweepout becomes significant even with beds of relatively narrow size distribution.
3. Sweepout of particles at a given velocity decreases with an increase in bed height and particle irregularity.

The upper limit of coolant flow rate in order to avoid sweepout can be approximated by the settling, or terminal, velocity U_t of the particles. Depending on the particle diameters, the values of U_t can be estimated from fluid mechanics by the following formulae [29]:

Settling Velocity	Law	
$U_t = \frac{g(\rho_s - \rho_f)d_p^2}{18\mu_f}$	(Stokes) Re < 0.3	(22a)
$U_t = \frac{0.153\ g^{0.71}(\rho_s - \rho_f)^{0.71}\ d_p^{1.14}}{\rho_f^{0.29}\ \mu_f^{0.43}}$	(Intermediate) 0.3 < Re < 1000	(22b)
$U_t = \frac{1.74\ \left[g(\rho_s - \rho_f)d_p\right]^{1/2}}{\rho_f^{1/2}}$	(Newton) 1000 < Re < 200,000	(22c)

To determine the rate of entrainment into the coolant flow, it is assumed that this rate is controlled by the particle characteristics, the fluid properties, and particle velocities above the bed. Applying dimensional analysis along with experimental data, a correlation for the specific sweepout rate constant (K) measured in kilogram per square meter of upper bed surface per second is given as [10]:

$$\frac{K}{\rho(U - U_t)} = 1.7\text{x}10^{-5} \left[\frac{(U - U_t)^2}{gd_p}\right]^{0.5} \left[\frac{d_p U_t \rho_f}{\mu}\right]^{0.725} \left[\frac{\rho_s - \rho_f}{\rho_f}\right]^{1.15} \left[\frac{U - U_t}{U_t}\right]^{0.1} \tag{23}$$

The above empirical correlation was obtained by using data based on gas as the working fluid and the following range of parameters:

$0.004\ \text{cm} < d_p < 0.015\ \text{cm}$

$0.22\ \text{m/sec} < U < 1.32\ \text{m/sec}$

To apply the above correlation, an equation must be derived from material balances to express the amount of each size particle swept-out during a specified time interval. If c is the concentration of the bed at any time

$$c = \frac{\omega_{oi} - \omega_{fi}}{W - \omega_{fi}} \tag{24}$$

where ω_{fi} is the amount of particles consisting of size, d_i, sweepout for a length of time, t, and ω_{oi}, is the weight of the particles of that size present initially, and W is the total weight of the bed.

Differentiating Eq. (24) with respect to t:

$$\frac{dc}{dt} = \frac{(\omega_{oi} - W)}{(W - \omega_{fi})^2} \tag{25}$$

but the change of concentration with time can also be written as

$$\frac{dc}{dt} = -M \frac{\omega_{oi} - \omega_{fi}}{W - \omega_{fi}} \tag{26}$$

where M is the sweepout rate constant measured in reciprocal time units. This constant may be expressed

$$M = \frac{K_i A}{W - \omega_{fi}} \tag{27}$$

where A is the bed cross section. Therefore combining Eqs. (25) through (27) yields

$$\left[\frac{\omega_{oi} - W}{(W - \omega_{fi})^2}\right] \frac{d\omega_{fi}}{dt} = -K_i A \frac{(\omega_{oi} - \omega_{fi})}{(W - \omega_{fi})^2} \tag{28}$$

or

$$\frac{d\omega_{fi}}{dt} = K_i A \frac{(\omega_{oi} - \omega_{fi})}{W - \omega_{oi}} \tag{29}$$

Integrating Eq. (29) from $0 \rightarrow t$ and $0 \rightarrow \omega_{fi}$

$$\int_0^{\omega_{fi}} \frac{d\omega_{fi}}{(\omega_{oi} - \omega_{fi})} = \int_0^t \frac{K_i A \, dt}{(W - \omega_{oi})}$$

or

$$\omega_{fi} = \omega_{oi} \left[1 - \exp\left(\frac{K_i A t}{\omega_{oi} - W}\right)\right] \tag{30}$$

The total amount of particles entrained and swept out in time t is obtained by the sum over all particle sizes:

$$\sum_i \omega_{fi} = \sum_i \omega_{oi} \left[1 - \exp\left(\frac{K_i A t}{\omega_{oi} - W}\right)\right] \tag{31}$$

3.5 Summary

The following summarizes the important conclusions of this chapter:

1) For a given height and porosity, the pressure drop through a fixed bed can be estimated theoretically using the Ergun equation.

2) In gas-fluidized systems there is a tendancy for the solid to aggregate giving rise to a non-ideal behavior. In liquid-solid system the dominant flow regime is that of the particulate fluidization, in which the bed expands uniformly as the liquid superficial velocity increases.

3) The relation between bed voidage and velocity in liquid fluidized bed has a simple form given by Eq. (18).

4) The minimum fluidization velocity can be calculated approximately from equations for flow through packed beds, by equating the pressure-drop through the bed at its maximum stable voidage to the buoyant weight per unit area of bed.

5) Particles entrainment and sweepout are significant for fluid flow rates that are higher than the terminal velocity of the smallest particles.

CHAPTER 4
HEAT TRANSFER CHARACTERISTICS OF HEAT GENERATING POROUS MEDIA

4.1 Introduction

Before the discussion of debris bed cooling by forced convection, it is worthwhile to throw some light on the present literature regarding natural convection cooling of particulate beds.

4.2 Natural Convection Heat Transfer

4.2.1 Previous Work

Considerable effort has been made in analyzing the thermal behavior of debris bed that result from a hypothetical core disruptive accident. Gasser and Kazimi [33] have carried out theoretical analysis for the onset of convection in a porous medium with volumetric heat source. They considered a fluid-saturated porous bed with a free surface as an upper boundary condition and a rigid surface as a lower boundary condition. For bottom surface temperature, greater or lower than the free surface temperature, they have obtained a relationship between the critical internal Rayleigh number and the external Rayleigh number.

Sparrow et al., [31] investigated analytically the linear stability problem for an internally heated fluid layer with both stabilizing and destabilizing temperature profiles in the layer, they showed that the fluid layer became more prone to instability as the heat generation rate increased. In other words, the critical Rayleigh number decreased with increasing departure from the linear temperature profile. Thirlby [32], among many other theoretical or experimental studies, performed numerical analysis of steady laminar natural convection in an infinite horizontal

layer of fluid. He showed that the convection cell size would decrease with increased Rayleigh number.

Numerous experimental investigations have also been carried out for the understanding of the debris bed dryout phenomena. Gabor and Sowa [34] measured the dryout fluxes for sodium or water cooled UO_2 particulated beds. The beds were either bottom heated or volumetrically heated. The bed was believed to have dried out when its temperature was found to increase rapidly without an increase in the heat input. The volumetric heated tests were performed by generating heat in the coolant (Joule heating) rather than in the particles. Gabor and Sowa also conducted experiments to study the formation of particulate beds and the dryout heat flux when induction heating rather than Joule heating of the coolant was employed. The work of Gabor et al, has revealed that the particulate beds can be classified into two categories, deep and shallow beds, according to the manner in which vapor escapes from the bed. It was observed that discrete vapor bubbles generated in the lower portion of a bed coalesce in the upper region to form vapor channels. These channels extend to the bottom in shallow beds and only part way into the deep beds. The particles are levitated in the region without channels. The dryout heat flux is found to be much higher in shallow beds as compared to deep beds. Lee and Nilson [35] gave experimental observations and qualitative interpretations for a series of steady state bench experiments in which decay heat in a debris bed is simulated by Joule heating of the liquid phase. Both single-phase and two-phase boiling phenomena were examined. More recently, Hardee and Nilson [36] performed an experimental and analytical study on the onset of convection and

convective heat transfer in a porous bed with rigid boundary walls. Rhee and Dhir [37] determined experimentally how a finite overlying free layer may enhance natural convection heat transfer and effect the onset of convective motion in a particulate bed having a uniform internal heat source.

Dhir and Catton [30] studied the effect of the particle size, bed porosity and fluid properties on the dryout heat flux in deep and shallow bottom and volumetrically heated particles. They have also studied and obtained data on the dryout heat flux when the particulate bed contains particles of widely different diameters or when both volume heated and non-heated particles are present in the bed. The effect on dryout heat flux of relative locations of volume heated and non-heated particles was also determined.

The studies of post accident heat removal phenomena in LMFBR's [38] at Sandia Laboratory have utilized for the first time fission heated experiments to better simulate the decay heating of debris beds by using the annular core pulse reactor operated at a steady-state mode to fission heat UO_2-fueled PAHR experiment capsules. In two of the experiments, threshold dryout of the fuel particulate were produced. During several runs, dryout was maintained for a long period. It was concluded that the observed temperature transients during dryout can be explained in terms of a conduction process in an expanding zone, and that the expansion is a displacement process. Expansion of the zone reduces the height of the overlying convection zone and that while the bed dryout may be a necessary condition for remelting of the fuel to occur, it is not always a sufficient condition.

4.2.2 Correlations Applied to Natural Convection Cooling

In the analysis of post-accident heat removal, it is important to know whether the fuel particulate can be adequately cooled by natural convection of coolant which lies within and above the debris bed. The fluid flow and heat transfer characteristics of heat-generating porous medium are strongly dependent on conditions at the boundaries of the region. If the walls of the containing vessel have high thermal mass and high conductivity they can be treated as constant temperature surfaces. Since the walls would be cooler than the generating bed, a descending boundary layer flow develops at the walls. If the walls of the containing vessel have negligible thermal mass and conductivity, they can be treated as adiabatic surfaces, and the onset of convection is determined by the balance between buoyant and viscous forces. Below some critical Rayleigh numbers, the heat flow is by conduction alone. Above this Raleigh number, cellular natural convection predominates. If the heat generation rate is large, boiling and eventual dryout of the bed can occur. For a heat-generating porous bed which is cooled from above, but otherwise insulated, the onset of convection has been calculated by Buretta and Berman [39] as $Ra_c = 33$, and the heat transfer data of these authors and that of Sun [40] can be represented by the correlation

$$Nu = 0.116\ Ra^{0.573} \tag{32}$$

where Ra is the Rayleigh number defined as

$$Ra = \frac{\rho g \beta L K}{\mu \alpha} \left(\frac{q'''_b H^2}{K_B} \right) \tag{33}$$

where K is the permeability of the bed for single phase coolant flow, β the linear thermal expansion coefficient, μ the viscosity, α the diffusivity and q'''_b the bed volumetric heating rate. According to the analysis, the onset of convection corresponds to a critical Raleigh number; $Ra_c = 33.0$. The permeability of typical particle beds can be obtained from the Kozeny equation as

$$K = \frac{1}{36} \frac{d_p}{C_K} \frac{\varepsilon^3}{(1-\varepsilon)^2} \tag{34}$$

where C_K is the Kozeny constant $C_K = 4.94$ [41].

An analytical model of a single-phase convective roll cell derived by an approximate technique [36] showed that the onset of convection can be given as $Ra_c = 32$, and the heat transfer by

$$Nu = 0.177\ Ra^{0.5} \tag{35}$$

Figure 3 shows the experimental findings of Hardee and Nilson [36]. The combined behavior for conduction and single-phase convection Eq. (35) is represented by the solid curve, the family of dashed branch lines extends into the boiling regime.

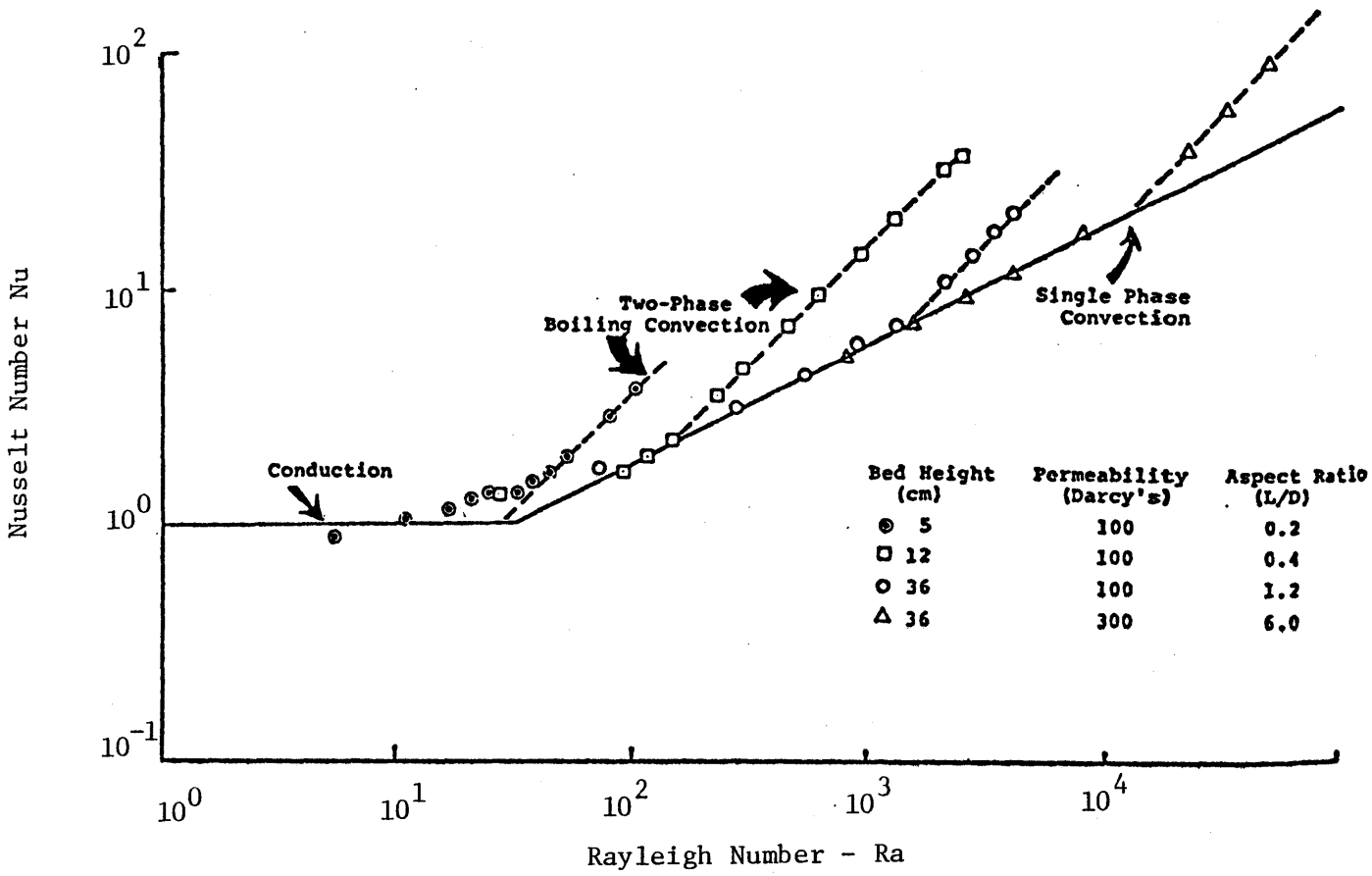

Figure 3: Heat Transfer for a Heat-Generating Porous Bed Cooled from Above [36]

Natural convection heat transfer can be improved by the presence of an overlying finite layer of coolant. Experimental observations [42] showed that increasing the height of the liquid layer over the bed tended to lower the internal Rayleigh number Ra_c at which onset of convection occurred. For overlying liquid layer height ratios of 4 or greater, the natural convection is given as $Ra \simeq 15$. The heat transfer for $Ra > 15$ is

$$Nu = 0.117\ Ra^{0.79} \tag{36}$$

Figure 4 shows the typical flow stream lines at the onset of convection.

4.2.3 Effective Thermal Conductivity of Particulate Bed

Upward heat removal can occur by conduction. Heat conduction is an effective heat removal mechanism for beds of oxide fuel and steel. The difficulty in calculating the thermal conductivity of a system composed of particles interspersed with a continuous liquid phase lies both in formulating a model that represents the system and in expressing mathematically an effective conductivity on the basis of the model. Any correlation to apply adequately over a range of conditions must account for variations in fluid thermodynamic properties as well as particle properties and dimensions.

If heat is considered as passing through a particulate bed by paths each composed of one or more discrete steps involving: 1) the solids, 2) the contact surface of the solids, 3) the fluid film near points of contact between the solids, an analytical expression can be developed for the bed effective thermal conductivity when the fluid is static [43] as

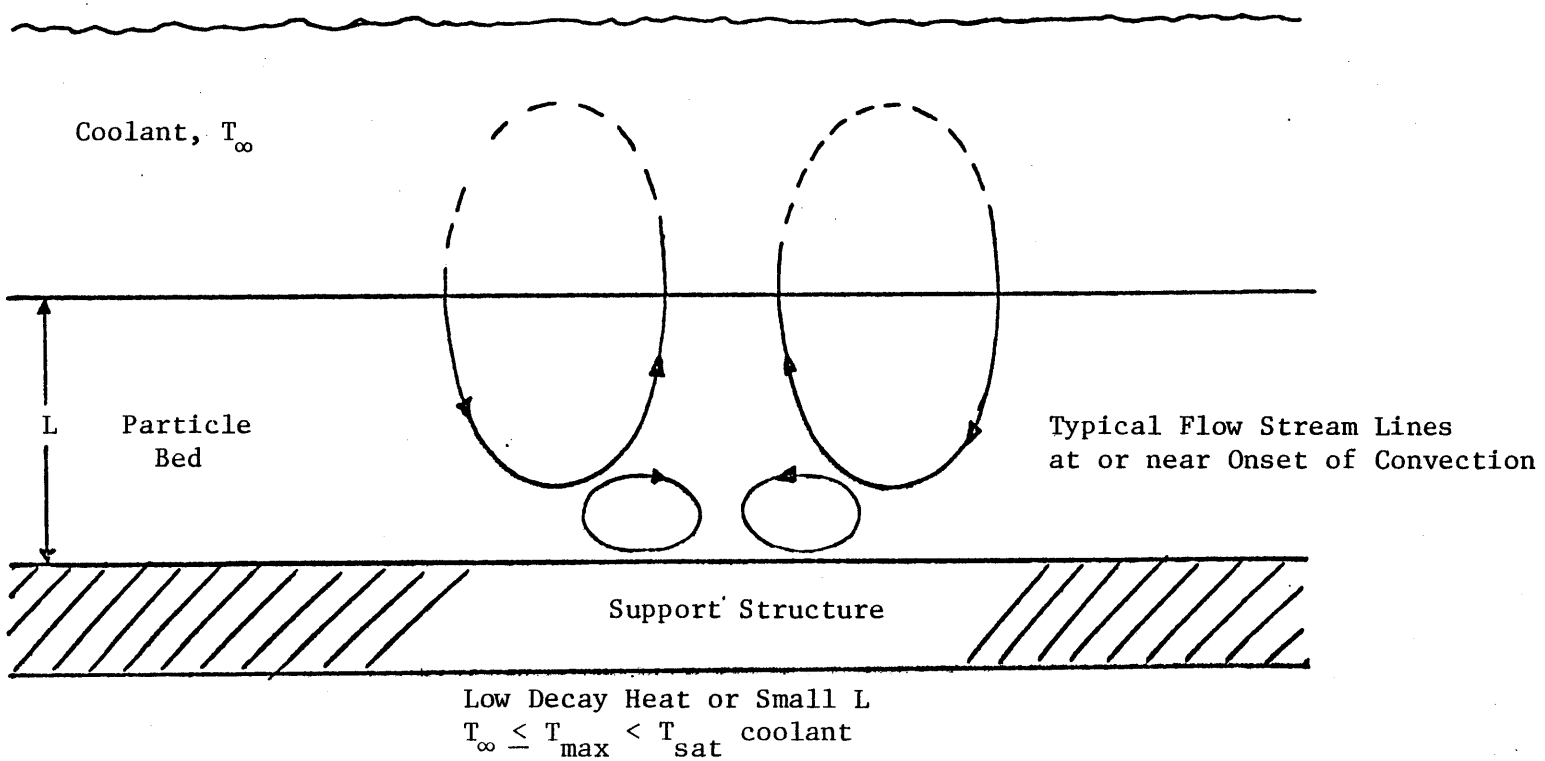

Figure 4: Natural Convection in a Porous Media with Internal Heat Generation

$$K_{eff} = K_f \left[1 - \frac{(1-\varepsilon)(1- K_f/K_w)}{K_f/K_w + (1-\varepsilon)^{1/3} (1- K_f/K_w)} \right] \quad (37)$$

Where the subscripts f and w denote fuel and water, respectively.

4.2.4 Boiling in Debris Bed

Upward heat removal from particulate beds in water is greatly enhanced by boiling within the bed. Boiling begins when either the bed loading or the heat generation rate is too great for heat removal by conduction or where there is insufficient subcooling of the overlying liquid (Fig. 5). Thicker debris beds and/or higher decay heat will result in more vigorous boiling (Fig. 6). Some of the debris may be at temperatures greater than the coolant saturation temperature, and the steel supporting the structure could be at temperatures approaching the coolant saturation temperature. The vapor and liquid may be beginning to interfere with one another.

At very high decay heats or in very deep beds, regions devoid of liquid will occur (see Fig. 7) because either the vapor blocks the fluid or the liquid does not have sufficient pressure gradient for it to penetrate the debris bed. The dry regions will begin to melt, and the molten particles will agglomerate. The final form will be a molten layer.

4.2.5 Dryout Heat Flux Correlations

Incipient dryout will occur in debris bed when the vapor generation rate is sufficiently large that it prevents the adequate flow of replenishing liquid. Incipient dryout thus depends on the fluid material properties (heat of vaporization, density, viscosity, etc.), particle sizes and shapes, bed depth, bed packing (space between particles), volumetric bed power, etc.

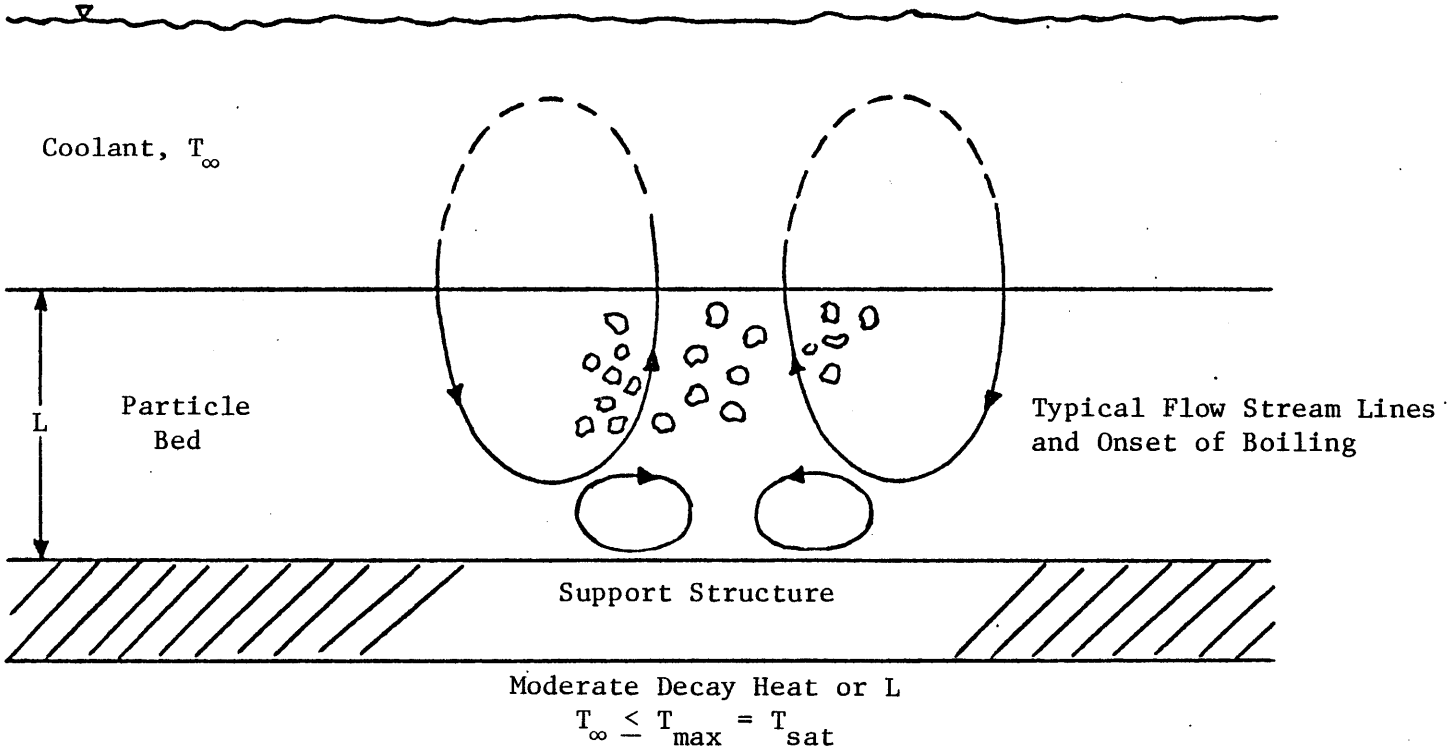

Figure 5: Natural Convection and Mild Boiling in a Porous Media with Internal Heat Generation

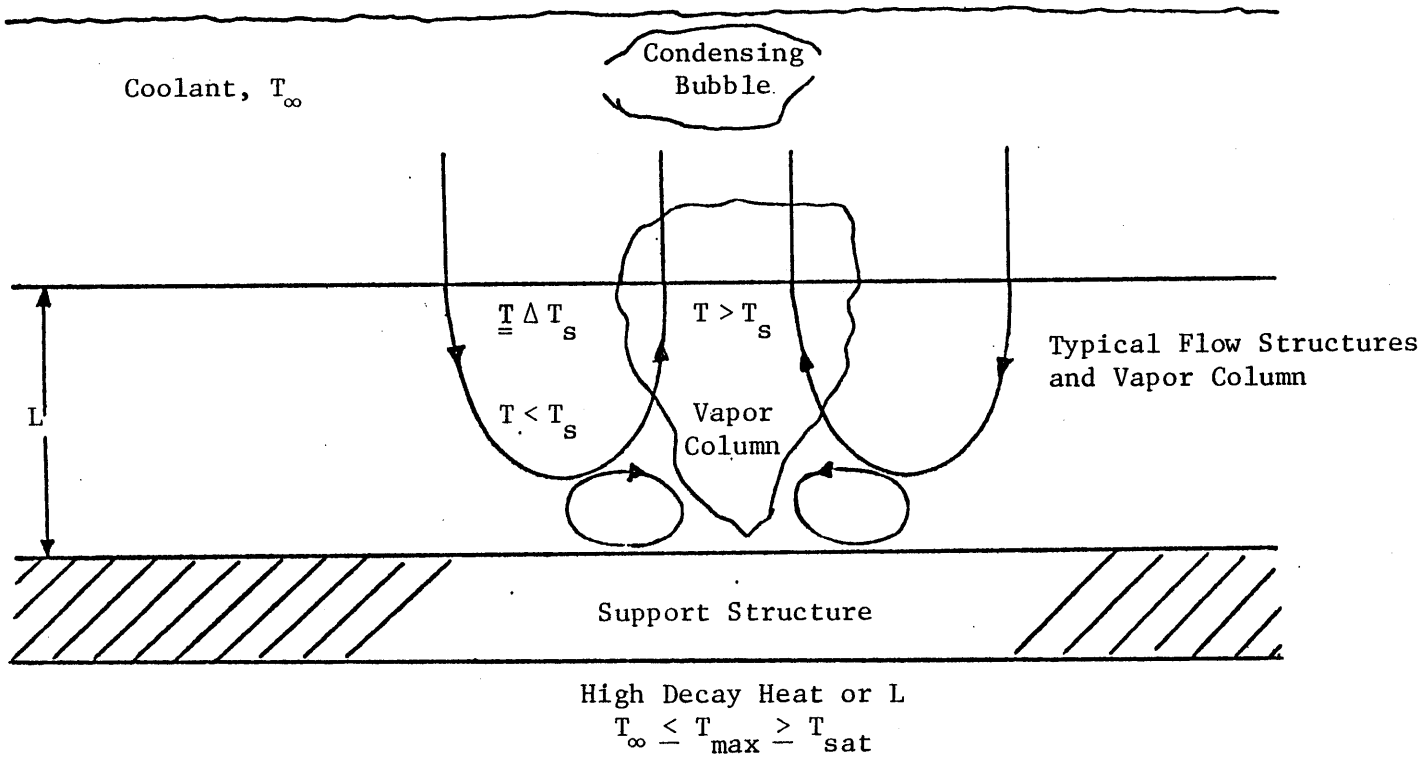

Figure 6: Natural Convection and Vapor Column in a Porous Media with Internal Heat Generation

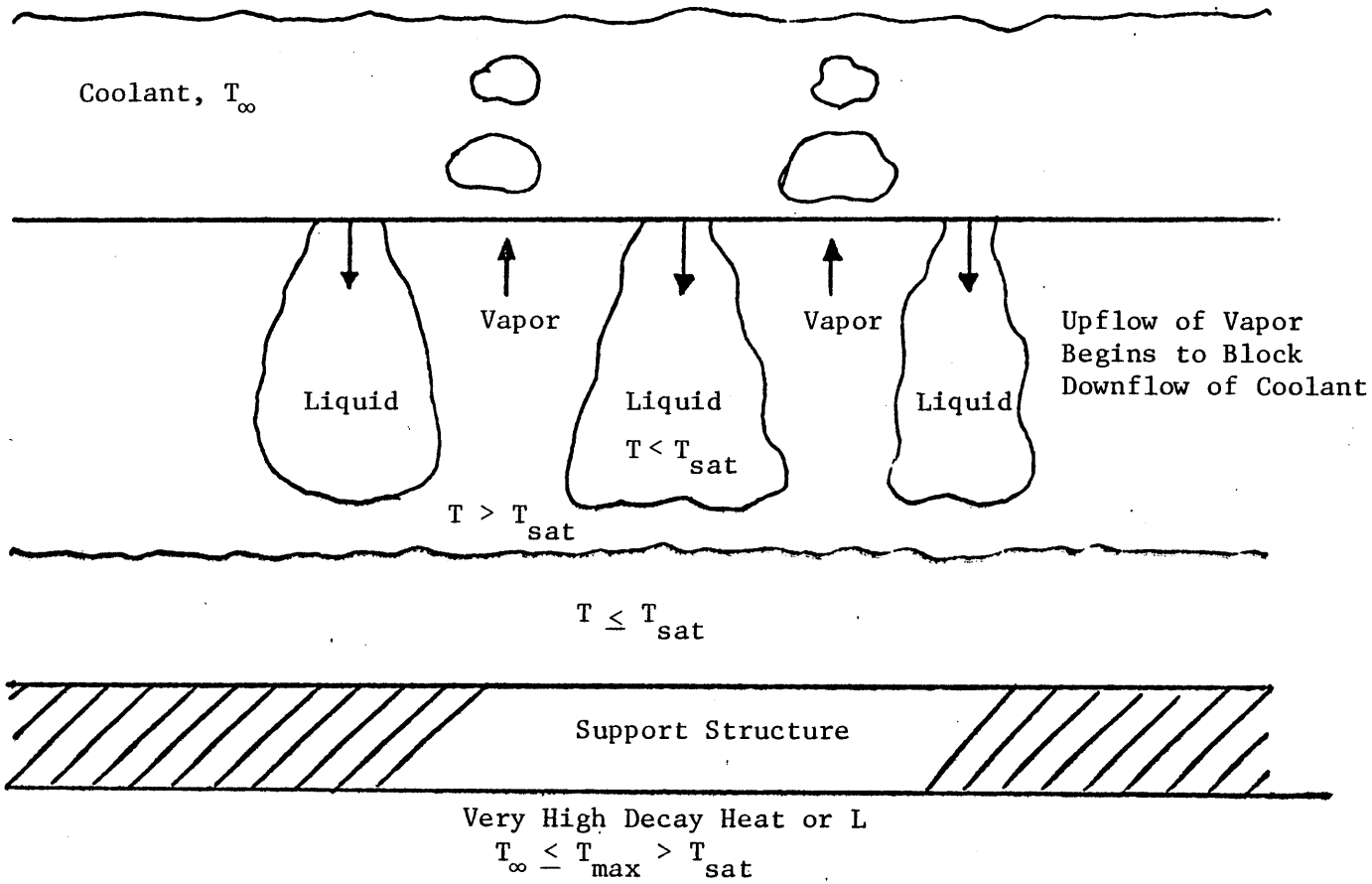

Figure 7: Beginning of Dryout and Melting of Debris Due to Internal Heat Generation

Considerable research has been performed on particle bed dryout in the LMFBR safety program [30,34,36,38]. Experiments involving water, acetone, methanol, and sodium as fluids with steel, lead, sand, and urania as particles have been performed.

Parametric studies on dryout have revealed various interesting phenomena. For example, debris beds formed with larger diameter particles (>>1 mm) have been found associated with a lower dryout heat flux as the bed height decreases, whereas beds composed of smaller diameter particles (<<1 mm) have lower dryout heat fluxes at deeper depths. Debris beds composed of mixtures of particles exhibit the worst characteristics as far as coolability is concerned. That is, mixtures of particle diameters, in general, exhibited lower dryout heat fluxes over the range of applicability than beds formed by particles of a single diameter [44].

Fluidization of a bed consisting of a wide range of particle sizes was shown to play an important role in the magnitude of dryout heat fluxes [34]. The partial fluidization of fine particles produces movement of the bed material, allowing the formation of channels for the escape of vapor. Further, the time average distance between particles is probably greater than that for a fixed bed so that lesser interference for upward vapor movement and downward fluid movement is encountered. The net effect is for higher heat transfer rates and consequently higher dryout heat fluxes as compared to a bed composed of uniformly sized particles.

Empirical correlations and phenomenological models have been developed to describe the dryout heat fluxes under the various physical conditions. A semi-empirical model based partly on an assumption of Darcy flow and partly on a correlational fit to the measured dryout data is that of Dhir

and Catton [30]

$$q_d = 0.0177 \frac{\rho_\ell \, gK \, h_{fg}}{\nu_\ell} \left(1 - \frac{\rho_v}{\rho_\ell}\right) \tag{38}$$

where q_d is the heat flux exiting the bed at incipient dryout, ρ_ℓ and ρ_v are the liquid and vapor densities, g is the gravitational acceleration, K is permeability, h_{fg} is the heat of vaporization, and ν_ℓ is the liquid kinematic viscosity.

A mechanistic model based on Darcy flow and optimizing liquid and vapor viscous drags is that of Hardee and Nilson [36]

$$q_d = \frac{\rho_\ell g K \, h_{fg}}{\left(\sqrt{\nu_v} + \sqrt{\nu_\ell}\right)^2} \tag{39}$$

where ν_v is the vapor kinematic viscosity. A semi-empirical model based on flooding correlations in packed beds is that of Ostensen [45]:

$$q_d = \frac{0.90 \, h_{fg} \sqrt{\rho_\ell \rho_v g} \sqrt[4]{K/\varepsilon}}{\left(1 + \sqrt[4]{\rho_v/\rho_\ell}\right)^2} \tag{40}$$

A mechanistic model (similar to the Hardee-Nilson model) which includes the effects of capillary forces is that of Shires and Stevens [46]

$$q_d = B \frac{(\rho_\ell - \rho_v) \, gK \, h_{fg}}{\left(\sqrt{\nu_v} + \sqrt{\nu_\ell}\right)^2} \left(1 + \frac{0.9 \, \lambda_c}{cL}\right) \tag{41}$$

where

$$\lambda_c = \frac{\sigma\sqrt{\varepsilon/K}}{2(\rho_\ell - \rho_v) g}$$

and where L is the bed depth, σ is the fluid surface tension, $c \simeq 1$ and B is empirically determined from dryout measurements.

A very general mechanistic model has been developed by Lipinski [47]. It allows for both laminar and turbulent flow in both the liquid and the vapor phases of the fluid. In addition, it includes both gravitational and capillaric forces. In the laminar limit it is similar to the model of Shires and Stevens. In the laminar limit and neglecting capillaric forces, the model is similar to the Hardee-Nilson model. In the turbulent limit (and again neglecting capillaric forces) the model is similar to the flooding model of Ostensen. The equation for dryout is

$$q_d = \rho_v h_{fg} \left[\left(\sqrt{V_L^2 + V_T} \right) - V_T \right] \tag{42}$$

where

$$V_L = \frac{\eta}{2K\rho_v} \left(\frac{\nu_v}{(1 - 1.11\gamma)} + \frac{\nu_\ell}{\gamma^3} \right) \Bigg/ \left(\frac{1}{\rho_v (1-\gamma)^3} + \frac{1}{\rho_\ell \gamma^3} \right)$$

$$V_T = \sqrt{\frac{\eta(\rho_\ell - \rho_v) g}{\rho_v^2} (1 + \lambda_c / L) \Bigg/ \left(\frac{1}{\rho_v (1-\gamma)^3} + \frac{1}{\rho_\ell \gamma^3} \right)}$$

$$\eta = \frac{d}{1.75} \frac{\varepsilon^3}{1-\varepsilon}$$

and where γ is varied from 0 to 1 until q_d is maximized.

When the models are compared with published dryout measurements. The Lipinski model appears to fit the data best [47]. This is partly due to the fact that the other models have only a limited range of capability, Fig. 8 compare the various models.

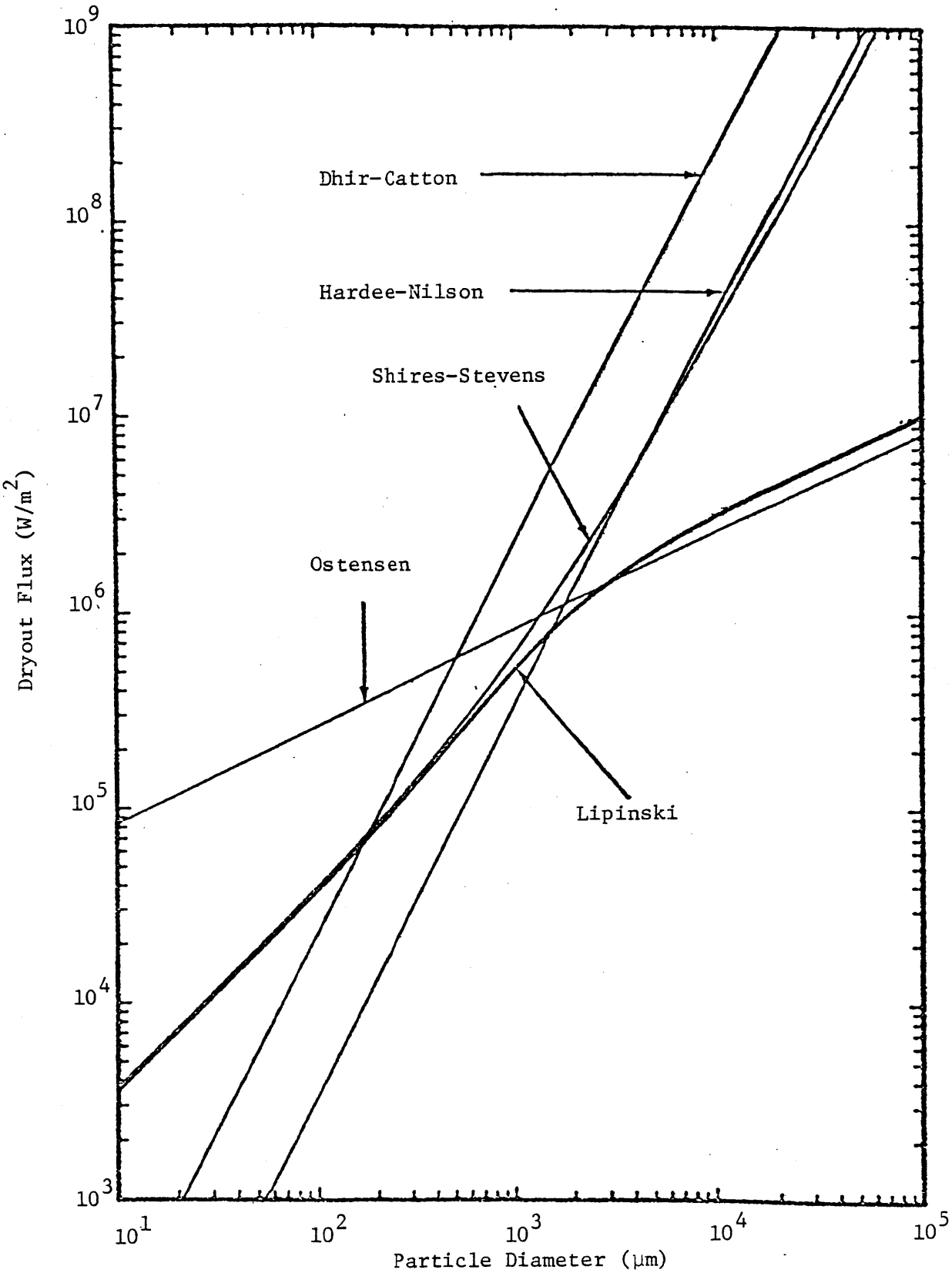

Figure 8: Comparison of Theoretical Dryout Heat Flux Correlations [47]

4.3 Convective Heat Transfer in Particulate Beds

4.3.1 Background

One of the inherent properties of particulate beds is the high rate of heat transfer between the bed particles and the fluid that is flowing through the bed, due to the large surface to volume ratio of the particles and to the enhanced heat transfer. The transfer of heat between particles and fluid is a complex problem as depends on many regimes of fluid flow in such two-phase systems.

Very few studies on post-accident heat removal PAHR from particulate beds with fluid flow seem to have been conducted. One investigation that can be cited is that of Squarer and Peoples et al. [48] who determined the minimum flow rate necessary to prevent the bed dryout. The authors concluded that a much thicker bed may be stored on a surface without experiencing bed dryout when a small amount of flow is forced through the heated bed.

D. H. Cho [49] studied the heat transfer from a heat generating blockage in two-dimensional geometry with conduction as the major heat transfer mechanism. The study gave a representation of the dimensions of the blockage that result in coolant boiling, also the minimum fuel mass and surface area required to produce coolant boiling.

Forced convection is an important mechanism of heat transfer from particulate beds though, up to the present time, there seems to be no experimental or analytical work in this area to assess the studies on PAHR from particulate beds. However, the problem is not new since extensive research has been conducted in the chemical industry on heat transfer from particulate beds in the fixed and fluidized states. Heat transfer

coefficient has been measured by using either steady state or unsteady state techniques. In the steady state techniques, rate data have been obtained either by estimating the heat changes accompanying evaporation of a liquid from the surface of porous particles forming the bed or by using induction heating or direct electrical heating of the bed. In the unsteady state techniques, temperature-time history graphs have been used to evaluate the heat transfer rate.

Fixed bed measurements have been made for beds of spheres oriented in a regular pattern, such as cubic, hexagonal, etc. and for randomly packed beds of spheres, cylinders and granules. Fluidized bed measurements have been made mostly with granules. Shallow beds have been used in most of the cases. Most of the measurements are confined to air. In the case of liquid fluidized beds water has been used as the fluid but in very few cases.

Most of the work is correlated in terms of the Chilton-Colburn J_h factor and particle Reynolds number. Nusselt numbers have also been used by many investigators. Correlations are often given to cover different ranges of particle Reynolds number and are valid within the range covered. Some have tried to improve those correlations by including other variables, such as $\frac{d_p}{D_T}$ (D_T being the bed diameter), $\frac{d_p}{D_H}$ (D_H being the bed height or shape factor). The lack of uniformity in the reporting of the results makes a comparison of the various studies difficult.

The problem of proper temperature distribution and difference is a source of much difficulty with fluidized bed measurements. The variation in data cannot be attributed to shortcomings in the experimental techniques alone, but also to the particular nature of the fluidized beds and fluidizing conditions.

The discrepancies in the results of various workers may be attributed to some additional factors. In analyzing the experimental results of heat transfer in fixed and fluidized beds, a uniform flow velocity over the entire cross-section of the bed has been assumed by many workers, and transport of heat by conduction and mixing in the direction of the flow is usually neglected with respect to convective transport. But this is not true in many cases. Bed inhomogeneity, which is often the case with beds of large particles, give rise to non-uniform flow distribution leading to radial temperature gradients.

For resolving these issues, it would be advantageous to obtain new data particularly in the fluidized bed region. These measurements must consider systematically the effects of all the variables affecting the transfer rate. Attention must be paid to the manner in which the bed is formed and whether or not it changes its geometry during the course of the experiment.

4.3.2 Heat Transfer Mechanisms

The phrases packed, fixed or particulate bed heat transfer are to describe a variety of phenomena, namely: (1) the convective heat transfer from the particles to the fluid flowing through the bed, (2) the conduction heat transfer between the individual particles in the bed, and (3) heat transfer by mixing of the fluid. These modes are illustrated schematically in Fig. 9. The second mode, namely the conduction between the particles, can be further subdivided into the axial and radial directions. The different modes may interact with one another. For example, the conduction between the particles and the fluid. This interaction among the different modes is one of the main reasons for the difficulty in

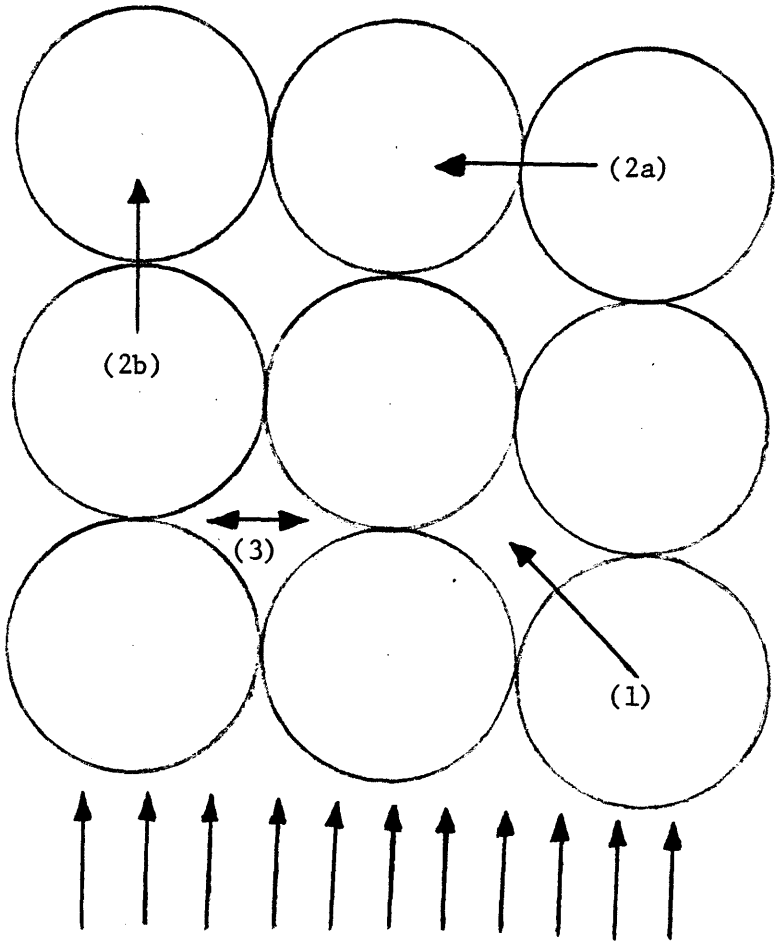

Figure 9: Modes of Heat Transfer in Packed Beds: (1) Particle to Fluid Convection; (2a) Radial Particle to Particle Conduction; (2b) Axial Particle to Particle Conduction; (3) Heat Transfer by Mixing of Fluid

correlating the total heat transfer and analyzing the experimental data in the field.

Two parameters, the effective or apparent conductivity, K_e, and the "total" heat transfer coefficient, h_t, are commonly used to express the heat transfer rate in packed beds. The effective thermal conductivity is an averaged parameter that describes the total thermal performance of the particulate medium that constitutes the bed. In other words, the effective conductivity is the conductivity the medium would have were it homogeneous. It is not the same as the conductivity of the material that constitutes the bed. The effective conductivity is dependent both on the thermal properties of the bed and on the flow rate, but in most experimental correlations it is generally expressed as a function of the Reynolds number only. This implies that these correlations are valid only for the particular bed materials which were used in developing them.

The total heat transfer coefficient is also an averaged parameter. This total heat transfer coefficient generally incorporates the conduction mode between the particle beds, and the convective mode between the bed particles and the flowing medium.

The effective conductivity of a particle bed through which fluid is flowing is greater than for the static case except when the Reynolds number ($Re = \frac{d_p G}{\mu}$, where d_p is the particle diameter), is below about 6.6 [50]. This is expected because, with flow, the mixing of fluid portions around particles transfers heat relatively rapidly. The physical situation is, of course, much more involved and difficult to describe. However, effective thermal conductivity of particle bed at right angle to the direction of liquid flow (K_{er}) is most reliably expressed by [51]

$$\frac{K_{er}}{K_f} = 6 + 0.026\left(\frac{K_p}{K_f}\right) + 0.00176\left(\frac{c_p\,\mu_f}{K_f}\right)\left(\frac{D_T G}{\mu_f}\right) \qquad (43)$$

Where D_T is the diameter of the bed and G the liquid mass velocity.

The overall bed conductivity (K_{ob}) which might be used to calculate the exit temperature of a fluid form entrance and bed boundary conditions is expressed by [52]

$$\frac{K_{ob} - K_b}{K_f} = K\left(\frac{D_T}{d_p}\right)^{1/2}\left(\frac{U_f S\, G}{\mu_f}\right)^{0.69} \qquad (44)$$

Where (K_b) is the bed's conductivity under static conditions given by Eq. (37), S the surface area of the particle and K a constant. For ceramic materials the constant has a value between approximately 0.05 and 0.06.

4.3.3 Experimental Findings and Available Correlations

A. Single Sphere

The heat transfer coefficient h_p between the surface of a sphere of diameter d_p and a fluid through which it is moving with relative velocity U is given by Ranz and Marshall [53].

$$Nu_p = \frac{h_p d_p}{K_f} = 2.0 + 0.6\ Pr^{1/3}\ Re_p^{1/2} \qquad (45)$$

Where K_f and Pr are the thermal conductivity and Prandtl number of the fluid respectively.

B. Packed Beds

Heat Transfer in beds of coarse solids may be approximated by

$$Nu_p = 2 + 1.8\ Pr^{1/3}\ Re_p^{1/2} \qquad Re_p > 100 \qquad (46)$$

Other correlations which are based on experimental measurements have been summarized in Table 2. However, some of the interesting work is discussed below.

It seems that a variety of techniques were used by the different investigators. The results form a consistent whole and show clearly that as the Reynolds number is lowered below 100, the Nusselt number drops sharply from the extrapolation of Eqs. (45) or (46), becoming very much smaller than the value for conduction alone into an infinite medium, or $Nu_p = 2.0$ (See Fig. 10).

Many investigators tried to explain the lower values of Nusselt number, as Cornish [83] suggested, turbulence of fluid in void spaces may degrade due to adjacent particles and boundary layers should develop on surfaces of packed particles in a similar manner to the case of an isolated particle. In the range of low Reynolds numbers, however, boundary conditions describing heat transfer in flowing media are quite different from those for an isolated particle system. Therefore, the theoretical value, 2.0, for single sphere in a stagnant medium does not have physical meaning anymore. Pfeffer [84] combined "free surface mode" introduced by Happel [85] with "thin boundary layer solution" [86]; he showed a simple relationship among heat transfer coefficients, Peclet number and void fraction as follows:

$$Nu_p = \frac{h_p d_p}{K_f} = 1.2\left[\frac{1-(1-\varepsilon)^{5/3}}{W}\right]^{1/3}\left[\frac{d_p C_p G}{K_f}\right]^{1/3} \qquad (47)$$

where

$$W = 2 - 3\gamma + 5\gamma^5 - 2\gamma^6$$

$$\gamma = \frac{R}{b} = (1-\varepsilon)^{1/3}$$

TABLE 2

Summary of Particle-to-Fluid Heat Transfer in Fixed Beds

Author(s)	Fluid	Particle		Bed Characteristics		Re	Pr	Correlation
		Material & Shape	Size (cm)	Height (cm)	Void Fraction (ε)			
Furnas [54]		iron, spheres	1.854-4.851	104.14	0.395-0.506	120 - 1200	0.7	$h = 0.000144G^{0.75}xTx10^{1.68\varepsilon-3.56\varepsilon^2}$
Saunders & Ford [55]	Air	steel, lead glass, spheres	0.1587-0.635	6.35 - 25.4	—	54 - 434	0.71	$St \approx 0.188$
Fedorov [56]	Air	Moscow coal grains	0.3 - 1.2	(2-10) x D_p	0.51-0.575	20-1850	0.6	$Nu = 0.23\ Re^{0.863}$
Kitayev [57]	—	iron, iron ore, coke; sphere, granules	1.85 - 4.86; 0.4 - 7.0	—	0.395-0.506; 0.485-0.585	67 - 1050 92-4830		$Nu = 0.14\ Re^{0.92}$ $Nu = 0.098\ Re^{0.9}$; $Nu = 0.104\ Re^{0.9}$; $Nu = 0.06\ [A/1-\varepsilon)]\ Re^{0.9}$ where $A = 10(1.68\varepsilon - 3.6\varepsilon^2)$
Sokol'skii [58]	Air	granules	—	—	—	—	0.6	$Nu = 2 + aRe^{0.5}$ for $Re > 100$ $Nu = 0.56\ Re^{0.5}$ for $Re \geq 100$
Gamson et al. [59]	Air	celite, spheres cylinders	0.3962-2.162	2.54 - 6.35	0.37 - 0.43	60 - 4000	0.72-0.75	$J_h = 18.1/Re$, for $Re < 40$ $J_h = 1.064\ Re^{-0.41}$ for $Re > 350$
Wilke & Hough [60]	Air	celite cylinders	0.3962-2.162	2.3368	—	40 - 350	0.7	$J_h = 1.95\ Re^{-0.51}$

Table 2 (continued)

Author(s)	Fluid	Particle		Bed Characteristics		Re	Pr	Correlation
		Material & Shape	Size (cm)	Height (cm)	Void Fraction (ε)			
Chukhanov and Shapatina [61]	—	copper-cylinder, fireclay-granules	0.2 x0.2; 0.2 - 0.7	—	0.4 - 0.52	—	—	$Nu = 0.24\ Re^{0.83}$
Glaser [62]	Air	ceramic, brass-sphere	1.0, 1.94, 1.60, 5.207	96.52	0.392 0.42	330 - 1500 300 - 4000	0.7	$Nu = 1.25\ Re^{0.58}$
Kichkina [63]	Air	ceramic-granules	1.0 - 1.5	—	0.465 - 0.473	270 - 1350	—	$Nu = 0.229\ Re^{0.815}$
Lof and Hawley [64]	Air	granitic granules	0.7975 - 3.33	91.44	0.426 - 0.545	50 - 500	0.7	$h' = 0.79(G/D_p)^{0.7}$
Lydersen [65]	Air	copper, celluloid spheres	3.785	22.71	0.2594 - 0.4764	120 - 4500	0.71	$J_h = 1.187\ Re^{-0.37}$
Dayton et al. [66]	Air	glass spheres	0.3275 - 0.6299	2.54 - 4.08	—	150 - 1000	0.71	$J_h = Re^{-0.41}$
Maeda and Kawazoe [67]	Air	celite, clay broken solids, Raschig rings, berl saddles	0.285 - 2.5		—	—	0.7	$Nu = 4.9\ Re^{0.60}\ \varepsilon^{-2.2}\ (D_p/D_t)$; Re>100 $Nu = 12.3\ Re^{0.4}\ \varepsilon^{-2.2}/(D_p/D_t)$; Re<100 (Nu Re based on tube diameter)

Table 2 (continued)

Author(s)	Fluid	Particle		Bed Characteristics		Re	Pr	Correlation
		Material & Shape	Size (cm)	Height (cm)	Void Fraction (ε)			
Dyakonov & Semenov [68]	Air	steel sphere	0.792 - 1.172	197	—	40 - 620	0.6	$Nu = 0.128\ Re(D_c/D_p)^{0.257}$
Glaser [69]	Air	olry, celite granules Raschig rings	0.8224 - 1.6764	96.52	0.519 - 0.677	140 - 2000	0.7	$Nu = 0.96\ \varepsilon^{0.75}\ Re^{0.61}$
Galloway et al. [70]	Air	celite, alundum, kasline spheres	1.7094	13.68	0.2595 - 0.4764	300 - 1200	0.718	$J_h = 0.197\ Re^{-0.159}$
Ball [71]	Air	lead, alumina spheres	0.4394, 0.419	12.7 - 63.5	0.355 - 0.402	68 - 116	0.73	$J_h = 0.913\ Re^{-0.324}$
Baumeister & Bennett [72]	Air	steel spheres	0.3175 - 0.3967	10.16	0.354	200 - 10400	0.73	$J_h = aRe^b$, a and b depend upon particle size
Glaser & Thodos [73]	Air	monel, brass spheres	0.4762 - 0.794	5.08	0.436 - 0.453	300 - 4000	0.71	$Nu = 1.25\ Re_p^{0.58}$
DcAcetis & Thodos [74]	Air	celite spheres	1.5875	4.763 - 7.938	0.482	13 - 2136	0.72	$J_h = 1.1/(Re^{0.41} - 1.5)$
Wadsworth [75]	Air	copper spheres	10.16	30.8	0.2595	8000 - 60,000	0.71	$J_h = St \approx 0.972\ Re^{-0.267}$

Table 2 (continued)

Authors(s)	Fluid	Particle		Bed Characteristics		Re	Pr	Correlation
		Material & Shape	Size (cm)	Height (cm)	Void Fraction (ε)			
Beek [76]	—	—	—	—	—	10 - 4000	—	$Nu = 3.22\ Re^{1/3}Pr^{1/3} + 0.177\ Re^{0.8}Pr^{0.4}$
Glaser [77]	Air	ceramic spheres	1.03, 1.21, 1.6, 5.2	96.0	0.392, 0.42	300 - 4000	0.7	$Nu = 1.40\ Re^{0.58}Pr^{1/3}$
McConnachie & Thodos [78]	Air	celite spheres	1.5875	6.579 - 8.484	0.416 - 0.778	235 - 7285	0.719	$J_h = 1.192/[(Re/1-\varepsilon)^{0.41} - 1.52]$
Sengupta & Thodos [79]	Air	celite spheres	1.5875	17.78	0.444 - 0.778	95 - 2500	0.718	$\varepsilon J_h = 2.06/Re^{0.575}$
Baldwin et al. [80]	Water	spheres	4.9112	—	0.48, 0.26	3000 - 70,000	5.8	$J_h = 0.99\ Re^{-0.33}$; cubic packing $J_h = 0.94\ Re^{-0.30}$; dense cubic packing
Zabrodsky & Zhitkevich [81]	Air		5.0	—	—	50 - 34,000	0.7	$Nu = 2 + 1.18\ Re^{0.53}$; $50 < Re < 3000$ $Nu = 0.263\ Re^{0.73}$; $2000 < Re < 40,000$ (for dense packed) $Nu = 0.87\ (\varepsilon_d/\varepsilon_1) - 0.19\ Re$ (for loosely packed)
Bradshaw et al. [82]	Air	steel, alumina, hematite spheres, pellets	0.9525 - 2.54	—	—	150 - 600	0.7	$J_h = 0.495\ Re^{-0.375}$
Balakrishnan & Pei [115]	Air	alumina spheres & cylinders	—	—	—	300 - 4000	0.7	$(J_h)_{fp} = 0.018\ (Fr_{pm})^{-0.5} \times \phi_s^{3.76}$

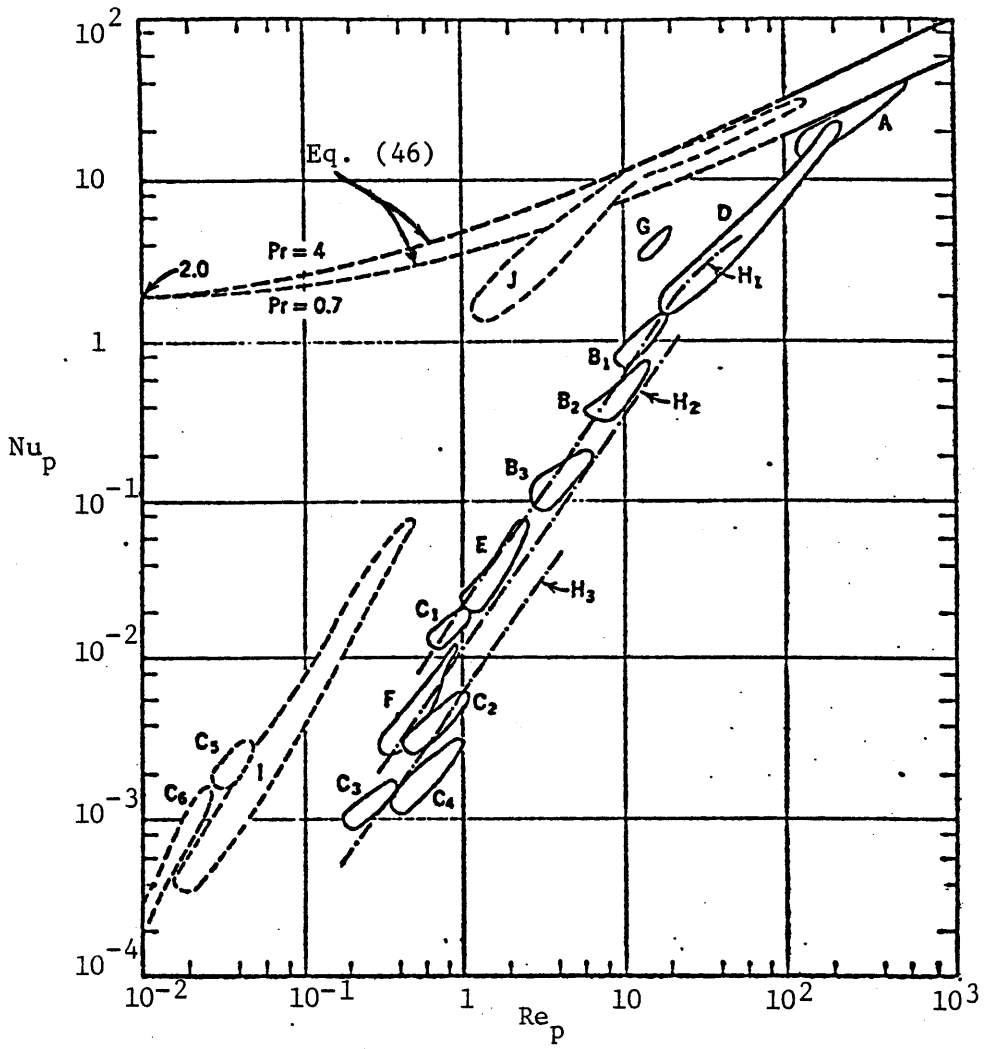

Figure 10: Reported Results for Heat Transfer in Fixed Beds, C_5, C_6, J for Liquid Water, the others for Air [12]. (A) Lof and Hawley [64]; (B's) Eichhorn and White [117]; (C's) Kunii and Smith [118]; (E) Mimura [119]; (F) Suzuki [120]; (G) Tokutomi [121]; (H's) Donnadieu [122]; (I) Harada [123]; (J) Mitsumori [127].

This equation is applicable to the high Peclet number -- low Reynolds number region, also assuming the existence of viscous flow and a thin thermal or diffusional boundary layer on the surface of a particle.

Zabrodsky [87] also tried to interpret experimental values of Nusselt number by means of a model with "micro-breaks" that is, local by-passing of gas due to non-uniformity of fluidization.

Kunii and Suzuki [88] suggested that channelling or local uneven contacting of fluids with solids is responsible for the apparent low heat transfer coefficient observed at low Reynolds number. Their correlation is of the form

$$Nu_p = \frac{\phi_s}{6(1-\varepsilon)\xi} Pe \qquad Pe < 10 \tag{48}$$

Where ϕ_s and ξ are the shape factor and the ratio of channelling length to particle diameter respectively.

Based on the analogy between heat and mass transfer Kato and Wen [89] correlated the Nusselt number for heat transfer between gas and particles in fixed beds to particles Reynolds number, Prandtl number and the ratio of the particle diameter to the bed height $\frac{d_p}{L_B}$,

$$Nu_p = 1.05\ Pr^{1/3} \left[Re_p \left(\frac{d_p}{L_B}\right) 0.6 \right]^{1.1} \qquad 0.1 \leq Re_p \left(\frac{d_p}{L_B}\right)^{0.6} \leq 2.5 \tag{49}$$

$$Nu_p = 1.5\ Pr^{1/3} \left[Re_p \left(\frac{d_p}{L_B}\right) 0.6 \right]^{1.1} \qquad 2.5 < Re_p \left(\frac{d_p}{L_B}\right)^{0.6} < 10^3$$

They attributed the low values of Nusselt number to the fact that for low Reynolds number and small Prandtl number regions, the individual thermal boundary layer for heat transfer does not exist. This is because the thermal boundary-layer thickness is much larger than the diameter of the particle causing overlapping of the thermal boundary layers in a multi-particle system, thereby reducing effective surface area for heat transfer. Consequently the calculation based on heat transfer area gives a much greater surface than the actual effective heat transfer area, thus the Nusselt number becomes smaller than the theoretical value of 2.0 for a single particle in a stagnant fluid when Reynolds number becomes very small.

C. Fluidized Beds

The phenomenon of heat transport in fluidized beds has been the subject of numerous studies. Kettering, Manderfield, and Smith were the first to report gas-to-solid heat transfer coefficient [90]. Both silica gel and alumina particles of narrow particle size range were used, with the particle diameter being varied from 360 to 1000 microns. The wet particles were heated and fluidized by air at 88 - 108 °F in a 2.3 inch diameter column and at gas mass velocities of 250 to 720 $lb/hr\text{-}ft^2$. Gas temperature was taken as that temperature indicated by a bare thermocouple inserted in the bed at various positions and the bed temperature was assumed equal to exit gas temperatures. Bed height was varied from 4 to 6 inches. A gas temperature gradient was found to exist over a small portion of the bottom of the bed. Heat transfer coefficients were determined and the data correlated by plotting the Nusselt group versus the Reynolds number.

Wamsley and Johanson [91] used a transient method to determine the heat transfer coefficient from various particles to air and carbon dioxide. Precooled particles were dropped into a heated gas stream, and the exit temperature of the gas leaving the fluidized column was recorded as a function of time. To analyze the data the authors assumed that:

(1) the solids temperature was uniform throughout the fluidized bed;

(2) the heat losses from the column were negligible;

(3) the gas in the column was perfectly mixed so that the gas temperature at any position is uniform and equal to the outlet temperature, and

(4) the heat capacity of the gas is negligible in comparison to the heat capacity of the solid particles.

The heat transfer coefficient was found to be independent of gas velocity and dependent only upon the particle diameter. The most serious assumption of Wamsley and Johanson is number (3); for the gas temperature obviously must vary throughout the column. Assumption (1) is also open to question because the particle temperature must vary along the length of the column in some manner similar to the variation of the gas temperature.

Walton, Olson, and Levenspiel [92] measured heat transfer coefficient between air and crushed coal. The particle size ranged between 360 and 730 microns. Gas temperatures were measured with suction thermocouples, and solids temperature were estimated by using bare thermocouples. In accordance with the reasoning pertaining to the rapid axial temperature equalization in the so-called active section of fluidized beds, the authors made an energy balance on a differential element in the active section. A constant solids temperature was assumed in order to obtain an expression for the heat transfer coefficient in terms of the axial gas temperature variation and the fluid properties. A graph was then plotted and used to

determine the heat transfer coefficient. The data were correlated with:

$$Nu_p = \frac{h_p d_p}{K_f} = 0.0028\ Re_p^{1.7} \left[\frac{d_p}{d_t}\right]^{-0.2} \tag{50}$$

Sunkoori and Kaparthi [93] performed heat transfer experiments with water, using granite and quartz particles in the range of 540 to 110 microns. The unsteady-state method used by Wamsley and Johanson [91] was used to evaluate the heat transfer coefficients in the liquid system; however, two serious faults are present in this paper. First, a Beckman thermometer was used to measure water temperature as a function of time. The total elapsed time for cooling the heated particles was of the order of 6 seconds. The time constant for the thermometer would surely be large enough to cause one to question the absolute accuracy of the cooling curve, although the relative behavior might be consistent. Second; the neglect of the heat capacity of the fluidizing medium (water) cannot be justified for a liquid as it was for the gaseous systems of Wamsley and Johanson. Consequently, the method of Sunkoori and Kaparthi appears invalid, since the heat capacity of the water in the column is of the same order of magnitude as that of the solid and hence cannot be neglected.

Frantz [94] in a survey article combines the liquid and gas data of [90,91] by using the equation:

$$Nu_p = \frac{h_p d_p}{K_f} = 0.016\ Re_p^{1.3}\ Pr^{0.67} \tag{51}$$

However, the data of Sunkoori and Kaparthi [93] do not fit the correlation too well.

Mann and Feng [113] studied the unsteady heat transfer between gas and solid particles in fluidized beds, 2 and 4 inches in diameter. A system of transient heating and cooling of glass beads, silica gel, and alumina between 130 °F and 233 °F was used. The effect of several variables, particle size (0.004 to 0.2411 inch) bed settled heights (0.8 to 16 inches), particle densities (8.5 to 206 pounds per cubic ft.), thermal conductivity [0.013 to 1.8 Btu/(hr)(ft^2)(°F/ft)] and air velocities (0.543 to 4.347 ft. per sec) on the space-averaged heat transfer coefficient, was investigated. A correlation for two ranges of Reynolds number was developed and shown to be

$$Nu_p = 0.08\ Pr^{0.4}\ Re_p^{-6.1} \left(\frac{L_s}{d_t}\right)^{-1.3} \left(\frac{d_f}{d_t}\right)^{4.3} \left(\frac{K_s}{K_f}\right)^{-4} \left(\frac{\rho_s}{\rho_f}\right)^{7.8} \qquad (52a)$$

$$10 \leq Re_p \leq 60$$

$$Nu_p = 0.011\ Pr^{0.4}\ Re_p^{-3.1} \left(\frac{L_s}{d_t}\right)^{-1.3} \left(\frac{d_f}{d_t}\right)^{4.3} \left(\frac{K_s}{K_f}\right)^{-4} \left(\frac{\rho_s}{\rho_f}\right)^{7.8} \qquad (52b)$$

$$60 < Re_p < 2200$$

Holman et al. [114] studied the heat transfer from particle to fluid in water fluidized system. Stainless steel and lead spheres were fluidized in water and heated by an induction heating field. Reynolds number based on particle diameter and superficial velocity ranged between 240 and 14,000. The heat transfer from the spherical particles to the water was correlated with

$$Nu_p = 0.291 \times 10^{-6} \, (Re_p F_\varepsilon)^{2.12} \, Pr^{0.67} \left(\frac{\mu}{\mu_o}\right)^{0.83} \tag{53a}$$

or

$$Nu_p = 1.28 \times 10^{-5} \, (Re_p F_\varepsilon)^{2.0} \, Pr^{0.67} \left(\frac{d_t}{d_p}\right)^{0.5} \left(\frac{\rho_f}{\rho_p}\right)^{2} \left(\frac{\mu}{\mu_o}\right)^{0.83} \tag{53b}$$

The second correlation of Eq. (53) deviates less from the data than the first correlation since the dimensionless groups $\frac{d_t}{d_p}$ and $\frac{\rho_f}{\rho_p}$ introduced. The velocity correction factor, F_ε is used to account for variation in porosity and is given by

$$F_\varepsilon = \frac{1}{1 - (1-\varepsilon)^{2/3} \, \pi^{1/3} \left(\frac{3}{4}\right)^{2/3}} \tag{54}$$

The experimental conditions were similar to those experienced in a fluidized nuclear reactor and the data obtained compared favorably with those of other investigators.

On examining the results of the various investigators one can observe a characteristic sharp drop in the Nusselt number with decreasing Reynolds number. Lack of agreement, with over a thousand fold variation, occur among many observers as shown in Fig. 11. This may be due to the different experimental conditions and data interpretations by different investigators.

The low values of Nusselt numbers at low range of Reynolds numbers are also apparent. Table 3 summarizes the experimental conditions and the results of the above investigators and many others.

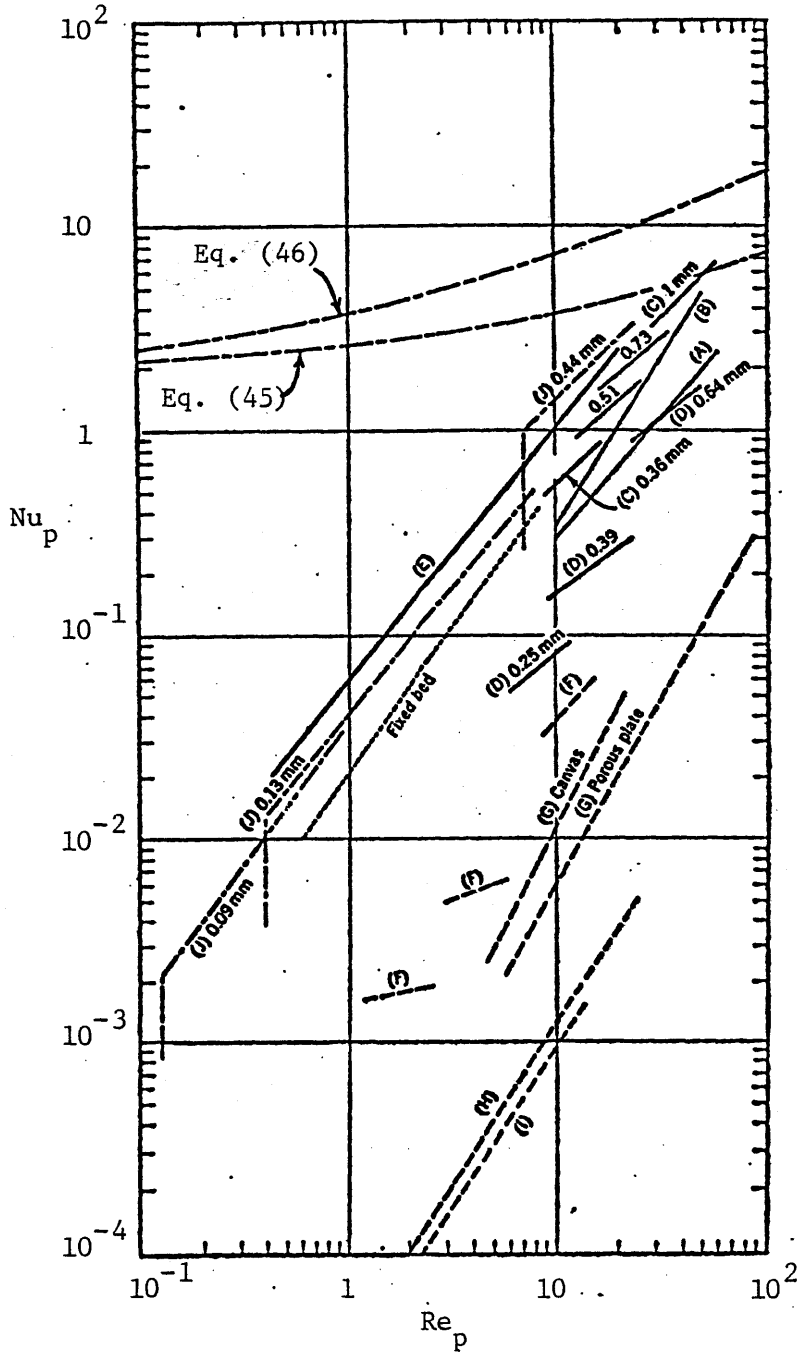

Figure 11: Reported Results for Heat Transfer in Fluidized Beds [12]. (A) Kettering et al., [90]; (B) Walton et al., [92]; (C) Heertjes and McKibbins [112]; (D) Sato et al., [124]; (E) Richardson and Ayers [97]; (F) Wamsley and Johanson [91]; (G) Yoshida [125]; (H) Ferron [126]; (I) Fritz [101]; (J) Donnadieu [122].

TABLE 3

Summary of Particle-to-Fluid Heat Transfer in Fluidized Beds

Author(s)	Fluid	Particle		Bed Characteristics		Re	Pr	Correlation
		Material & Shape	Size (cm)	Height (cm)	Void Fraction (ε)			
Fedorov [111]	Air	active carbon, Moscow coal, cardboard granules pieces	0.3 - 0.5 0.5 - 1.0 5 x 6 x 3 - 10 x 5 x 3 mm piece	0.6 - 4.5	—	Ge = 0.9 4.0 kg/m^{2}sec	0.7	$Nu = 0.23\ Re^{0.863}$; $20 < Re < 500$ $Nu = 0.0151\ Fe^{0.74}\ Re^{0.65}\left(\frac{Ho}{de}\right)^{-0.34}$ For $30 < Fe < 100$
Kettenring et al. [90]	Air	alumina, silica gel granules	0.0502 - 0.0713	10.16 - 20.32	0.6 - 0.8	g - 55	0.72	$J_h = 0.0151\ Re^{0.30}$
Walton et al. [92]	Air	coal granules	0.12 - 0.33	25.4 - 71.12	—	10 - 32	0.689	$Nu = 0.00285\ Re^{1.7}(D_p/D_t)^{-0.2}$ $h = 0.00762G^{1.7}D_p^{0.5}$
Wamsley & Johnson [91]	Air	alumina, glass, dowex-granules, spheres	0.045 - 0.3	—	0.4 - 0.47 (static)	1 - 40	0.7 - 0.76	$Nu_p = 0.0028\ Re_p^{1.7}\left(\frac{d_t}{d_p}\right)^{0.2}$
Fritz [101]	Air	silica alumina micro-spherical	0.006	11.43 - 120.7	—	1.2 - 13	0.7	$h = \frac{U_o}{116 + 52.4(L/D_t)} + \frac{1 - 0.6(L + D_t)}{274 + 447(L/D_t) + 146(L/D_t)^2}$

Table 3 (continued)

Author(s)	Fluid	Particle		Bed Characteristics		Re	Pr	Correlations
		Material & Shape	Size (cm)	Height (cm)	Void Fraction (ε)			
Heertjes & McKibbins [112]	Air	silica gel sphere	0.0299 - 0.1198	—	—	8.8 - 52.3	0.708	$h = 1.310\ Re^{0.76}$ $J_h = 95.7\ (D_p/Re^{0.24})$
Frantz [95]	Combustion gas	—	0.0225	—	—	1.3 - 2.8	0.65	$Nu = 0.018\ Re_p^{1.2}$
Rosenthal [96]	Air	gelatine cubes, cylinders, rings	0.8382 - 0.9906	7.62 deep settled	—	630 - 3200	0.68	$Nu = 0.00064\ Re^{1.48}$ or $J_h = 0.000719\ Re^{0.48}$
Richardson & Ayers [97]	Air	glass, lead, petunia seeds	0.011 - 0.067	1.016 (static)	0.5 - 0.64	0.53 - 34.4	0.72 - 0.76	$Nu = 0.054\ (Re/\varepsilon)^{1.28}$
Blickle & Nemeth [98]	Gas	—	—	—	—	30 - 10,000	0.7	$J_h = 5.7(Re/1-\varepsilon)^{-0.78}$ for $30 < Re/1-\varepsilon < 10^4$ $J_h = 1.77\ (Re/1-\varepsilon)^{-0.44}$ for $(Re/1-\varepsilon) < 30$
Donnadieu [99]	Air	granules	0.043	43.43	0.39	6 - 25	0 - 72	$J_h = 0.0097\ Re^{1.3}$ $J_h = 0.0449\ Re^{0.637}$

Table 3 (continued)

Author(s)	Fluid	Particle		Bed Characteristics		Re	Pr	Correlation
		Material & Shape	Size (cm)	Height (cm)	Void Fraction (ε)			
Ruckenstein & Teoreanu [100]	—	—	—	—	—	—	—	$Nu = 0.426\ Re^{0.30}\ Ar^{0.17}\ Pr^{1/3}$; for $Re\ Ar^{-0.4} < 2.15$ $Nu = 0.943\ Re^{-1.0}\ Ar^{0.69}\ Pr^{1/3}$; for $ReAr^{-0.4} > 2.15$
Sunkoori & Kaparthi [93]	Water	quartz, granite granules	0.054 - 0.11	20.32 - 45.72	0.68 - 0.885	12 - 42	5.93	$Nu = 0.00381\ Re^{2.1}$
Yeh [102]	—	sphere, Raschig rings, berl saddles	—	—	—	0.2 - 5000	—	$Nu = 1.91 \times 10^{0.04}\ RePr^{1/3}$; $10 > Re$ $Nu = 0.8\ Re^{0.65}\ Pr^{1/3}$; $Re > 50$
Holman et al. [103]	Water	steel, lead spheres	0.1587 - 0.4762	58.42	0.50 - 0.85	6 - 70	1.9 - 4.4	$Nu = 3.07 \times 10^{-6}\ (ReF_\varepsilon)^2\ Pr^{1.5}\ (D_t/D_p)^{0.5} \times (\rho_f/\rho_p)^2$
Moore	Water	steel, lead spheres	—	—	—	—	5.0	$Nu = C(Re\ F_\varepsilon)^a\ Pr^b (D_t/D_p)^{0.5}\ (\rho_f/\rho_s)^d$
Solntsev et al. [105]	Air	basalt, silica-gel activated carbon granular	0.2032 - 0.6096; 0.4318, 0.3048	3.048 - 12.7	0.5	380 - 3500	0.71	$St = 0.095\ Re^{-0.13}$

Table 3 (continued)

Author(s)	Fluid	Particle		Bed Characteristics		Re	Pr	Correlations
		Material & Shape	Size (cm)	Height (cm)	Void Fraction (ε)			
Fujishige [106]	Air	quartz, cinder, pyrite coke, resin granular	—	—	—	—	0.7	$Nu = 2.90 \times 10^{-2}\ \phi Re^{0.945}(u/U_{mf})^{-0.223}$ ϕ = function of particle shape
Holman et al. [114]	Water	steel, lead spheres	—	—	—	240 - 14,000	5.9	$Nu = 1.28 \times 10^{-5}(ReF_{\varepsilon})^{2.0}\ Pr^{0.67}$ $(D_t/D_p)^{0.5} \times (\rho_f/\rho_p)^{2.0}(\mu/\mu_o)^{0.82}$
Lindin & Kazakova [107]	Air	polymer, slag, corundum sphere, granules	0.04-0.2	—	—	5 - 450	0.7	$Nu = 0.01\ (Re/\varepsilon)^{1.4}$; $5 \leq Re \leq 120$ $Nu = 0.18\ (Re/\varepsilon)^{0.85}$; $120 \leq Re \leq 450$
Vasanova & Syromyankikov [108]	Air	—	—	—	—	80 - 500	—	$Nu = 0.001185\ Re^{1.6}$
Chang & Wen [109]	Air	aluminum steel, brass spheres	0.4762 - 0.635	—	0.425 - 0.879	580 - 5000	0.7	$J_h = 0.097\ (Re/1-\varepsilon)^{-0.502}\ Ar^{0.198}$
Petrovic & Thodos [110]	Air	celite sphere	0.1831 - 0.3086	—	0.426 - 0.753	100 - 1000	0.72	$J_h = 1.12\ Re^{-0.363}$

Table 3 (continued)

Author(s)	Fluid	Particle		Bed Characteristics		Re	Pr	Correlation
		Material & Shape	Size (cm)	Height (cm)	Void Fraction (ε)			
Kato & Wen [89]	Gases	—	—	—	—	0.1 - 1000	0.7	$Nu = 1.05\ Pr^{1/3}\ [Re(D_p/L)^{0.6}]^{1.1}$; $0.1 \leq Re(D_p/L)^{0.6} \leq 2.5$ $Nu = 1.5\ Pr^{1/3}\ [Re(D_p/L)^{0.6}]^{0.63}$; $2.5 \leq Re(D_p/L)^{0.6} \leq 1.03$
Frantz [94]	Air	salt granules	0.0225	15.24 - 27.94	—	1.3 - 2.8	0.65	$Nu = 0.016\ Re^{1.3}\ Pr^{0.67}$; for apparent heat transfer coefficient.

In summary, the turbulent motion and rapid circulation rate of the solid particles within the fluid stream and the high heat capacity of the solids which deters rapid temperature changes, fluidized beds tend to have uniform temperature profile throughout the system.

For correlating particle-to-fluid heat transfer coefficient, investigators have applied the technique of dimensional analysis relating all the variables affecting particle-to-fluid heat transfer, however, there is no one single correlation that can be used to cover all range of variables and conditions.

Finally, channelling and the overlap of the thermal boundary layers may have resulted in the low values of Nusselt numbers measured at the low range of Reynolds number.

CHAPTER 5
HYDRODYNAMICS AND FLUID FLOW CHARACTERISTICS OF A DEGRADED REACTOR CORE

5.1 Physical Model

The postulated damaged core configuration and the assumptions made regarding the assessment are given below. The TMI reactor core parameters given in Table 4 will be used for this analysis. A schematic representation of the reactor core is shown in Fig. 12.

Further, two cases are studied. The first assumes part of the fuel rods (of initial length Li= 0.523 m) that is standing between the first and second grids to have suffered the damage. The collapsed core in the form of spherical or nearly spherical particles is then settled on the second grid to a height L_B. All fuel rods below this grid remain in their intact geometry. Depending on the extent of the damage, there may exist a portion of the fuel rods above the second grid in its intact geometry so that particles may fill the flow area forming a debris bed that may extend to a height determined by the spacing between the fuel rods and the amount of collapsed fuel. There may also exist a configuration where the debris filling the flow area extends only to a small height above which the core may still have the channel geometry. Another configuration exists in which the debris bed occupies the entire cross sectional area of the core.

The second case assumes that any damage to the initial fuel rods, length L_o, will fall on the bottom spacer grid forming a debris bed above this grid. The bed configurations may be looked at in a similar fashion as discussed in the first case.

TABLE 4

TMI Core Parameters

Total heat generating rate Q MW (th)	=	2,452
Core volumetric heat generation rate q''' (MW/m3)	=	79.6
Core mass flow rate at full power in (Kg/sec)	=	16,546
Core active height L_o (m)	=	3.66
Number of fuel rods per assembly	=	208
Number of fuel assemblies	=	177
Pitch spacing P (m)	=	0.218
Core equivalent diameter d_c (m)	=	3.28
Core flow area A_T (m^2)	=	4.436
Distance between spacer grids L_i(m)	=	0.5229

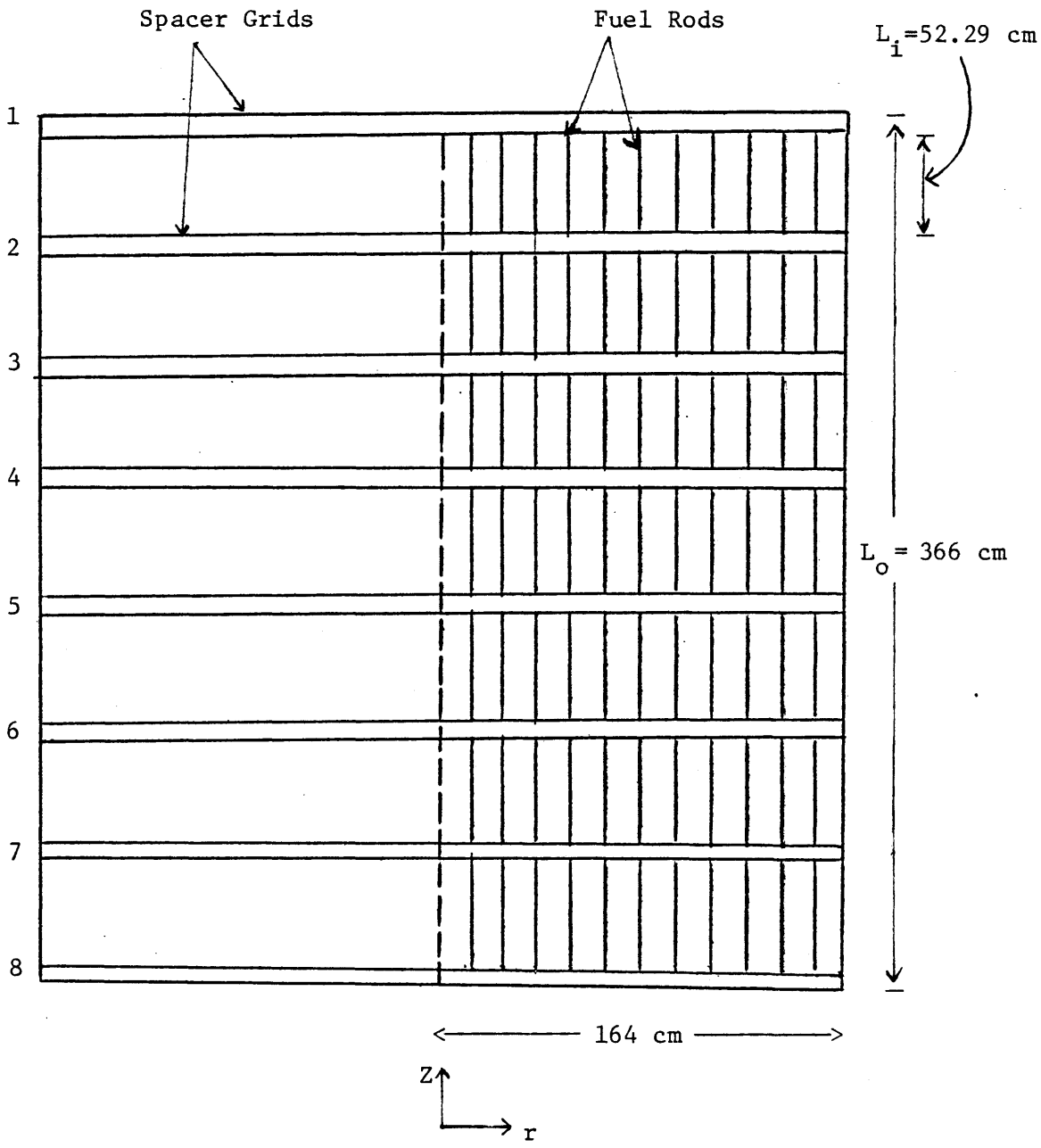

Figure 12: Reactor Core Schematic

The assumptions made in the analysis are:

1. The rubblized bed is assumed to behave as a heat generating porous medium. Heat is generated uniformly in the bed due to the decay of contained fission products.
2. Values of bed porosity , are assumed to take into account the inter-particle volume fraction as well as the interstitial voids that may exist within the fuel debris and formed by the presence of fission gases.
3. It is assumed that the inter-particle spacing is unifrom so that the flow encounters no local plugging or blockage, i.e., the debris has passages for the coolant to remove heat uniformly from the bed.
4. Analysis is restricted to single phase subcooled liquid flow with no phase change.
5. Reactor initially operating at 2,452 MW(t) full power.
6. The reactor system pressure has dropped to 1,000 psi following the accident.

Appendix A illustrates the above model and the determination of debris bed height above the spacer grid for the different configurations. Values of debris bed height that may form above the spacer grid for a specified fraction of the original length of fuel rods which suffered damage and fragmentation are listed in Tables 5 and 6 for the two cases respectively, taking the porosity ε to be 0.47. It can be seen, for example, that if half of the initial 0.523 m fuel rods length above the second grid fragmented, the debris bed will extend to a height equal to 0.31 m above this grid, the debris particles in this case will partially fill the flow area between the remaining intact part of the rods that suffered the damage; whereas, if the fuel rods above the second grid totally fragmented,

TABLE 5

Values of bed height L_B when the length L of an initial fuel rod length L_i remains intact, and debris bed formed on the second grid

L/L_i	L (m)	L_B (m)
1.00	0.522	0.000
0.90	0.470	0.071
0.80	0.418	0.141
0.70	0.366	0.212
0.60	0.313	0.283
0.57	0.300	0.300
0.50	0.261	0.310
0.40	0.209	0.322
0.30	0.157	0.334
0.20	0.104	0.347
0.10	0.052	0.359
0.00	0.000	0.371

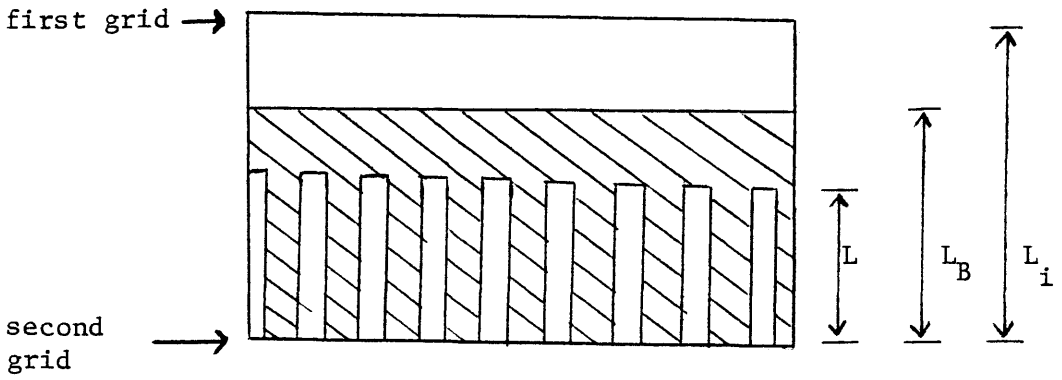

TABLE 6

Values of bed height L_B when the length L of an initial fuel rod length L_o remains intact, for the case where the debris settle on the core bottom grid

L/L_o	L (m)	L_B (m)
1.00	3.66	0.000
0.90	3.29	0.495
0.80	2.92	0.989
0.70	2.56	1.484
0.60	2.19	1.979
0.57	2.10	2.106
0.50	1.83	2.170
0.40	1.46	2.256
0.30	1.09	2.342
0.20	0.73	2.427
0.10	0.36	2.513
0.00	0.00	2.599

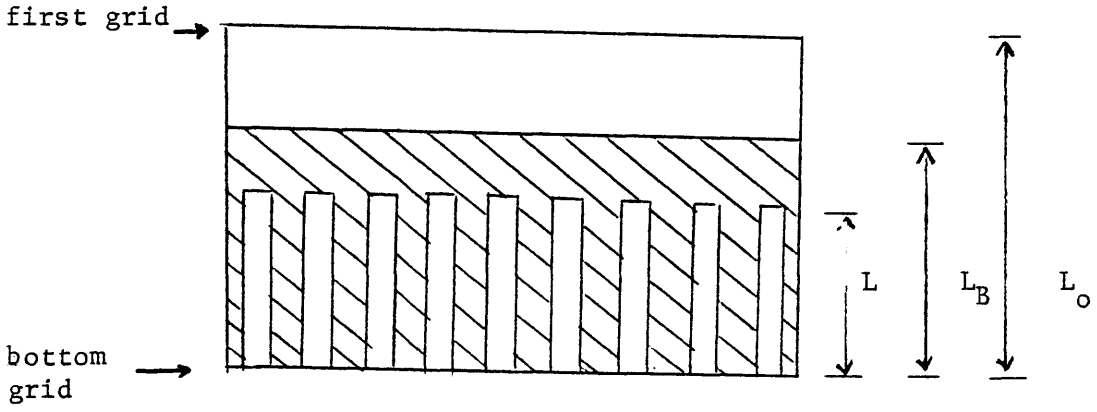

the debris bed is approximately equal to 0.37 m which occupies the entire cross sectional area of the core. Similarly if the fuel in the entire core fragmented, the debris bed height expected above the bottom grid is 2.6 m (occupying the entire cross section area of the core).

5.2 Analysis of Flow Through Core Rubblized Bed

Decay heat removal from debris bed is controlled by the rate of in-situ forced coolant flow. The higher the flow rate, the more heat can be removed and the less is the risk that further particles heat up and melt. However, as discussed earlier, an increase in fluid velocity beyond the minimum fluidization velocity will result in bed expansion, and at large fluid velocity either channelling or slugging and entrainment may take place, which is undesirable in a reactor environment.

Experiments have shown that particle to fluid heat transfer in particulate beds is much higher when the bed is in a state of fluidization than when it is in a fixed state. Thus, better heat transfer exists for fluid velocities of magnitude higher than the minimum fluidization velocity U_{mf}. However, to avoid the sweepout of small particles from the bed, the coolant velocity for fluidized bed should be kept somewhere between U_{mf} and particle terminal velocity U_t. This indicates the fact that the total pressure drop in the damaged core (pressure drop in the rubblized bed and intact fuel) be such that the superficial coolant velocity in the core is near the minimum fluidization velocity. Therefore, it is important to make some quantitative analysis to show the effect of the various physical parameters on the characteristics of debris bed.

5.3 Parametric Effect of Fluidization Characteristics

As mentioned before, the analysis here will assume that the rubblized bed has settled on the top of a spacer grid to a height represented by L_B and porosity ε and the particles have a size distribution with mean diameter $\overline{d}_p$ and mean sphericity $\overline{\phi}_s$. For spheres and broken solids, $\overline{\phi}_s$ is given as 1.0 and 0.63 respectively. These values have been used in the present calculations.

It is further assumed that the bed is in a state of incipient fluidization. Hence, the pressure drops across it may be obtained with the use of Eq. (3) and (9) at the minimum fluidization conditions given as

$$\left(\frac{\Delta P}{L_B}\right)_{mf} = 150 \frac{(1-\varepsilon_{mf})^2}{\varepsilon_{mf}^3} \frac{\mu U_{mf}}{(\overline{\phi}_s \overline{d}_p)^2} + 1.75 \frac{(1-\varepsilon_{mf})}{\varepsilon_{mf}^3} \rho_f \frac{U_{mf}^2}{\overline{\phi}_s \overline{d}_p} \qquad (3)$$

and

$$\left(\frac{\Delta P}{L_B}\right)_{mf} = (1-\varepsilon_{mf})(\rho_s - \rho_f) g \qquad (9)$$

Equation (15) is used to compute the minimum fluidization velocity U_{mf}, and, hence, Eqs. (3) and (9) to calculation $\left(\frac{\Delta P}{L_B}\right)_{mf}$ and ε_{mf}.

If $(L_B)_{mf}$ were to exceed the height of the rubblized bed L_B, the bed would expand further, the voidage "ε" and fluid velocity would increase.

and channelling would result. Otherwise, the pressure drop, ΔP, would not be enough to support the bed. Further, in the case of bed height less than $(L_B)_{mf}$, an unstable condition exists, and the flowing coolant would sweep the particles out, re-establishing a stable condition. Particle sweepout and entrainment velocity is calculated by using Eq. (22) in the appropriate range of Reynolds numbers.

5.3.1 Results and Discussion

The system variables as assumed and the calculated values of U_{mf}, ε_{mf}, and $\left(\frac{\Delta P}{L_B}\right)_{mf}$ are given in Table 7, along with the Reynolds number for each data set.

The first three data sets display the dependency of the bed porosity and $\left(\frac{\Delta P}{L_B}\right)_{mf}$ on the mean size of the particles of the bed, and emphasize that the porosity is not much sensitive to this parameter whereas the pressure drop slightly increases as the mean particle diameter decreases. Data sets 1, 4, and 5 illustrate the effect of ρ_s on bed porosity and $\left(\frac{\Delta P}{L_B}\right)_{mf}$ as ρ_s is changed from 6,551 to 10,956, representing materials typical of LWR core, the bed porosity remaining almost constant, while $\left(\frac{\Delta P}{L_B}\right)_{mf}$ increases from 32.99 to 58.38 Kpa. This is understandable because the bed height should certainly decrease as the density of the bed material increases to accommodate the same pressure drop.

Data set 1 and 6 together highlight the influence of bed temperature T on ε_{mf} and $\left(\frac{\Delta P}{L_B}\right)_{mf}$. Understandably, the bed porosity remains unaffected while $\left(\frac{\Delta P}{L_B}\right)_{mf}$ is influenced by a very small extent through the changes in fluid density and viscosity. Data set 1 and 7 illustrate the effect of

TABLE 7

Calculated values of $\left(\frac{\Delta P}{L_B}\right)_{mf}$ and ε_{mf} for particulate debris beds at various conditions. P = 1000 psi

Set Number	T(°C)	$\bar{d}_p$ (mm)	$\bar{\phi}_s$	$\rho_s \left(\frac{Kg}{m^3}\right)$	$\rho_f \left(\frac{Kg}{m^3}\right)$	μ(μpa•s)	$U_{mf} \left(\frac{m}{sec}\right)$	Re_{mf}	ε_{mf}	$\left(\frac{\Delta P}{L_B}\right)_{mf} \left(\frac{KPa}{m}\right)$
1	200	1.00	1.00	10956 (UO_2)	870	135	0.06309	406	0.409	58.38
2	200	0.10	1.00	10956	870	135	0.00426	2.75	0.384	60.95
3	200	10.00	1.00	10956	870	135	0.21489	13848	0.414	57.91
4	200	1.00	1.00	7977 (S•S)	870	135	0.05219	336	0.408	41.22
5	200	1.00	1.00	6551 (ZrO_2)	870	135	0.04616	297	0.408	32.99
6	250	1.00	1.00	10956	803	107	0.06679	501	0.409	58.70
7	200	1.00	0.63	10956	870	135	0.06309	406	0.484	51.01

the particle shape or the mean sphericity $\overline{\phi}_s$. The results show a slight increase in bed porosity as the value of $\overline{\phi}_s$ changes from 1 (spheres) to 0.63 (broken solids) while the pressure drop decreased from a value of 58.38 to 51.01 $\frac{Kpa}{m}$ respectively. Thus, in summary, the height of the bed is altered only if the density of the bed particles changes, Eq. (9) dominates with the bed porosity, ε_{mf}, varying minutely.

Figure 13 shows the minimum fluidization velocity as a function of particle mean diameter for the different reactor materials. The system pressure was taken to be 1,000 psi with coolant inlet temperature at 240 °C. The bed porosity was chosen to be $\varepsilon = 0.48$ and, for simplicity, the particles are assumed to be spherical, $\phi_s = 1$. It is apparent that because of their higher density, spherical particles of uranium dioxide of a given diameter will fluidize at a relatively higher coolant velocity than stainless steel or zirconium dioxide particles of the same diameter. Therefore, to ensure that no particles be entrained in the flow stream, the pressure drop across the bed should be such that the superficial fluid velocity is less than the terminal free velocity of the smallest possible debris.

The coolant superficial velocity required to ensure adequate particle coolability may result in debris fluidization and possible sweepout. The minimum superficial velocity that results in a specified temperature rise across debris bed is plotted against the various decay power levels in Figs. 14 through 16 for bed temperature rise of 10, 20, and 50 °C respectively. The graphs also indicate the corresponding fluidization and sweepout diameters calculated by using Eqs. (11) and (22). Again, for simplicity, the particles assumed to be spherical, i.e., having spherical surface

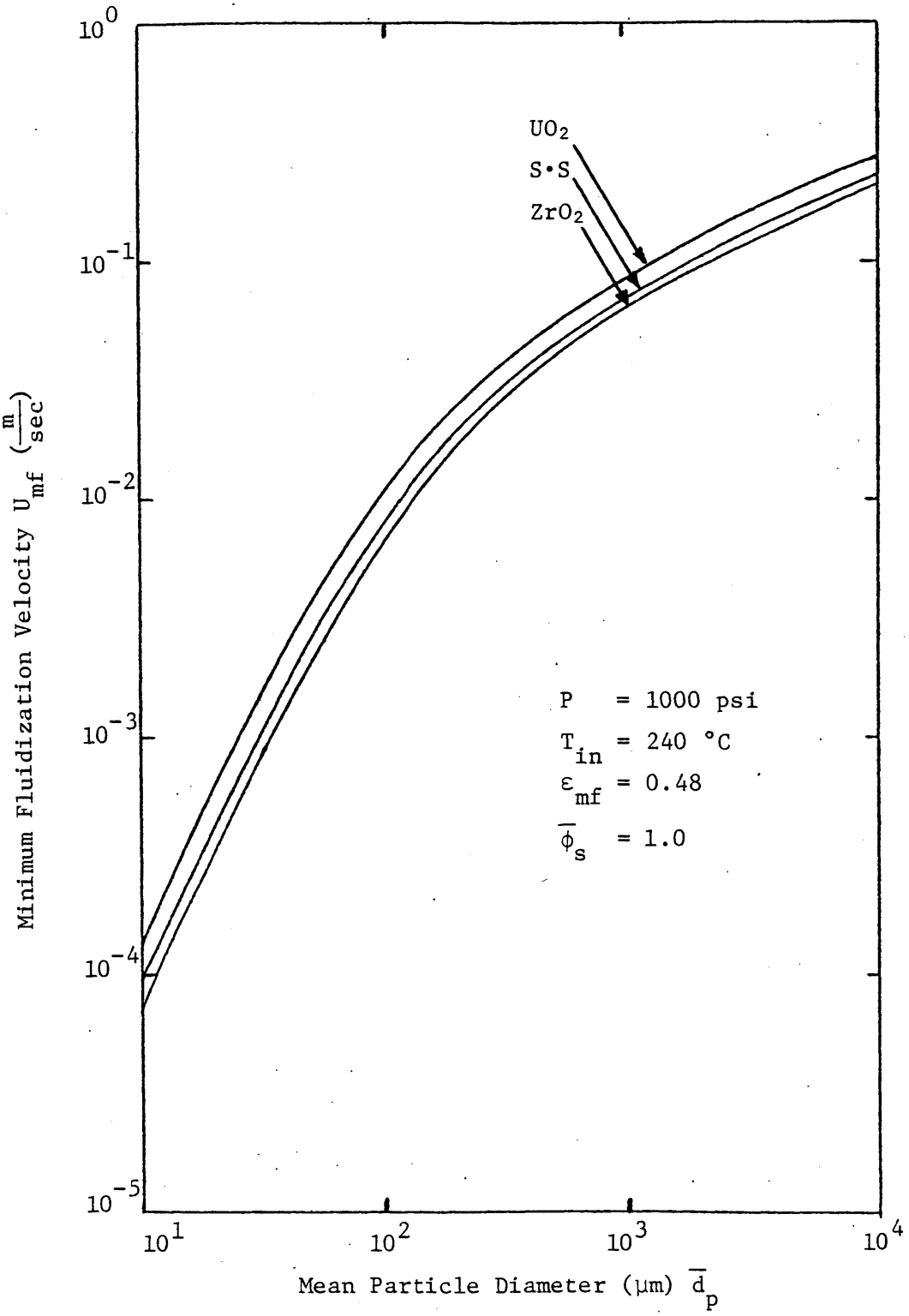

Figure 13: Minimum Fluidization Velocity as a Function of Particle Diameter and for Various Reactor Materials.

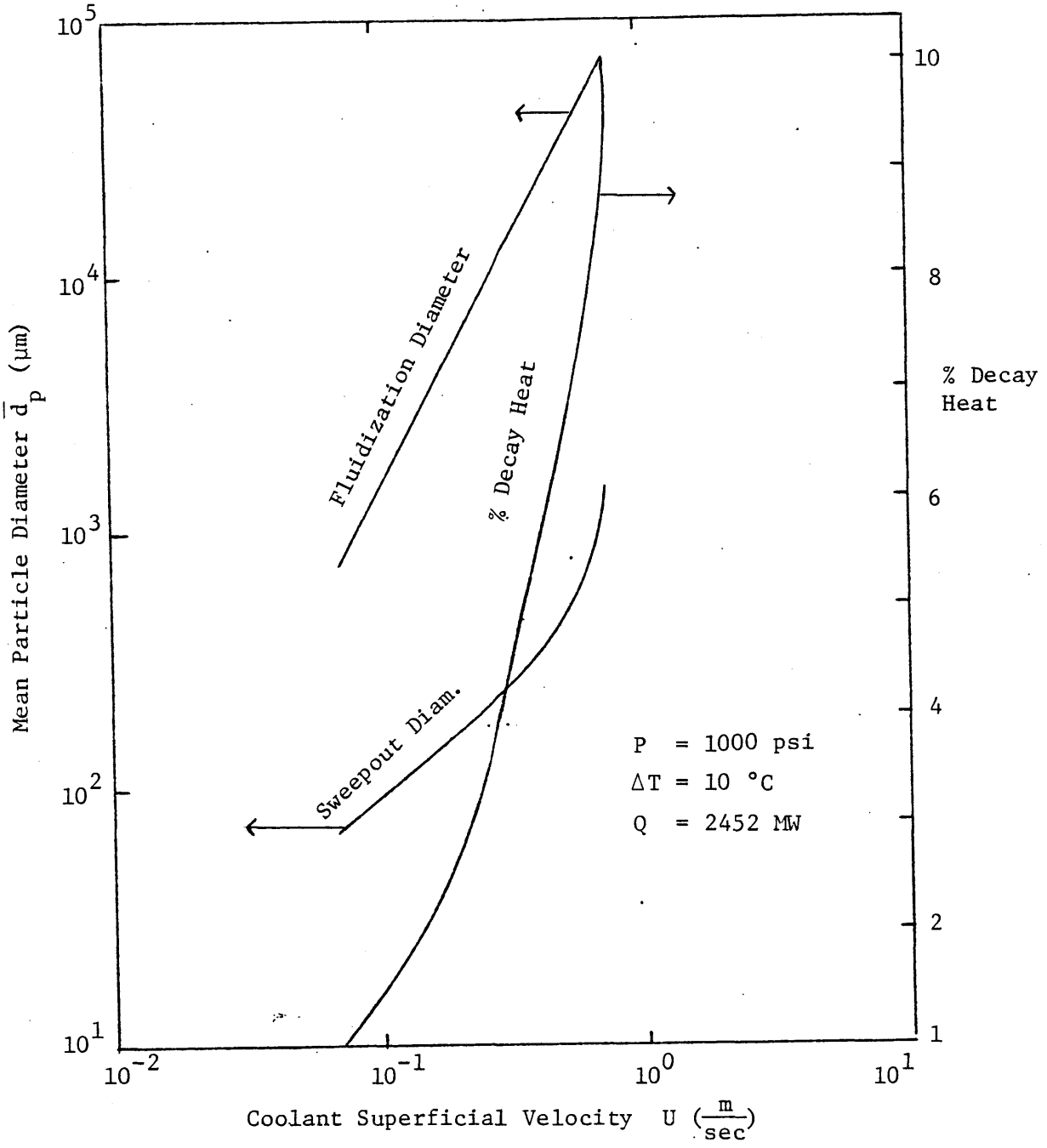

Figure 14: Fluidization and Sweepout Particle Diameter as a Function of Single Phase Coolant Superficial Velocity

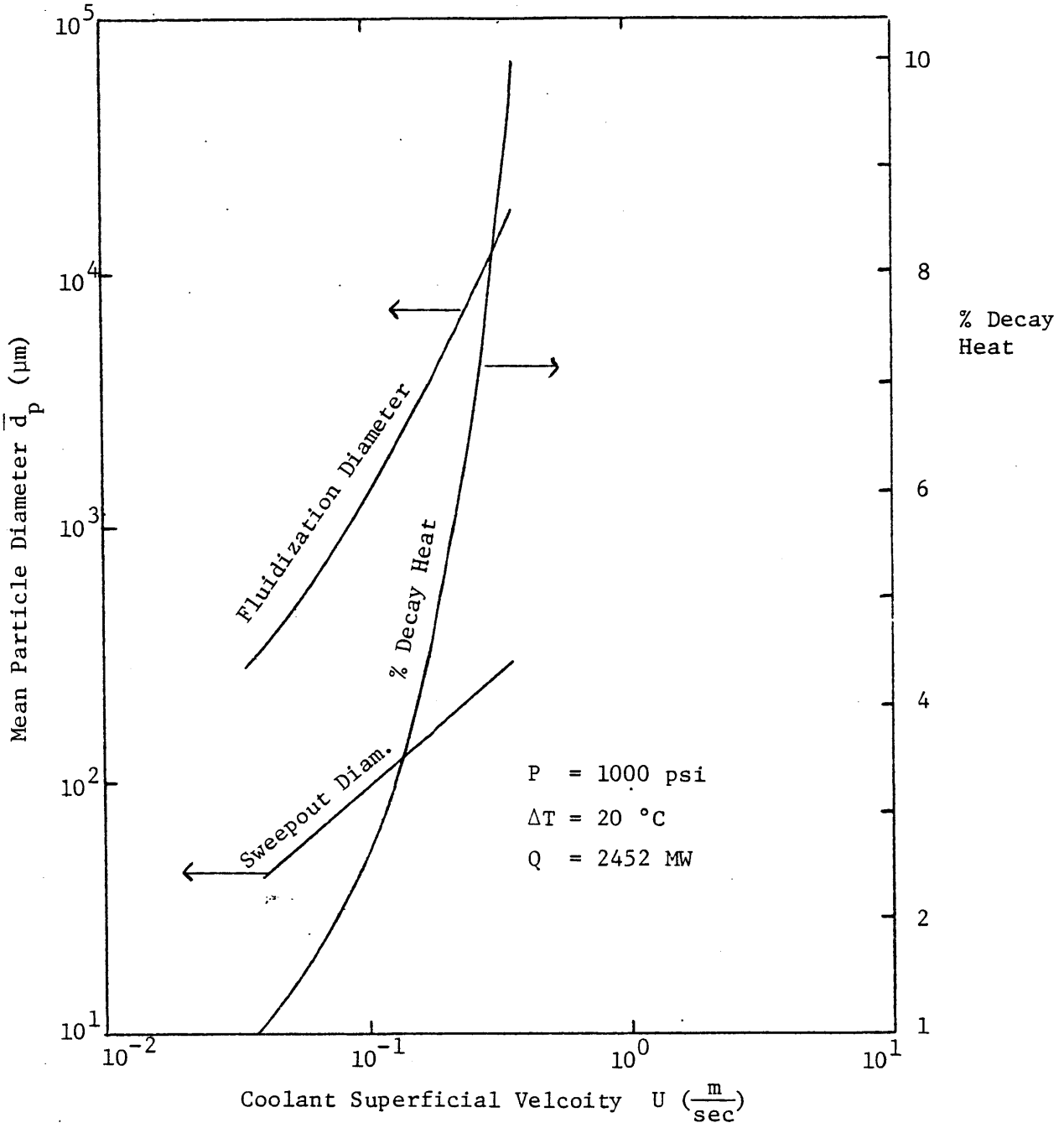

Figure 15: Fluidization and Sweepout Particle Diameter as a Function of Single Phase Coolant Superficial Velocity

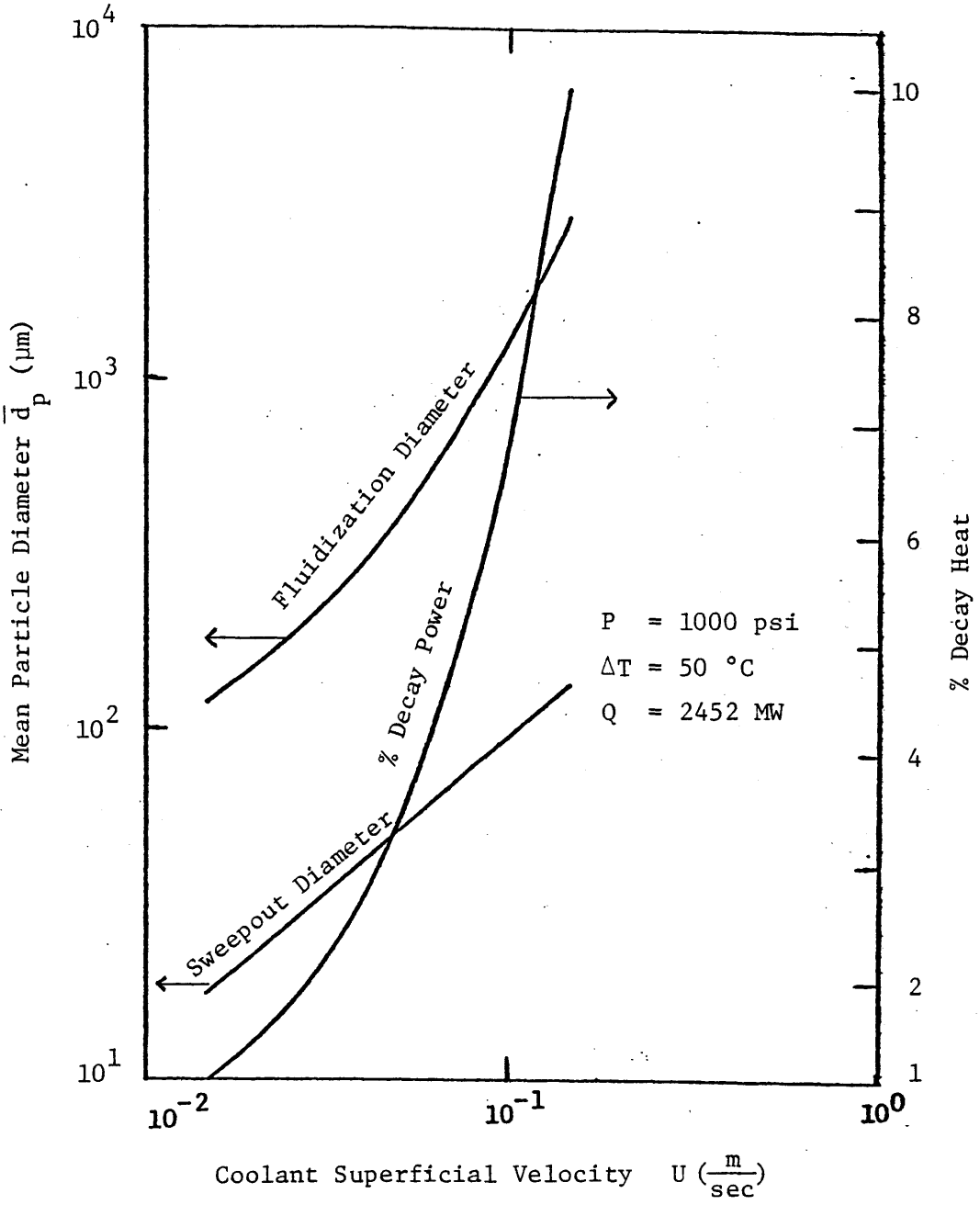

Figure 16: Fluidization and Sweepout Particle Diameter as a Function of Single Phase Coolant Superficial Velocity

$\phi_s = 1$ and the initial power level was taken to be 2,452 MW (typical of TMI reactor core).

From the plots one can determine the range of mass flow rate through the bed which result in adequate coolability and at the same time ensures that none of the smallest particles expected in the core are swept out by the flow. For example, if the decay heat is about 2% of the initial total power, the mass flow rate that results in 50 °C temperature rise across the bed is 204.3 kg/sec which corresponds to coolant superficial velocity of 0.0301 m/sec. At such velocity particles of diameter of the order of 220 μm will be fluidized whereas particles with a diameter smaller than 32 μm will be swept out by the flow.

In summary, depending on the temperature rise across the bed, the implication is that the potential for sweepout of particles with a diameter larger than 20- 100 μm is small when ΔT is of the order of 50 °C. Even fluidization appears to occur only for particle diameters less than 3 mm. For water coolant temperature rise of 10 °C sweepout of particles of diameter of the order of 1 mm may occur if the required decay heat removal is about 10% of the total initial power.

5.4 Pressure Drop in Degraded Core

It is important to determine the magnitude of the pressure drop within the damaged core in order to obtain an estimate for the required pumping power. However, because of the complexity of the postulated core configuration after the accident together with the uncertainties concerning the particle characteristics such as shape, dimensions, and distributions only a gross estimate of the pressure drop will be given here that is based on the proposed model and the assumptions given earlier.

It should also be noted that the debris bed has been assumed to behave like a porous media with uniform porosity ε, and that the core does not have blocked parts that prevent the flow. Also, the pressure drop due to abrubt changes in flow area and flow restrictions have been neglected.

The pressure drop per unit height of the bed has been plotted as a function of the fluid superficial velocity in Fig. 17 for uranium dioxide particles having density equal to 95% of the theoretical density and mean diameters of 0.1, 1, and 10 mm. The Ergun formula, Eq. (3) was used in the fixed bed region with porosity equal to ε=0.48, the particles assumed to be spherical (ϕ_s=1). As expected, the smaller the particle diameter, the higher is the pressure drop per unit bed height at a given water coolant superficial velocity. For superficial velocity of 10^{-2} m/sec, the pressure drop is four orders of magnitude and ten orders of magnitude greater when the debris bed mean particle diameter is 0.1 mm than when it is 1 mm and 1 cm respectively. Therefore, particle diameters play a significant role in determining an effective coolable geometry.

The effect of porosity (ε) on pressure drop evaluation is shown in Fig. 18, where ΔP per unit bed height is plotted as a function of coolant superficial velocity for various bed porosities, taking the particles mean

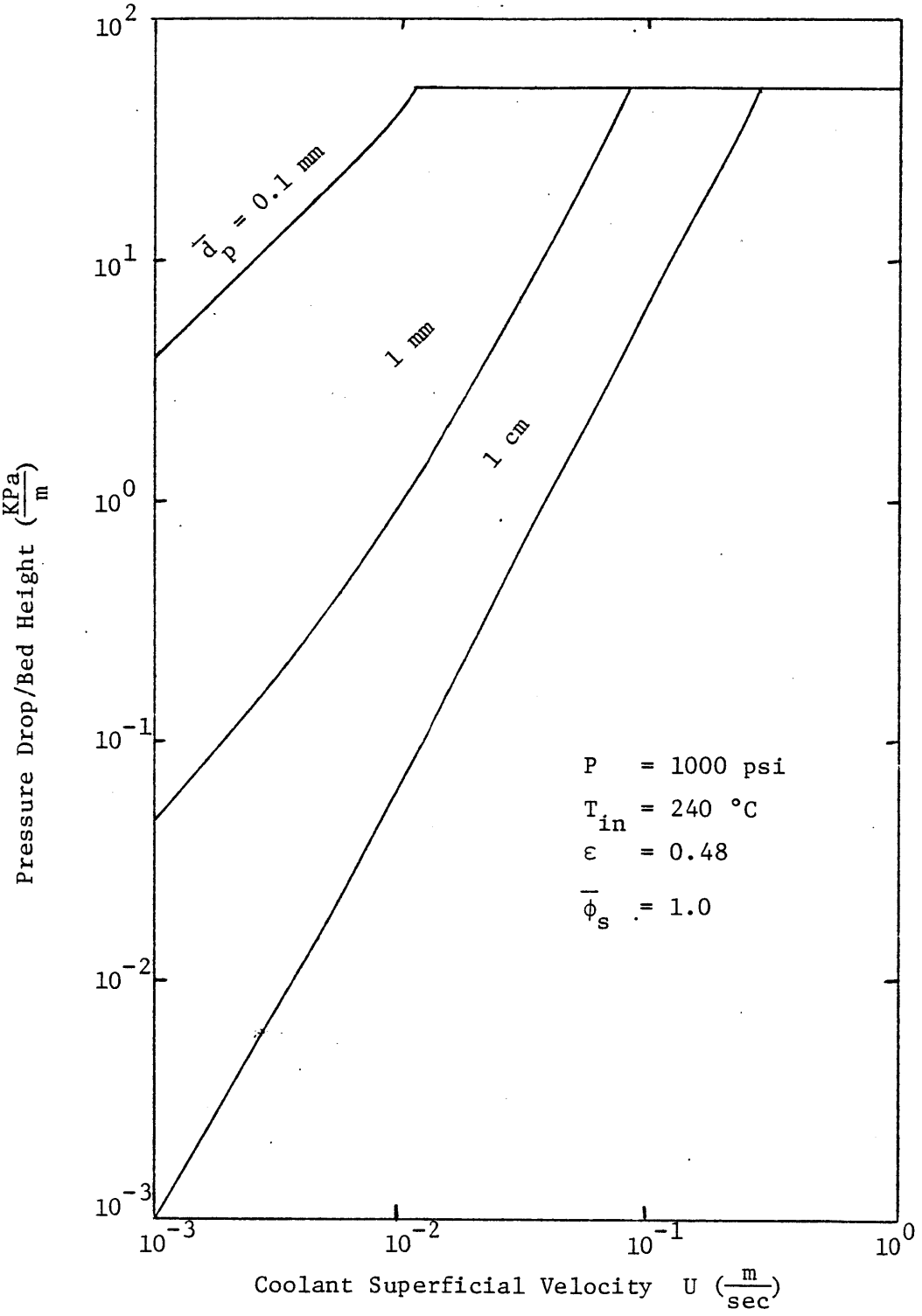

Figure 17: Pressure Drop Per Unit of Initial Debris Bed Height as a Function of Coolant Superficial Velocity

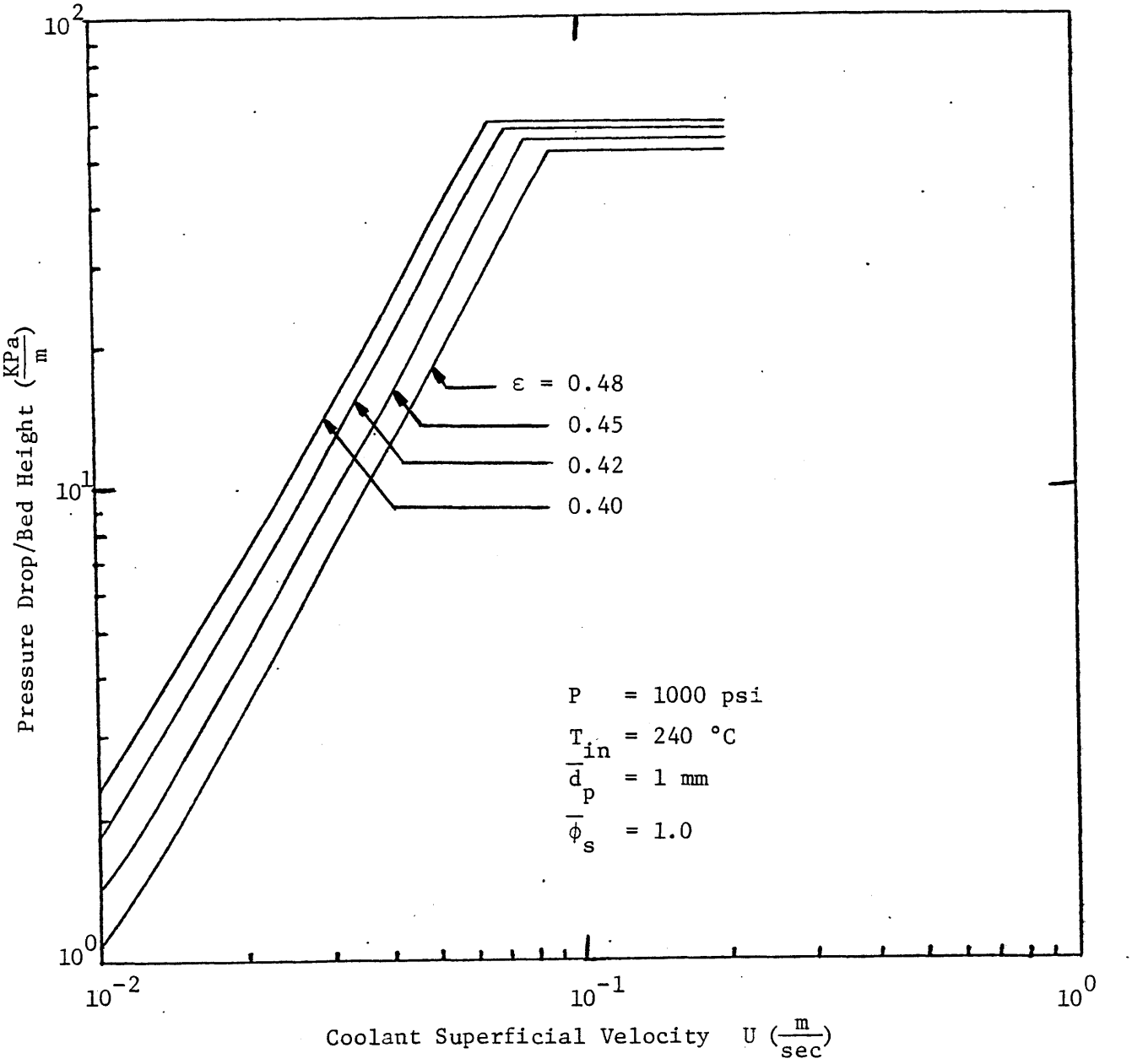

Figure 18: Pressure Drop Per Unit of Initial Debris Bed Height as a Function of Coolant Superficial Velocity and Porosity

diameter to be 1 mm. The variation in porosity also influences the magnitude of pressure drop to some extent. The pressure drop increases as the value of ε decreases for a given superficial velocity; almost two times greater for beds with porosity equal to 0.40 than when it is 0.48.

The relative variation of ΔP caused by a relative variation in the value of ε is discussed in Appendix A.2. It is found that for $\varepsilon = 0.45$, a positive relative variation of ε causes a negative relative variation in the pressure drop which is about five times larger. For example, if one assumes a porosity of 0.46 instead of 0.45, ΔP is then subjected to a change of about -10%.

The total pressure drop in the core is also calculated for the two cases considered; i.e., for the case where all the fuel above the second grid collapsed on the second grid in the form of particulate debris bed of a height equal to 0.37 m. The fuel rods below this grid remained in the intact geometry. The second case involves the total core being disrupted and settled on the bottom spacer grid to form a bed of a height equal to 2.6 m.

The total pressure drop is shown in Fig. 19 as a function of superficial velocity; also shown in the figure are the corresponding pressure drop values of the core in its initial undamaged geometry. In the first case the pressure drop is calculated as the sum of the pressure drop in the debris bed piled on the second grid plus that in the remaining intact fuel rods below the second grid; however, the latter seems to be negligible in magnitude in comparison to the former.

If the temperature rise across the entire core is to be 20 °C the minimum water coolant superficial velocity required to remove a decay heat of the order of 2% of the initial total power is 7.5×10^{-2} m/sec.

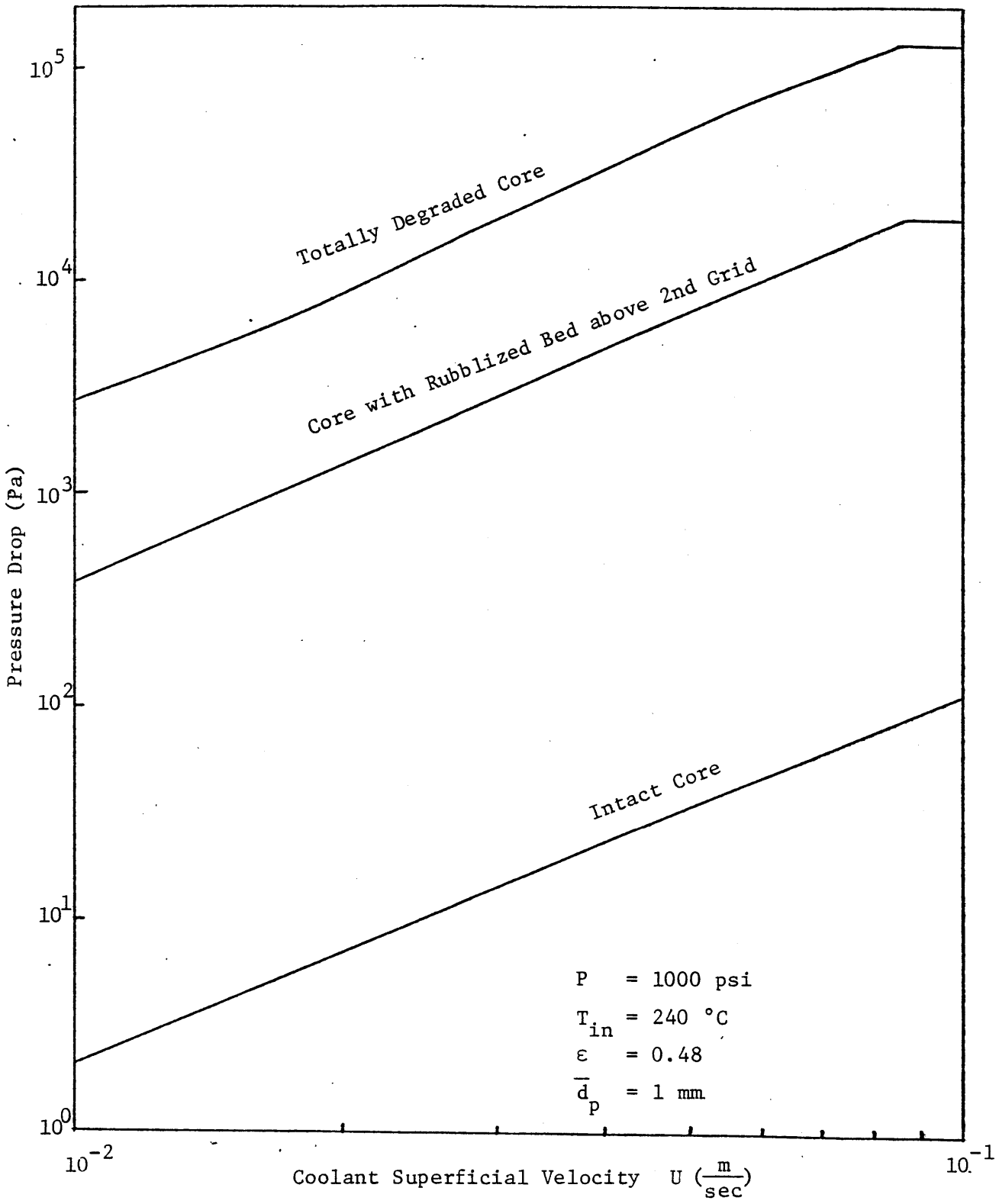

Figure 19: Pressure Drop as a Function of Coolant Superficial Velocity for Core with Intact Fuel Rods, Partially Degraded and Totally Degraded Core

At such velocity the total pressure drop in the initial intact core is only 70 pa whereas in a totally degraded core that consists of spherical particles of mean diameter equal to 1 mm it is about 110 Kpa, which corresponds to almost 14 m of water pressure head. For the case where the rubblized bed settles on the second grid to a height of 0.37 m the total pressure head required is 1.9 m. Therefore, in the cases of totally disrupted core high pumping power is rquired to assure adequate collability of the particles.

Again, for the two cases, the total pressure drop in the core is plotted as a function of the ratio of the particulate debris bed height L_B to the corresponding initial fuel rod length before it suffers the damage, L_i and L_o and for different coolant temperature rise ΔT. The core decay heat level is 2% of the initial total power. The values of L_i and L_o are 0.523 and 3.66 m corrseponding to the initial fuel rod length above the second grid and the full fuel rod length respectively. Values of debris bed height L_B (given in Tables 5 and 6) are calculated using Eqs. (2) and (5) from Appendix A and TMI core parameters of Table 4; the plots are shown in Figs. 20 and 21. It should be noted that, in calculating the pressure drops, particles having mean diameter $\overline{d}_p$ equal to 3 mm and mean specific surface $\overline{\phi}_s$ of 0.63 (value for broken glass) were chosen.

From the plots, it is seen that the total pressure drop in the core varies exponentially with the height of the debris pile as long as a constant cooling temperature rise is maintained. High values of pressure drop are observed as a result of the assumption that the particles are non-spherical with specific surface $\phi_s = 0.63$. For instance, in a totally disrupted core that has spherical particles with diameter equal to 3 mm, a water coolant flow that is capable of removing decay power equal to 2% of

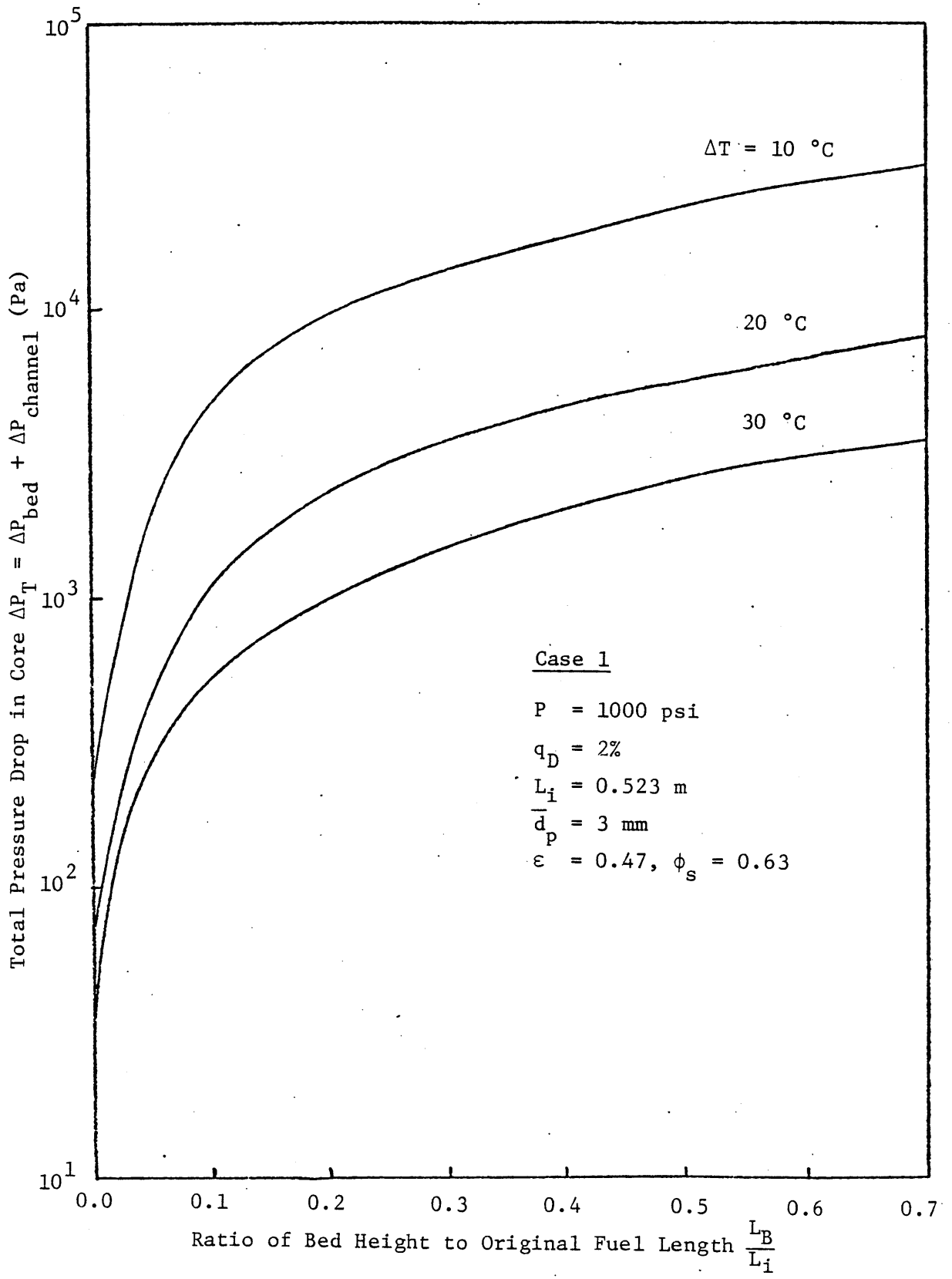

Figure 20: Total Pressure Drop in the Degraded Core as a Function of the Ratio of Particulate Bed Height to the Corresponding Intact Fuel Rod Length, Case 1

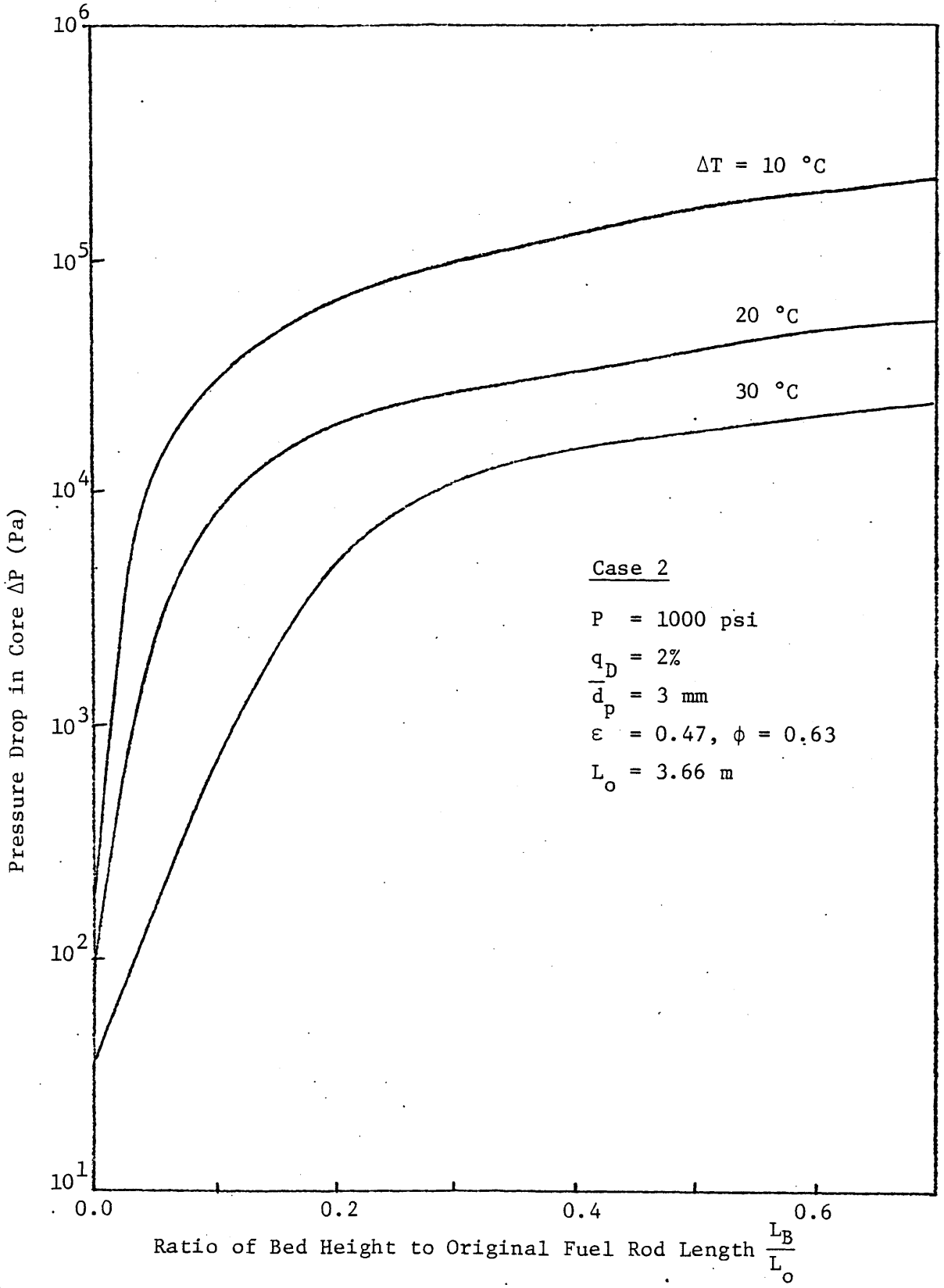

Figure 21: Pressure Drop in the Degraded Core as a Function of the Ratio of Bed Height to Original Fuel Rod Length, Case 2

the total initial power with 20 °C temperature rise will result in a pressure drop equal to 35 Kpa, where from Fig. 21 it can be seen that for similar conditions but for particles having specific surface equal to 0.63 the total pressure drop is 56 Kpa which is larger by a factor of 1.6.

It is also important to observe the variation of the mass flow rate in the core with the amount of debris present for a given core pressure drop. In Fig. 22 the percentage ratio of the mass flow rate $\dot{m}$ in the damaged core to that of the intact core $\dot{m}_o$ is plotted as a function of the ratio of debris bed height to the initial fuel rod length, for the case where all the debris particles settled on the bottom grid (case 2). The applied pressure drop was 50 Kpa which gave an initial mass flow rate $\dot{m}_o$ in the undegraded core of 22,000 Kg/sec; particle diameter was also a variable. It is clear that the higher the debris bed the lower is the mass flow rate. Moreover, the smaller the particle diameter the more resistance that is offered to the flow and hence the mass flow rate decreases further.

At bed heights up to approximately 0.5 m (L_B/L_o equal to 0.14) the mass velocity through a rubblized core, having particles with mean diameter $\overline{d}_p$ = 1 mm, is found equal in magnitude to the case when the bed consists of particles having $\overline{d}_p$ = 3 mm. This is because the pressure drop available is high enough to fluidize the particles and at such a state the total pressure drop depends on the particle density but does not depend on the particle diameter. Beyond $L_B/L_o = 0.14$ the pressure drop available is not enough to fluidize the particles with the result that the bed transfers to a fixed state and the pressure drop then depends on the particle diameter as described by the Ergun equation, Eq. (3).

In conclusion, relatively high pressure drops are required to cool a totally disrupted core. However, the magnitude of the pressure drop depends

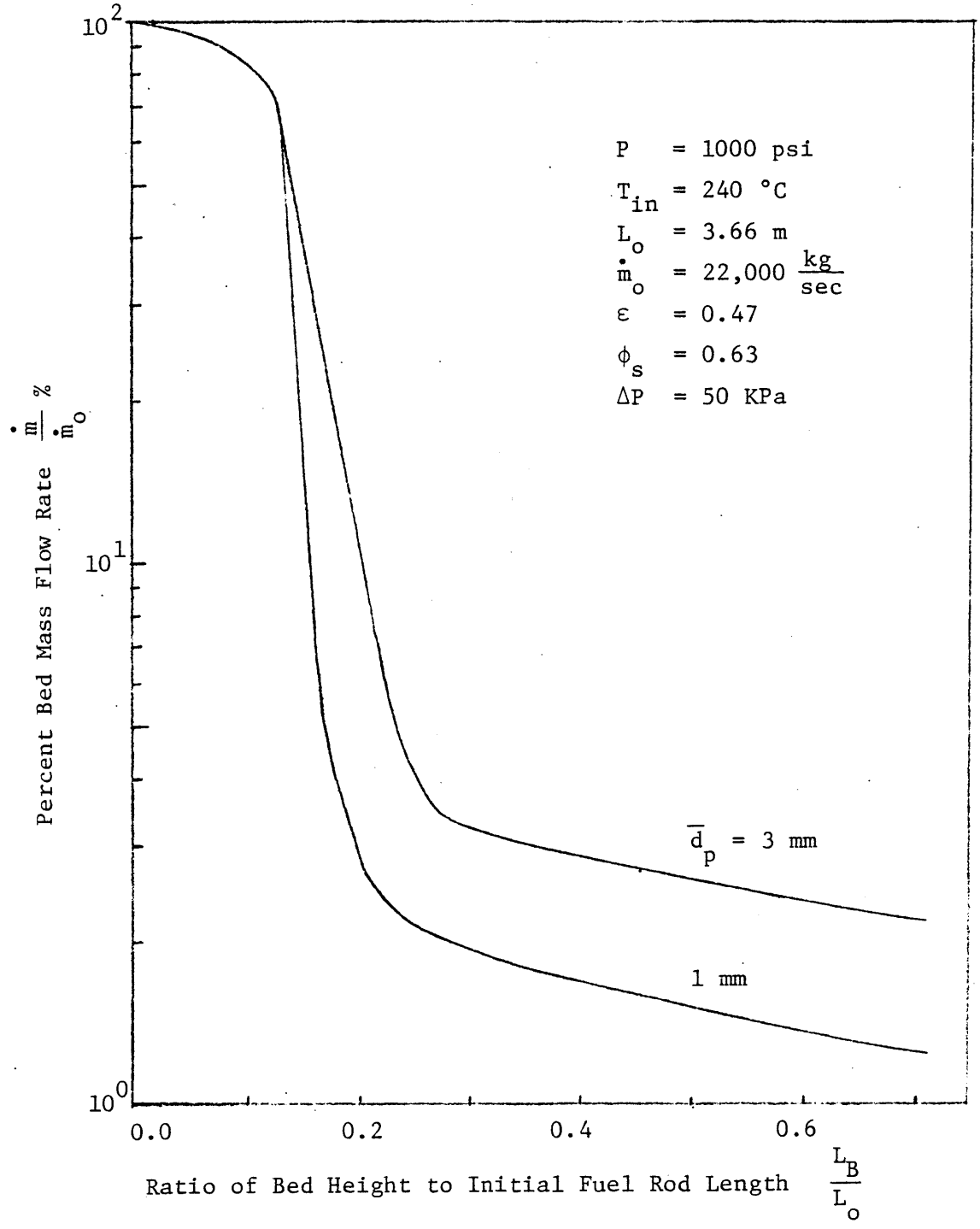

Figure 22: Percentage Ratio of Mass Flow Rate in Degraded Core to Initial Core Flow Rate, $\dot{m}_o$, as a Function of the Ratio of Bed Height to Initial Fuel Rod Length, Case 2

to a large extent on bed characteristics such as bed height, particle diameter and shape and to a lesser extent on bed porosity. It is important to realize that for a given pressure drop the coolant mass flow rate decreases with an increase in bed height. The result being that at a certain height boiling may occur, and depending on the heat flux undercooling conditions may be reached.

CHAPTER 6
ASSESSMENT OF DEGRADED CORE COOLING

6.1 Analysis of One Dimensional Heat Removal in Particulate Beds

For the determination of coolable particle bed heights the momentum equation and the energy equation for coolant temperature distribution inside the particle bed have to be solved. The hydrodynamic characteristics of particulate bed and the determination of pressure drops have been discussed in Chapter 5 through the use of the Ergun equation, Eq. (3) and the concept of fluidization. For heat transfer calculations two cases are considered.

(1) A lumped mass approach: For this case the coolant temperature at the exit of the bed T_{out} can be calculated by using an energy balance between the solid particles and the fluid.

$$A_B \times L_B \times q_b''' = \dot{m}_B C_p \, (T_{out} - T_{in}) \tag{55}$$

where q''' is the bed volumetric heat generation rate given by

$$q_b''' = \frac{V_o}{V_B} \, q_o''' \, , \tag{56}$$

where q_o''' , V_o and V_B are the initial core power density, initial core volume before the damage and the corresponding volume of the degraded core.

q_b''' can therefore be written as

$$q_b''' = \frac{V_o}{V_B} \, q_o''' = \frac{D_c^2(1-\varepsilon)}{N_f d_f^2} \, q_o''' \tag{57}$$

where D_c, d_f and N_f are the core diameter, fuel rod diameter and total number of fuel rods respectively. Using Eqs. (55) and (57), the core volumetric heat generating rate q_o''' can be calculated such that the coolant exit temperature equals the boiling point of the water coolant which is taken as 284 °C at 1000 Psi in the present calculation.

(ii) A one-dimensional approach: A one-dimensional porous bed of porosity ε is considered. The coolant enters at $z = 0$ at temperature T_{fo}, and leaves at $x = L_B$ and temperature T_{fL_B}. The energy is generated in the bed at uniform volumetric rate q_b'''. The solid phase transfers all the energy generated to the fluid, while the latter is flowing through. The governing differential equations, in the steady state, assuming constant properties are:

$$K_f\varepsilon \frac{d^2T_f}{dz^2} - G\varepsilon C_p \frac{dT_f}{dz} - h\psi(T_f-T_s) = 0 \tag{58}$$

$$K_s(1-\varepsilon) \frac{d^2T_s}{dz^2} + h\psi(T_f-T_s) + q_b''' = 0 \tag{59}$$

Order of magnitude calculations have shown that the conduction terms are small in comparison to the other terms in both equations. Hence axial conduction is neglected and Eqs. (58) and (59) become

$$Gc_p \frac{dT_p}{dz} = h\Psi(T_s-T_f) = q_b''' \tag{60}$$

where G is the superficial mass velocity. Eq. (60) has the following solutions:

$$T_f(z) = T_{fo} + \frac{q_b'''}{GC_p} z \tag{61}$$

$$T_s(z) = T_{fo} + \left(\frac{z}{GC_p} + \frac{1}{h\psi}\right) q_b''' \tag{62}$$

Eqs. (61) and (62) represent the axial temperature distribution in the coolant and the solid particles respectively. The heat transfer coefficient h can be calculated by using particle fluid heat transfer correlations for fixed and fluidized particle beds in the approximate range of validity as given in Tables 2 and 3.

The rate of heat transfer to the coolant inside the particle bed may be written as

$$q_b = hA(T_s - T_f) = h(T_s - T_f)\ \psi L_B \left(\frac{\pi}{4} D_B^2\right) \tag{63}$$

where A is the total surface area of particles for heat transfer, L_B and D_B are bed height and diameter respectively, and ψ is particles' specific surface area given as

$$\psi = \frac{6(1-\varepsilon)}{d_p} \tag{64}$$

Eq. (63) will be used to compare the adequacy of various correlations of heat transfer coefficient with the experimental data of Peoples and Squarer [48] for flow in inductively heated particulate beds.

The heat flux exiting the top surface of the bed may also be written as

$$q_b''' = h \left[\frac{6(1-\varepsilon)}{d_p}\right] L_B \, (T_s - T_f) \qquad (65)$$

6.2 Results and Discussion

Calculation of particle coolability depends on the following parameters: inlet temperature T_{in}, decay heat production q_b''', driving pressure Δp, bed porosity ε, and effective particle diameter. Dependence on inlet temperature is small and not discussed here. The influence of other parameters are shown in Figures 23, 24 and 25. If one parameter is investigated all other parameters are fixed at values judged to be conservative.

Figure 23 shows the influence of decay heat production (% of initial power) on coolable particle bed height. Obviously, the higher the decay power density, the smaller is the bed height that can be cooled.

For bed height of 2.599 m which corresponds to a totally disrupted core (case 2), it can be seen that the bed may remain coolable up to a power density equivalent to 2.0% of the initial total power. For higher decay powers up to 10%, a considerable amount of fuel debris can still be cooled stationary. If the axis for the power density is changed into a time scale taking the transient decay heat development as a measure, it follows that a considerable amount of core debris can be cooled this way only if particle beds are established more than several minutes after neutronic shut down.

The effect of bed porosity is small; however, coolable bed heights increases with an increase in porosity.

The coolable bed heights vary, too, depending on the driving pressure difference for the coolant mass flow. It is clear that the larger

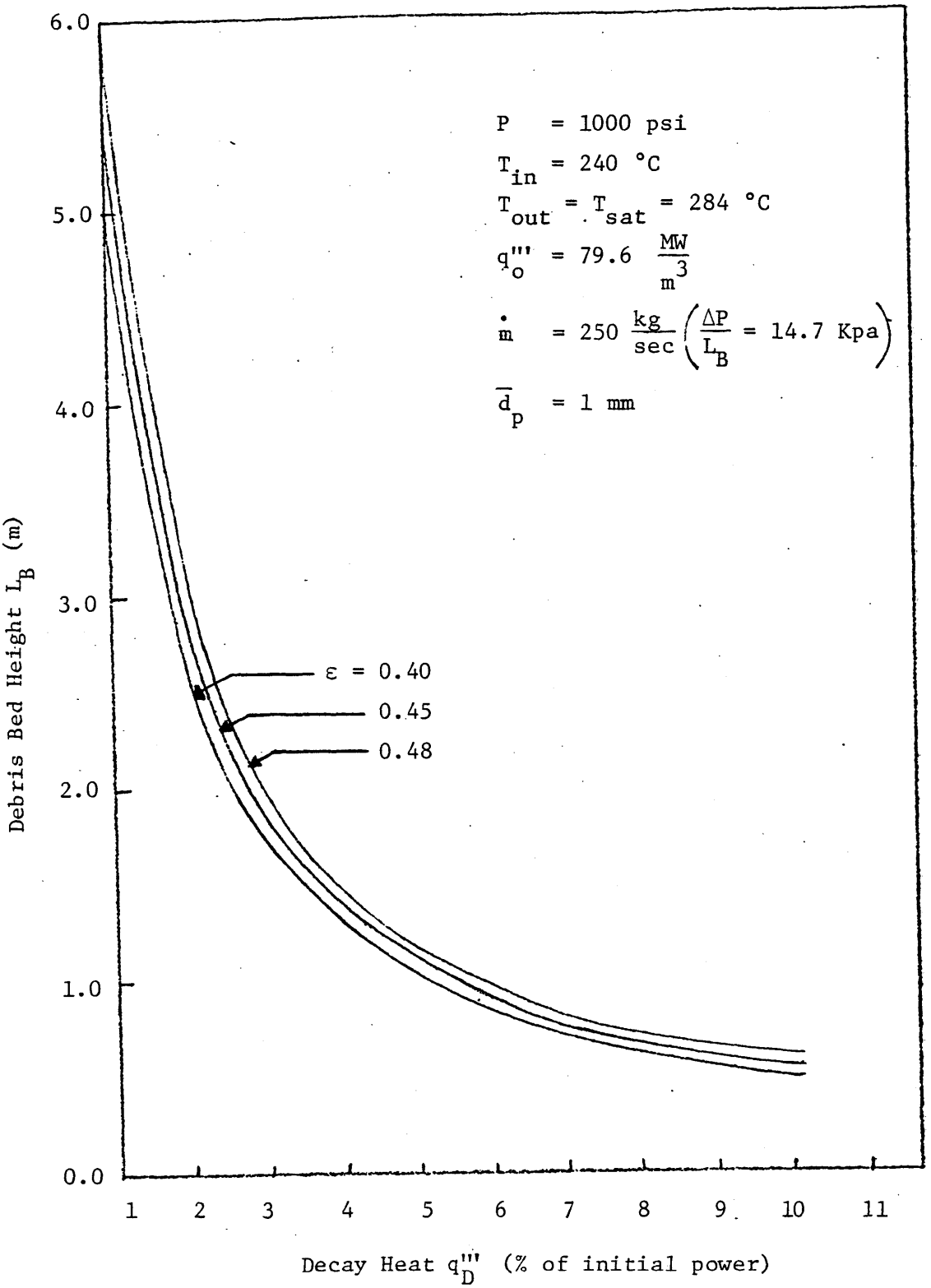

Figure 23: Coolable Particle Bed Heights Dependence on Decay Heat Production q'''_D

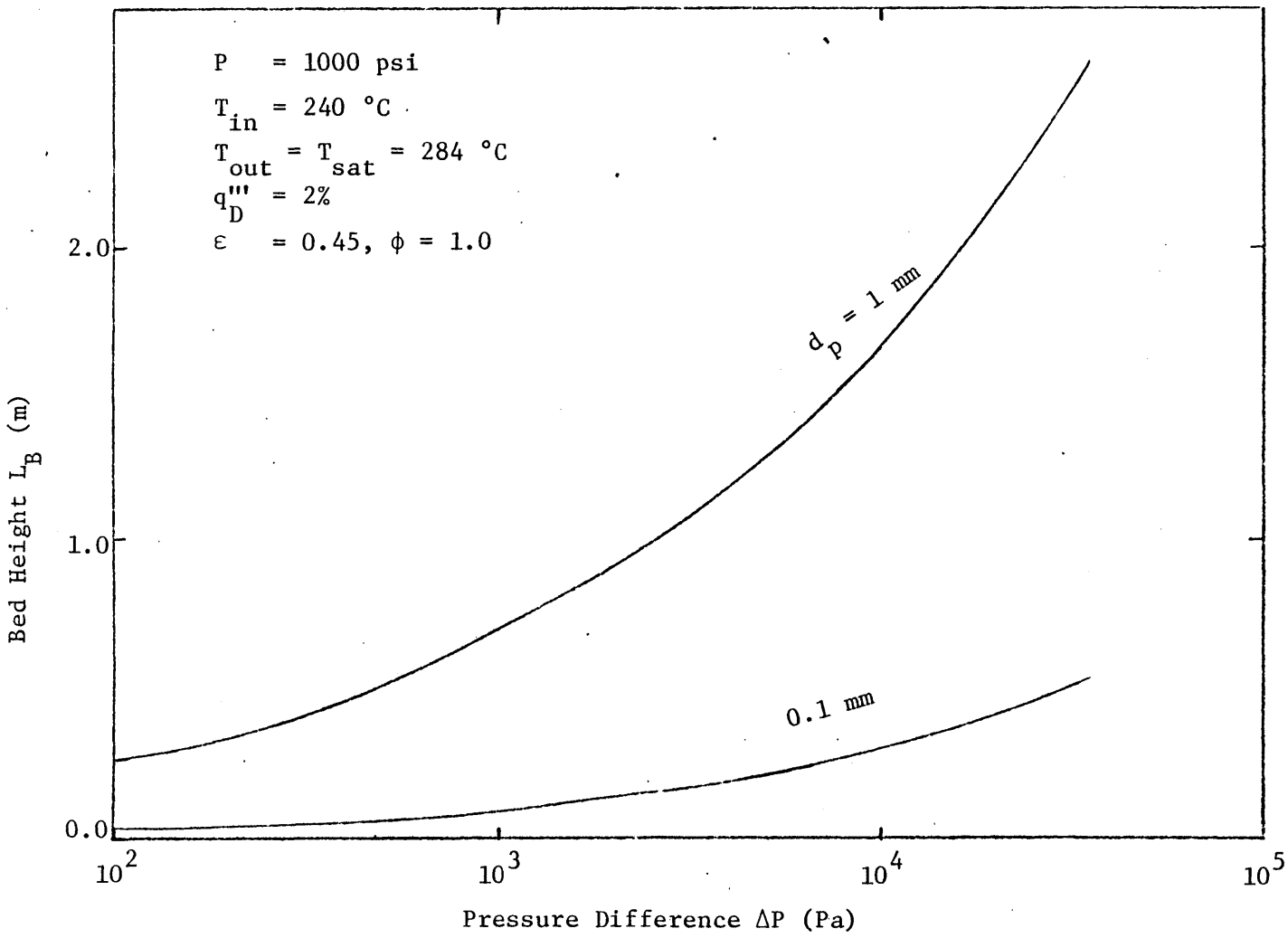

Figure 24: Coolable Particle Bed Heights Dependence on Driving Pressure Difference

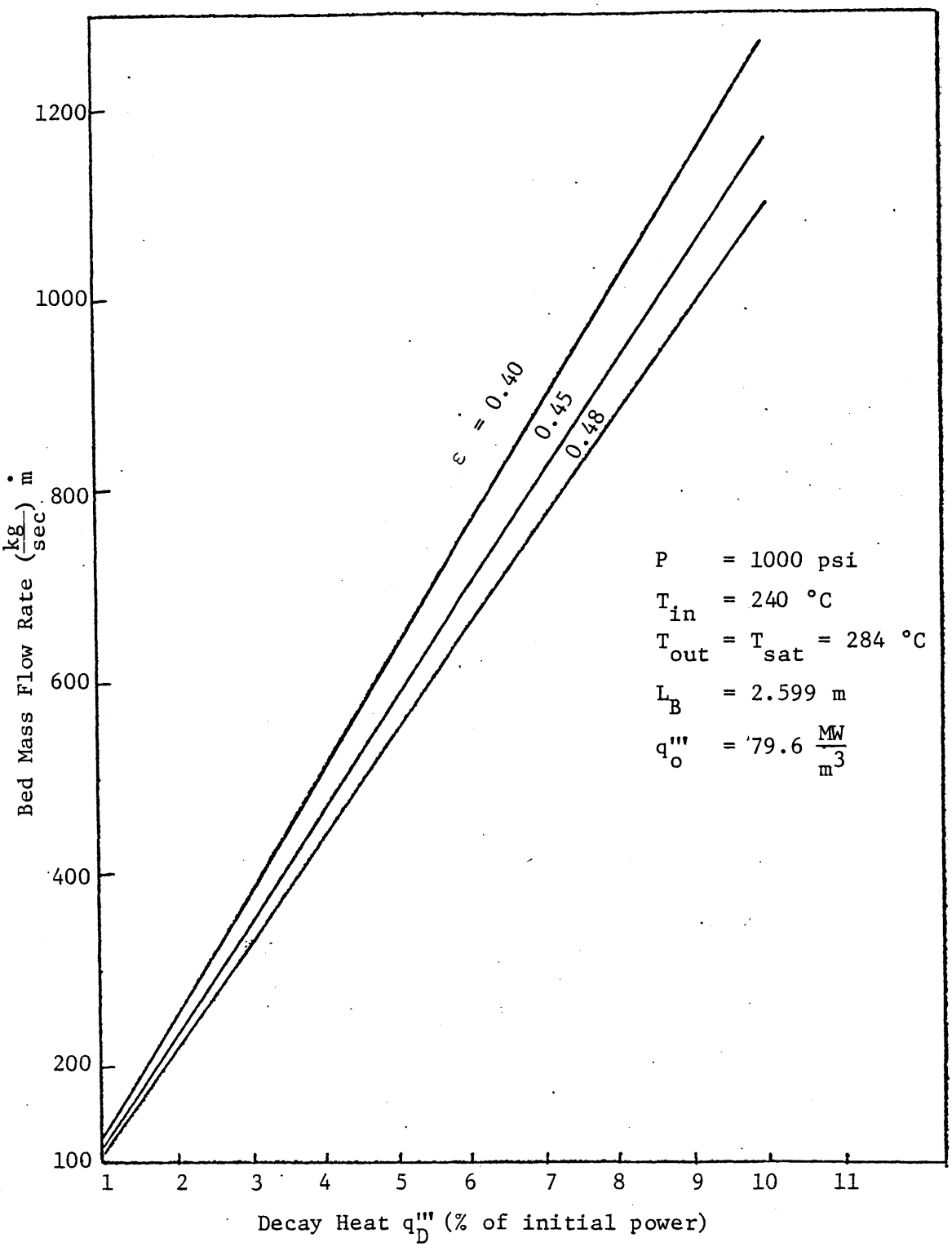

Figure 25: Coolant Mass Flow Rate for Saturation at Bed Exit Dependence on Decay Heat Production, in a Totally Disrupted Core, Case 2

the driving pressure difference, the higher the coolable bed height for a given particle diameter. Particle diameter does also influence coolable bed heights in this case; for beds having particles with mean diameter of 1 mm the coolable bed heights increases approximately by a factor of 5, as compared to beds with particles having mean diameter equal to 100 μm, Figure 24.

Figure 25 shows the coolant mass flow rate required for saturation conditions at bed exit as a function of decay power percentage and for a core that is totally disrupted (case 2). The increase in mass flow rate with decay heat is a linear function as described by Eq. (55). The effect of bed porosity is also shown. It can be seen that the percentage of decay heat increases with ε for a given mass flow rate.

In the one dimensional approach, an appropriate correlation for the heat transfer coefficient is required for the calculations of solid temperature distribution. However, there are only two correlations for the heat transfer coefficient that use water as the working fluid; these are the correlations of Holman [114] and Sunkoori [93]. The others use gas as fluid. The appropriateness of those correlations in the analysis of degraded core cooling is checked with the experimental data of Peoples et al. [48]. The latter workers have reported that a superficial velocity U_o of 0.0007 m/sec is needed to adequately cool a bed of particles with uniform size equal to 650 μm and power density of 2.3 $\frac{KW}{Kg}$.

If we assume that the temperature difference between the solid particles and the coolant is 10°C and that cooling of particles is controlled by single phase force convection, the values of superficial velocity U_o calculated using the different correlations for heat transfer

coefficient under similar experimental conditions as employed by Peoples are shown in Table 8. A comparison of the results indicates that the correlations which are derived from the use of gas as fluid give lower values for the superficial velocity than the reported value of Peoples, whereas correlations derived from the use of water as fluid give higher values of U_o. This results in the conclusion that the latter correlations are more conservative, i.e., demand more flow than experimentally observed. Therefore, the Holman's correlation will be used for the assessment of heat transfer in the degraded reactor core of the present work.

Figure 26 shows the variation of the heat flux exiting the particulate bed against coolant superficial velocity for a totally disrupted core (case 2). The effect of particle size is also shown. The temperature difference between the bed and the coolant is assumed to be 1°C. The physical properties of the coolant are taken at 1 atmosphere. Values of dryout heat flux in the absence of forced convection cooling calculated by using the Lapinsky dryout model are also indicated as a function of particle diameter for the purpose of comparison with bed top surface heat fluxed under forced cooling.

It is clear that forced flow is capable of removing considerably higher heat fluxes than natural convection. For example, particles of diamter equal to 1 cm may dryout under heat flux of the order of 3.2 MW/m^2 if they were to be cooled by an overlying layer of coolant. Forcing a flow at a rate of 4.5×10^{-2} m/sec will provide an adequate cooling for such a value of heat flux. However, flow rates below these values do not necessarily result in a bed dryout.

TABLE 8

Comparison of Correlations for
Heat Transfer Coefficient in Particulate Beds*

Author	Fluid	Bed	U_o (m/sec)
Holman [114]	water	fluidized	0.0207
Sunkoori [93]	water	fluidized	0.0034
Glaser [73]	gas	packed	0.00001
Bradshaw [82]	gas	packed	0.00002
Peoples [48]	water	packed	0.0007

*The bed conditions are those in the experiment of Peoples and are the following

bed diameter d_T	= 10.16 cm
particle diameter d_p	= 650 μm
bed height L_B	= 20.32 cm
bed loading	= 890 kg/m^2
power density	= 2.3 KW/kg

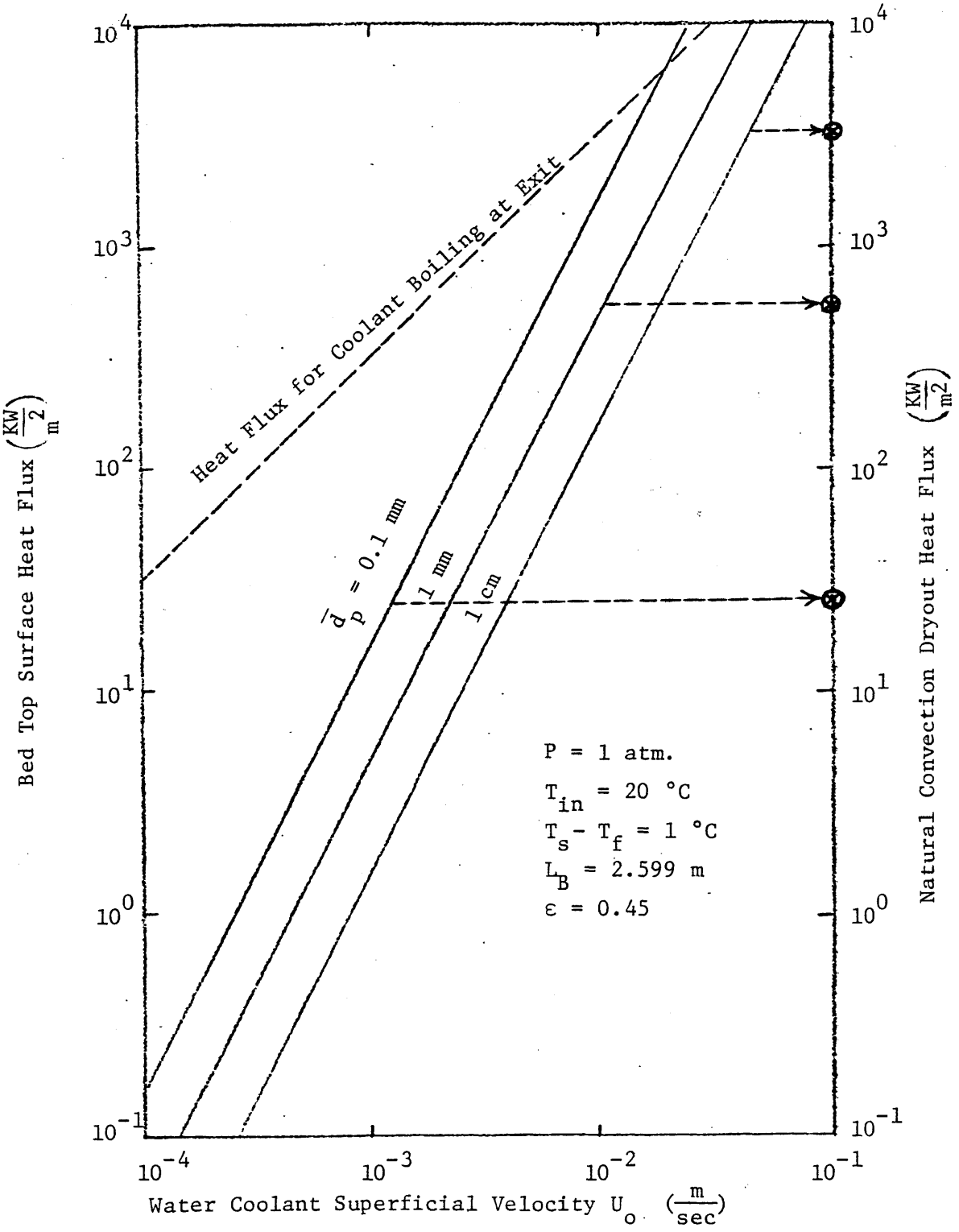

Figure 26: Heat Flux Leaving Bed Top Surface Dependence on Coolant Superficial Velocity in a Totally Degraded Core

Peoples [48] has also investigated dryout phenomena under forced convection, and showed that at a power density of 1.4 KW/Kg, dryout conditions may be reached in the bed at coolant superficial velocity of 0.0003 m/sec.

The graph of Figure 26 also shows that the heat flux leaving the top of the bed increases as the particle diameter decreases for a given superficial velocity. Values of heat flux that result in boiling at bed exit are also plotted on the same figure. This shows that the particles remain coolable within a single phase coolant at considerably high heat fluxes.

The temperature distribution in a partially degraded core with a debris bed height equal to 0.37 m (case 1) is shown in Fig. 27. The water coolant superficial velocity is 1×10^{-2} m/sec and the volumetric heat generation rate is 2% of the initial total power. The solid and coolant temperatures increased linearly with bed height and particles remaining coolable. Since decrease in particle diameter is accompanied by an increase in particle specific surface area ψ, particles seem then to have lower solid temperature and, as can be seen for particles of mean diameter equal to 0.1 mm, the solid temperature approaches that of the coolant.

The effect of increases in coolant velocity is illustrated in Fig. 28 for a totally disrupted core (case 2). An increase in coolant velocity from 1×10^{-2} m/sec to 4×10^{-2} m/sec resulted in a decrease in solid temperature by a factor of 4.

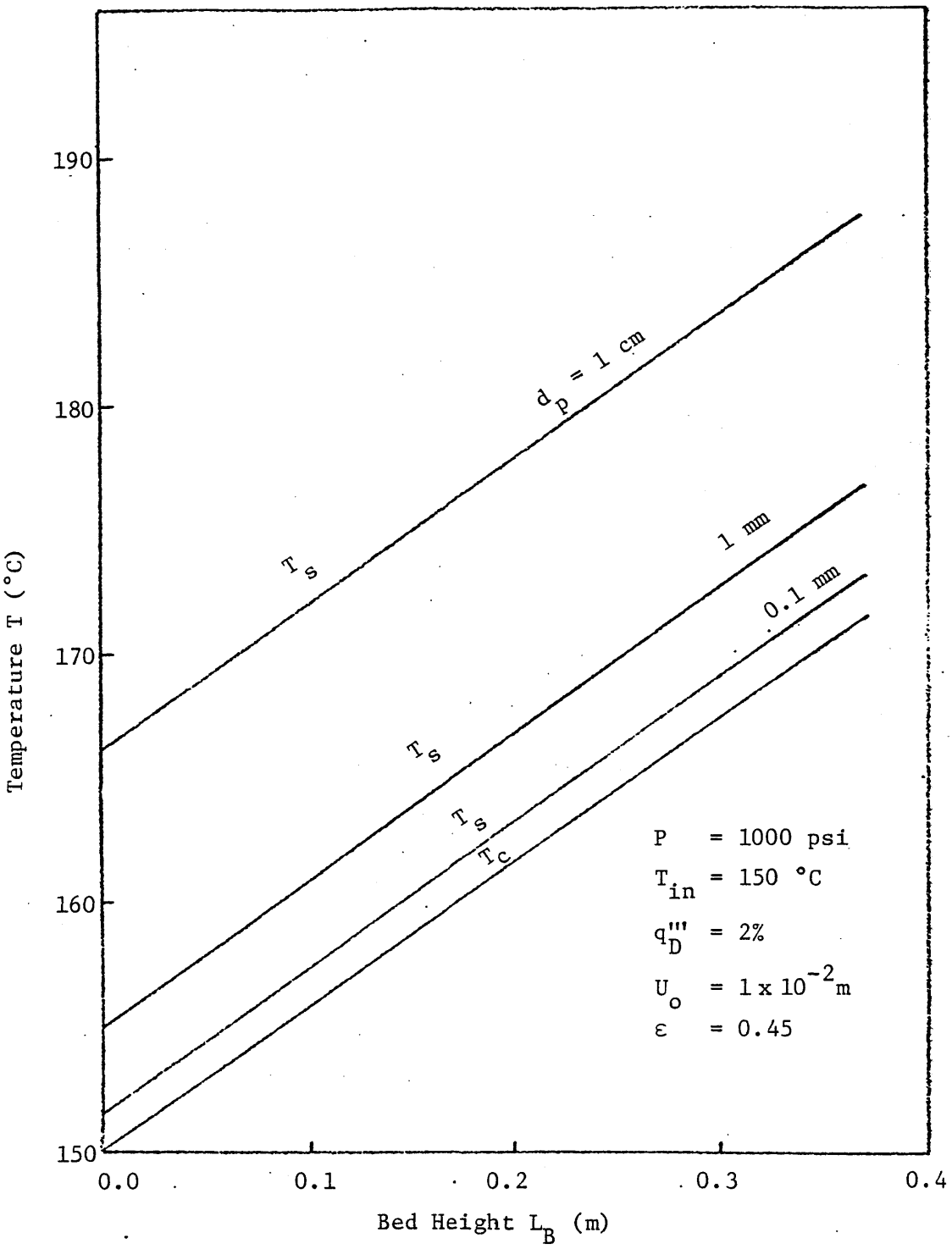

Figure 27: Coolant and Debris Bed Axial Temperature Distribution in Partially Degraded Core, Case 1

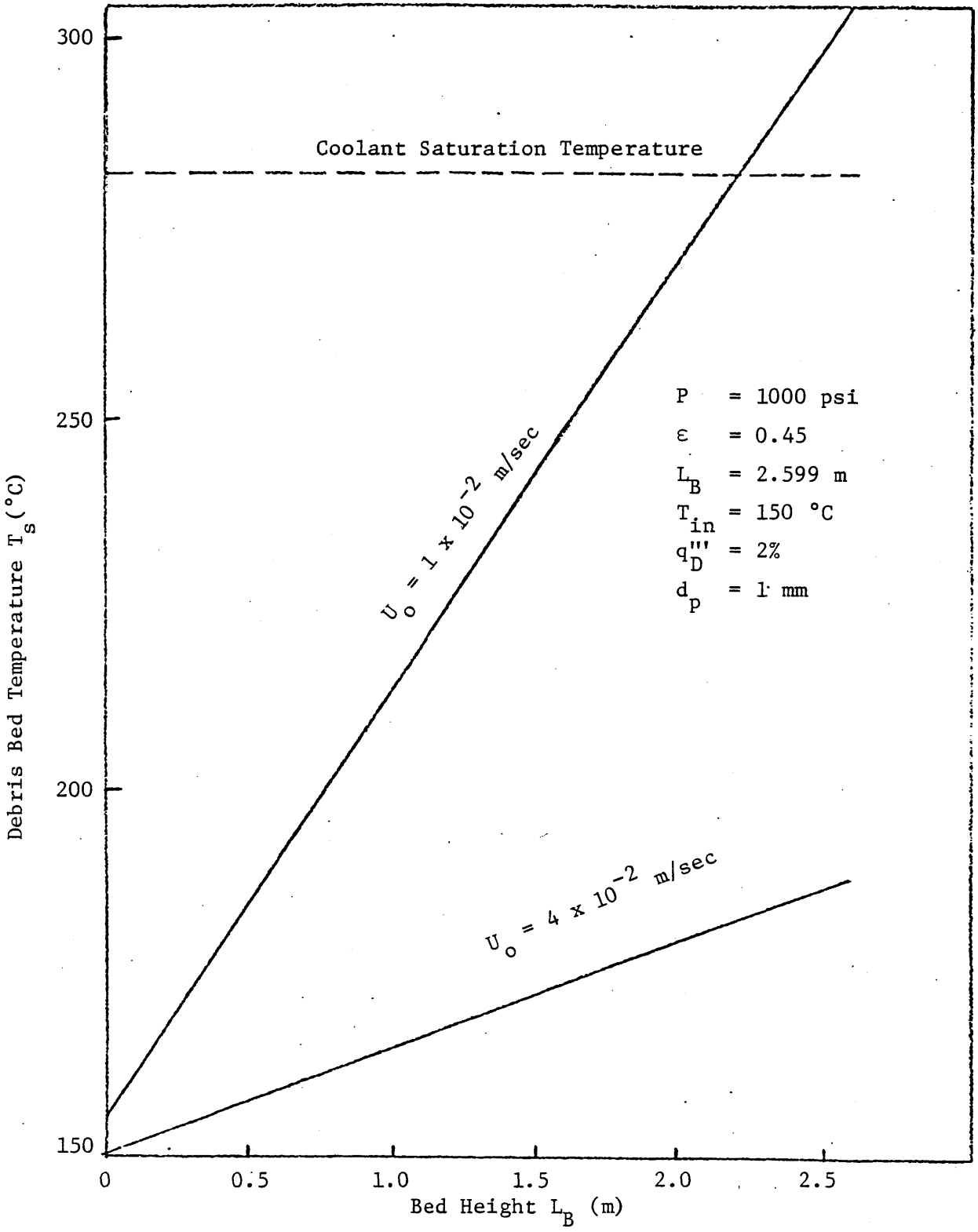

Figure 28: Debris Bed Axial Temperature Distribution in a Totally Degraded Core, Case 2

CHAPTER 7
CONCLUSIONS AND RECOMMENDATIONS

I. Literature Review

The results of the reviews in Chapters 3 and 4 can be summarized as follows:

1. There exists a large volume of information on the behavior of particulate beds of uniform size particles but considerable uncertainty about the behavior of beds of non-uniform particle sizes, which what would be expected under LWR accident conditions.

2. The major parameters for characterization of bed behavior are the porosity, the particle size distribution, particle geometry, bed size and particle-to-fluid density ratio.

3. Most of the heat transfer experiments have been performed on beds consisting of small particles with gas as the working fluid. Experiments on beds of large particles with water as a fluid are relatively sparse and restricted to a narrow range of conditions.

4. Experiments to study the hydrodynamic behavior of particle beds have mainly employed non-heated particles. The effects on the hydraulic and thermal behavior of internal heat generation have not been investigated widely. For instance, it was observed that in heated beds "thermal fluidization" may occur under certain conditions. The limited or partial fluidization produced movement of the bed material, with small particles being moved toward the top of the bed at the same time channeling may be formed which allows the escape of vapor.

5. Experimental studies on particle-to-fluid heat transfer in both fixed and fluidized beds have used either steady state techniques or unsteady state techniques. The experiments were directed toward correlating the total heat transfer rates (generally in dimensionless form) with Reynolds and Prandtl numbers. However, the many variables

involved and the different experimental methods employed resulted in poor agreement among the reported data. Particle-to-fluid heat transfer correlations that are based on experiments with water as the coolant yield lower heat transfer coefficient, and hence higher values of bed temperatures, than the more commonly available correlations based on experiments with gas as a fluid. In general, it is found that there is no one single correlation that can satisfy the range of variables and conditions of interest.

II. Needed Experiments

To resolve these issues and to improve the certainty with which the safety analysis of degraded LWR cores may be performed, the following suggestions are made:

1. More experimental data on flow through heat generating particle beds under conditions that characterize disrupted light water reactor core materials are needed. Of the important issues to be addressed are the self-pumping capability and the pressure drop as a function of quality and flow rate in beds of mixed size particles. Nucleate and film boiling that may commence locally in the bed are also important phenomena that require investigation.

2. Further experiments are needed to study the dryout in particulate beds under forced convection cooling. Data for a wide range of particle sizes, density, bed porosity, power, bed loading, effects of subcooling and flow rates should be generated before any dryout correlation can be developed. A variety of liquid pressures should also be investigated to determine the effect of vapor density on dryout heat flux.

3. Experiments with the proper range of particle size distribution are needed in which stratification and sweepout of the different particle sizes are studied.

4. For resolving the problem of the discrepancies in results of the various workers on particle-to-fluid heat transfer, it would be advantageous to obtain new data particularly in the fluidized bed region. These must consider systematically the effects of all the variables affecting the transfer rate. Attention must be paid to the manner in which the bed is formed and whether or not it changes its geometry during the course of the experiment.

III. Degraded Core Cooling Characteristics

In analyzing the potential of single phase forced convection cooling for the reference core conditions, given in Chapter 5, the calculations indicate that relatively large pressure heads are required to cool a totally degraded core. For example, if the temperature rise across the core is to be 20 °C, the minimum water coolant superficial velocity required to remove a decay heat of the order of 2% of the initial total power is 0.075 m/sec. At such velocity the pressure drop in the intact core is only 70 Pa whereas in a totally degraded core, that consists of particles of mean diameter equal to 1 mm, it is about 110,000 Pa. Furthermore, at such coolant velocity particles of diameter of the order of 850 μm will be fluidized and particles with diameter smaller than 80 μm will be swept out by the flow. However, depending on the temperature rise across the bed, the implication is that the potential for sweepout of particles with a diameter larger than 40 - 200 μm is very small.

It should be mentioned that if the particle bed consisted of particles with diameters larger than 1 mm, as likely to happen, the pressure drop requirement will be reduced. Even with the above conservative numbers, the pressure head is within the capabilities of the main reactor pumps.

APPENDIX A
CORE CONFIGURATION AND DEBRIS BED HEIGHT

Configuration A

Assume that part of the fuel rods has been damaged and collapsed on the spacer grid to form a particulate debris bed. Depending on the extent of the damage, the fuel particles may fill the flow area between the fuel rods; then the height of the bed is determined by the size of flow area and the amount of collapsed fuel. As shown in Figure A.1, there may still be some intact fuel rods above the debris bed; therefore, for a coolant to flow in such a configuration it will first encounter a particulate bed of porosity ε and height L_B. Above this bed the flow is again represented by channel flow characteristics, and the debris bed height can be determined as follows, writing a mass balance equation.

Total mass of fuel rods that suffered damage =

mass of debris bed that occupies the channel flow area

$$N_f A_f L_o \rho_f = A_T L_B (1-\varepsilon)\rho_f + N_f A_f \rho_f L \ , \qquad L_{lim} \leq L \leq L_o \qquad (A.1)$$

where N_f is the total number of fuel rods, A_f is the cross sectional area of fuel rod, L_o is the initial fuel rod length, ρ_f is the fuel density, A_T is the total channel flow area, L_B is the debris bed height, and L is the remaining intact fuel rod length. Eq. (A.1) is valid only to the extent where the bed height equals the height of the remaining fuel rods, i.e., when $L = L_{lim} = L_B$.

The height of the debris bed is hence given as

$$\frac{L_B}{L_o} = \left(1 - \frac{L}{L_o}\right) \frac{N_f A_f}{A_T(1-\varepsilon)} \tag{A.2}$$

when $L = L_B = L_{lim}$. Eq. (A.2) is written as

$$N_f A_f L_o = \left[A_T(1-\varepsilon) + N_f A_f\right] L_{lim}$$

hence

$$L_{lim} = \frac{L_o}{\left[1 + \frac{A_T}{N_f A_f}(1-\varepsilon)\right]} \tag{A.3}$$

Configuration B

In this configuration fuel debris fill the flow area and may extend to a height above the remaining intact rods forming a bed that occupies the entire cross sectional area of the core, as shown in Figure A.2. From mass balance on the amount of fuel degraded, we can write

$$N_f A_f L_o \rho_f = A_c(1-\varepsilon)\rho_f(L_B - L) + A_T(1-\varepsilon)\rho_f L + N_f A_f \rho_f L \ ,$$

$$0 \leq L \leq L_{lim} \tag{A.4}$$

The height of the debris bed is then given by

$$\frac{L_B}{L_o} = \frac{1}{A_c(1-\varepsilon)} \left\{ N_f A_f - \left[A_T(1-\varepsilon) + N_f A_f - A_c(1-\varepsilon) \right] \frac{L}{L_o} \right\} \qquad (A.5)$$

where A_c is the core cross sectional area. Eqs. (A.2) and (A.5) are used to determine the bed height for the core configurations expected under the proposed model.

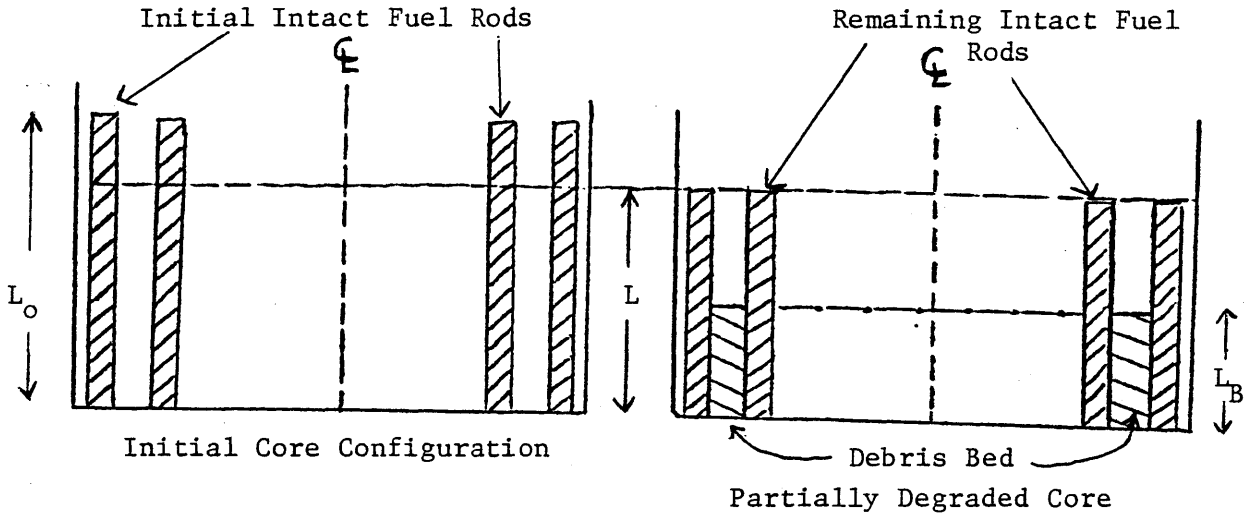

Figure A.1: Reactor Core Schematic, before and after the Accident with Debris Particles Settled in Flow Channels

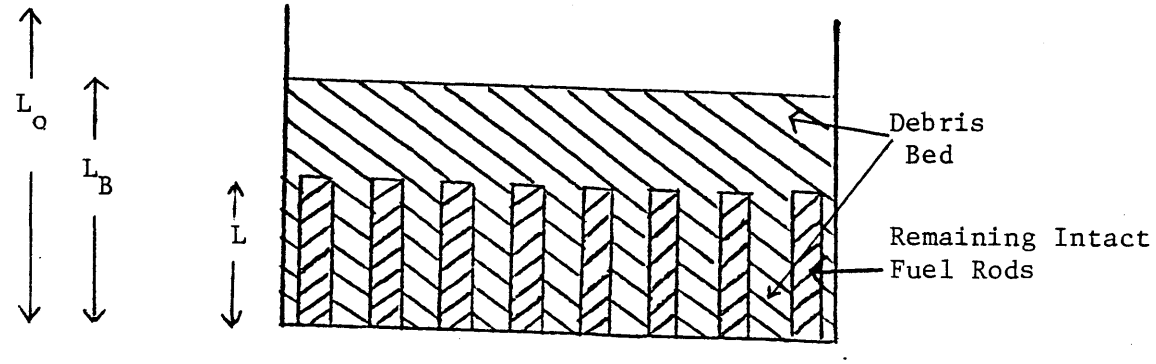

Figure A.2: Schematic of Core Configuration after the Accident with Debris Filling the Entire Core Cross Sectional Area

APPENDIX B

EFFECTS OF UNCERTAINTY IN POROSITY ON PRESSURE DROP

The accurate determination or prediction of the porosity, ε, is of importance since the pressure drop is strongly dependent on this quantity. Experimentally, if a small error in the value of ε is introduced during measurements the pressure drop results seem then to scatter considerably [116].

Using the Ergun pressure drop correlation, Eq. (3), one can find quantitatively the effect of ε on Δp. Hence if

$$\frac{\Delta p}{L_B} = 150 \frac{(1-\varepsilon)^2}{\varepsilon^3} \frac{\mu U}{d_p^2} + 1.75 \frac{(1-\varepsilon)}{\varepsilon^3} \rho_f \frac{U^2}{d_p} \tag{3}$$

or

$$\frac{\Delta p}{\rho U^2 \left(\frac{L_B}{d_p}\right)} \frac{\varepsilon^3}{(1-\varepsilon)} = \frac{150}{\left(\frac{Re}{1-\varepsilon}\right)} + 1.75 \tag{B.1}$$

Writing

$$\gamma = \frac{150}{\left(\frac{Re}{1-\varepsilon}\right)} + 1.75 \tag{B.2}$$

where γ is the pressure drop coefficient. The pressure drop coefficient (γ) consists of two contributions representing the viscous and inertia effects. Both terms have the form

$$\gamma = A \left(\frac{Re}{1-\varepsilon}\right)^{-n} \tag{B.3}$$

where

$n = 1$ when $A = 150$ (viscous flow)

$n = 0$ when $A = 1.75$ (inertia flow)

Eq. (B.1) can then be written as

$$\frac{\Delta p}{\rho U^2 \left(\frac{L_B}{d_p}\right)} \quad \frac{\varepsilon^3}{(1-\varepsilon)} = A \left(\frac{Re}{1-\varepsilon}\right)^{-n} \tag{B.4}$$

or

$$\Delta p = K \frac{(1-\varepsilon)}{\varepsilon^3} \left(\frac{1}{1-\varepsilon}\right)^{-n} \tag{B.5}$$

where

$$K = \rho U^2 \left(\frac{L_B}{d_p}\right) A \, (Re)^{-n}$$

We can also write

$$\frac{d(\Delta p)}{\Delta p} = \frac{d(\Delta p)}{d\varepsilon} \cdot \frac{d\varepsilon}{\Delta p} \tag{B.6}$$

Substituting Eq. (B.5) into Eq. (B.6),

$$\frac{d(\Delta p)}{\Delta p} = \left[\frac{-(n+1)}{1-\varepsilon} + \frac{(-3)}{\varepsilon}\right] d\varepsilon$$

or

$$\frac{d(\Delta p)}{\Delta p} = -\left[3 - \varepsilon(2-n)\right] \frac{d\varepsilon}{\varepsilon(1-\varepsilon)} \qquad \text{(B.7)}$$

Eq. (B.7) yields the relative variation of Δp caused by a relative variation of ε. The relationship is plotted in Fig. B.1 for $n = 0, 1$.

If $\varepsilon=0.45$, a positive relative variation in ε causes a negative relative variation in the pressure drop which is about five times larger. For example, if one assumes a porosity of 0.46 instead of 0.45, Δp is then subjected to a change of about -10%.

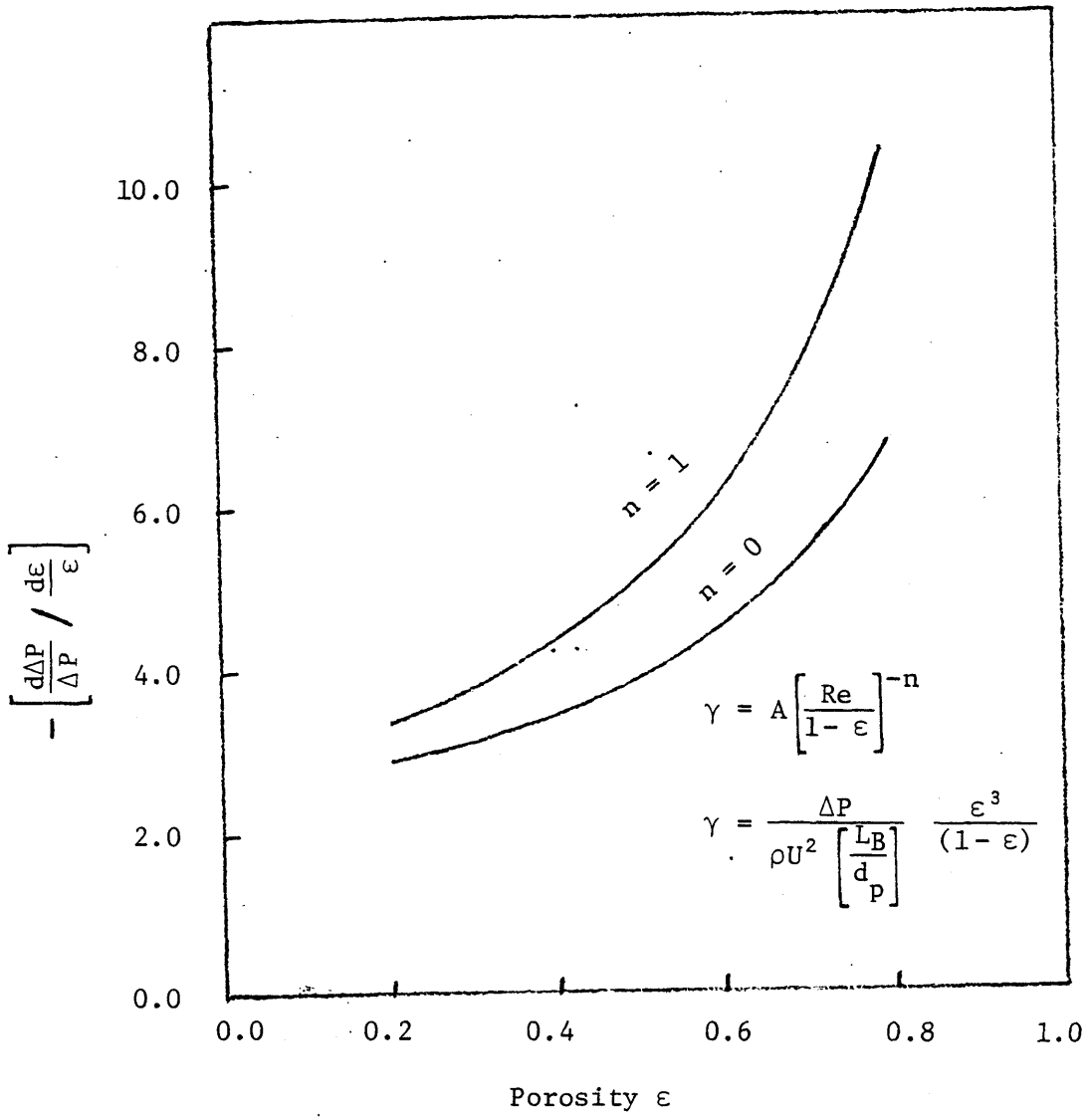

Figure B.1: The Effect of Void Fraction on Pressure Drop

REFERENCES

1. "Analysis of Three Mile Island - Unit 2 Accident," NSAC-80-1, March 1980.

2. El-Genk, M.S., "Molten Fuel-Coolant Interaction Occurring During a Severe Reactivity Initiated Accident Experiment," NUREG/CR-1900, March 1980.

3. El-Genk, M.S., "Fragmentation Mechanisms Occurring During an Energetic Fuel-Coolant Interaction," Transactions of the American Nuclear Society, 35, p. 348, 1980.

4. Bowden, F.P., "The Formation of Microjets in Liquid Under the Influence of Impact or Shock," Royal Society Philosophical Transactions, A-260, p. 94, 1966.

5. Fontana, M.H., "Core Melt-Through as a Consequence of Failure of Emergency Core Cooling," Nuclear Safety, 9, 1, p. 14, 1968.

6. Hagen, G., Ann. Phys. Chem., 46, pp. 423-442, 1839.

7. Poisenville, Compte Rendus, 11, pp. 961 and 1041, 1840.

8. Scheidegger, The Physics of Flow through Porous Media, U. of Toronto Press, Toronto, 1974.

9. Kozeny, J., Sitzber. Akad. Wiss. Wien., Math - Naturw. Kl. Abt. IIa, 136, p. 271, 1927.

10. Davidson, J.F. and Harrison, D., Fluidization, Academic Press, 1971.

11. Ergun, S., Chem. Eng. Progr. 48, 89; 1952.

12. Kunii, D. and Levinspiel, Fluidization Engineering, John Wiley, New York (1975).

13. Handley, D. and Heggs, P.J., "Momentum and Heat Transfer in Regular Shaped Packings," Trans. Inst. Chem. Engrs., Vol. 46 (1968).

14. Leva, M., Weintraub, M., Grummer, M., with Pollchik, M., and Storch, H, Chem. Eng. Progr. 44, 511, 619, 707; 1948.

15. Uchida, S. and Fujita, S., J. Chem. Soc. (Japan), (Ind. Eng. Section), 37, pp. 1578, 1583, 1589, 1707; 1934.

16. Shirai, T., Ph.D. Thesis, Tokyo Institute of Technology, 1954.

17. Lewis, W.K., Gilliland, E.R., and Bauer, W.C., "Characteristics of Fluidized Particles," Ind. Eng. Chem., 41, pp. 1104-1117, 1949.

18. Wilhelm, R.H. and Kwauk, M., "Fluidization of Solid Particles," Chem. Eng. Progr. 44, pp. 201-217, 1948.

19. Narsimhan, G., AIChE J., 11, p. 550, 1965.

20. Wen, C.Y. and Yu, Y.H., Chem. Eng. Progr. Symp. Ser. No. 62, 62, 1966.

21. Leva, M., Fluidization, McGraw-Hill Book Company, New York (1959).

22. Wen, C.Y. and Yu, Y.H., AIChE J., 12, p. 610, 1966.

23. Frantz, J.F., Chem. Eng., 69, p. 161, 1962.

24. Schwartz and Smith, In. Eng. Chem., 45, p. 1209, 1953.

25. Hancock, R.T., Trans. Inst. Mining Eng., 94, p. 114; 1937, 1938.

26. Steinour, H., Ind. Eng. Chem., 36, p. 618, 1944.

27. Lewis, W.K., Gilliland, E.R., and Bauer, W.C., Ind. Eng. Chem., 41, p. 1104, 1949.

28. Richardson, J.F. and Zaki, W.M., Trans. Inst. Chem. Eng., 32, p. 35, 1954.

29. Perry, J.H., Chemical Engineer's Handbook 2nd Ed., McGraw-Hill, 1941.

30. Dhir, V.K. and Catton, I., "Study of Dryout Heat Fluxes in Beds of Inductively Heated Particles," NUREG-0262, NRC-7, 1977.

31. Sparrow, E.M., Goldstein, R.J., and Jonsson, V.K., "Thermal Instability in a Horizontal Fluid Layer: Effect of Boundary Conditions and Non-Linear Temperature Profile," J. Fluid Mech., 18, pp. 513-528, 1964.

32. Thirlby, R., "Convection in an Internally Heated Layer," J. Fluid Mech., 44, part 4, 1970.

33. Gasser, R.D. and Kazimi, M.S., "Onset of Convection in a Porous Medium with Internal Heat Generation," J. Heat Transfer, Trans. ASME, Series C., 98, No. 1, 1976.

34. Gabor, J.D., Sowa, S.E., Baker, L., and Cassulo, J.C., "Studies and Experiments on Heat Removal from Debris in Sodium," ANS Fast Reactor Safety Meeting, Beverly Hills, 1974.

35. Lee, D.O. and Nilson, R.H., "Flow Visualization in a Heat Generating Porous Media," Sandia Lab., Albuquerque, NM, SAND 76-0614.

36. Hardee, H.C. and Nilson, R.H., "Heat Transfer Regimes and Dryout in a Porous Bed of Fuel Debris," Trans. Am. Nucl. Soc., 24, 1976.

37. Rhee, S.J. and Dhir, V.K., "Natural Convection Heat Transfer in Beds of Inductively Heated Particles," NUREG/CR-0408, 1978.

38. Rivard, J.B., "First In-Reactor Experiment with Simulated LMFBR Debris Bed," ANS Trans., 27, 1977.

39. Buretta, R.J. and Berman, A.S., J. App. Mech., 98, p. 249, 1976.

40. Sun, W., "Convection Instability in Superposed Porous and Free Layers," Ph.D. Dissertation, Univ. of Minnesota, 1973.

41. Shneider, K.J., "Investigation of the Influence of Free Thermal Convection on Heat Transfer Through Granular Material," XIth Int. Cong. Refrigeration, paper 11-4, Munich, 1963.

42. Rhee, S.J., Dhir, V.K., and Catton, I., "On the Natural-Convection Cooling of a Bed of Fuel Debris," Trans. ANS, 26, 1977.

43. Kampf, H. and Karsten, G., "Effects of Different Types of Void Volumes on the Radial Temperature Distribution of Fuel Pins," Nucl. App. Tech., 9, No. 3, 1970.

44. Koewen, R.S. and Catton, I., "Dryout of a Fluidized Particle Bed with Internal Heat Generation," UCLA-ENG-7519, March 1975.

45. Ostensen, R.W., "Advanced Reactor Safety Research Program Quarterly Report," Sandia Lab., 1980.

46. Shires, G.L. and Stevens, G.F., "Dryout During Boiling in Heated Particulate Beds," AEEW-M1779, Uk. AEA, 1980.

47. Lipinski, R.J., "Particle Bed Dryout," Sandia Lab., 80-1452A, 1981.

48. Squarer, D. and Peoples, J.A., "Dryout in Inductively Heated Bed With and Without Forced Flow," Trans. ANS, 34, 1980.

49. Cho, D.H., "A Simple Analysis of Heat Generating Blockages," Trans. ANS, 33, 1979.

50. Willhite, G.P., Kunii, D. and Smith, J.M., "Heat Transfer in Beds of Fine Particles," AIChE J., 8, p. 340, 1962.

51. Gopalarathnam, C.D., Chenakesavan, B., and Laddha, G.S., "Heat Transfer in Packed Beds," J. Sci. Ind. Res. (India), A23, pp. 186-195, 1962.

52. Verschoor, H. and Schuit, G.C.A., "Heat Transfer to Fluids Flowing Through a Bed of Granular Solids," Appl. Sci. Res., A-2, pp. 97-119, 1950.

53. Ranz, W.E. and Marshall, W.R., Jr., Chem. Eng. Progr., 48, p. 141, 1952.

54. Furnas, C.C., Ind. Eng. Chem., 22, p. 26, 1930.

55. Saunders, O.A. and Ford, H., J. Iron Steel Inst., 141, p. 291, 1940.

56. Fedorov, I.M., in Collection of Contemporary Problems of Drying Technique, Vol. 2, edited by Yu M. Lurye (Water Power Institute), 1941.

57. Kitayev, B.I., Heat Exchange in Shaft Furnaces, Moscow, 1941.

58. Sokolskii, A.P., "Experimental Investigation of Combustion, Diffusion and Heat Exchange Processes During Dust Combustion," Ph.D. Thesis, Polytechnique Institute, Leningrad, 1941.

59. Gamson, B.W., Thodos, G., and Hougen, O.A., Trans. Am. Inst. Chem. Eng., 39, p. 1, 1943.

60. Wilke, C.R. and Hougen, O.A., Trans. Am. Inst. Chem. Eng., 41, p. 445, 1945.

61. Chukhanov, Z.F. and Shapatina, E.A., Izv. Akad. Nauk SSSR (Otd. tekh. Nauk), 4, 1946.

62. Glaser, H., MAP-VG, 96-818T, March 1947.

63. Kichkina, E.S., Dissertation, Kalinin Polytechnical Institute, Leningrad, 1947.

64. Lof, G.O.C. and Hawley, R.W., Ind. Eng. Chem., 40, p. 1061, 1948.

65. Lydersen, A., "Investigation of Heat Transfer and Pressure Loss in Stacked Spheres Traversed by Air," Dissertation Technische Hochschule Trondheim, 1950.

66. Dayton, R.W., Fawcett, S.L., Grimble, R.E., and Sealander, C.E., Rep. BMI-747, Battelle Memorial Institute, Columbus, Ohio, 1952.

67. Maeda, S. and Kawazoe, K., Chem. Eng., Tokyo, 17, p. 276, 1953.

68. Dyakonov, G.K. and Semenov, G.A., Izv. Akad. Nauk SSSR (Otd. tekh. Nauk) 7, p. 109, 1955.

69. Glaser, H., Chemie-Ingr.-Tech., 27, p. 637, 1955.

70. Galloway, L.R., Komarnicky, W., and Epstein, N., Can. J. Chem. Eng., 35, p. 139, 1957.

71. Ball, W.E., Dissertation Abstr., 19, p. 494, 1958.

72. Baumeister, E.B. and Bennett, C.O., AIChE J., 4, p. 69, 1958.

73. Glaser, M.B. and Thodos, G., AIChE J., 4, p. 63, 1958.

74. DcAcetis, J. and Thodos, G., Ind. Eng. Chem., 52, p. 1003, 1960.

75. Wadsworth, J., Int. Heat Transfer Conference ASME, New York, 4, p. 760, 1961.

76. Beek, J., Advances in Chemical Engineering, Vol. 3, edited by T.B. Drew, J.W. Hoopes, and T. Vermeulen, Academic Press, New York, p. 204, 1962.

77. Glaser, H., Chemie-Ingr.-Tech., 34, p. 468, 1962.

78. McConnachie, J.T.L. and Thodos, G., AIChE J., 9, p. 60, 1963.

79. Sengupta, A. and Thodos, G., AIChE J., 9, p. 751, 1963.

80. Baldwin, D.E. Jr., Beckman, R.B., Rothfus, R.R., and Kermode, R.I., Ind. Eng. Chem. Process Des. Dev., 5, p. 281, 1966.

81. Zabrodsky, S.S. and Zhitkevich, L.K., Issled. Jeplo. Massoobmena Tekhnol. Protsessak Appl. Inst. Teplo. Massoobmena Akad. Nauk SSSR, p. 42, 1966.

82. Bradshaw, A.V., Johnson, A., McDachlan, N.H., and Chiu, Y.T., Trans. Inst. Chem. Eng., 48, p. T77, 1970.

83. Cornish, A.R.H., Trans. Inst. Chem. Eng., 43, p. T332, 1965.

84. Pfeffer, R., "Heat and Mass Transport in Multi-Particle Systems," I/EC Fundamentals, 3, pp. 380-383, 1964.

85. Happel, J., "Viscous Flow in Multi-Particle System: Slow Motion of Fluids Relative to Beds of Spherical Particles," AIChE J., 4, 1958.

86. Levich, V.G., Physicochemical Hydrodynamics, Prentice-Hall, New York, 1962.

87. Zabrodsky, S.S., "Heat Transfer Between Solid Particles and Gas in a Non-Uniform Aggregated Fluidized Bed," Int. J. Heat Mass Transfer, 6, pp. 23-31, 1963.

88. Kunii, D. and Suzuki, M., "Particle-to-Fluid Heat and Mass Transfer in Packed Beds of Fine Particles," J. Heat Mass Transfer, 10, pp. 845-852, 1966.

89. Kato, K. and Wen, C.Y., Chem. Eng. Prog. (Symp. Ser. No. 105), 66, p. 100, 1970.

90. Kettenring, K.N., Manderfield, E.L., and Smith, J.M., Chem. Eng. Prog., 46, p. 139, 1950.

91. Wamsley, W.W. and Johnson, L.N., Chem. Eng. Prog., 50, p. 347, 1954.

92. Walton, J.S., Olson, R.L., and Levenspiel, O., Ind. Eng. Chem., 44, p. 1474, 1952.

93. Sunkoori, M.R. and Kaparthi, R., Chem. Eng. Sci., 12, p. 166, 1960.

94. Frantz, J.F., Chem. Eng. Prog., 57, p. 35, 1961.

95. Frantz, J.F., "Fluid-to-Particle Heat Transfer in Fluidized Beds," Ph.D. Thesis, Louisiana State University, 1958.

96. Rozental, E.O., Teplo-i, Massoobmen V Protses. Ispareniza, Akad. Nauk SSSR, Energet. Inst., p. 87, 1958.

97. Richardson, J.F. and Ayers, P., Trans. Inst. Chem. Eng., 37, p. 314, 1959.

98. Blickle, T. and Nemeth, J., Magy. Kem. Lap., 15, p. 551, 1960.

99. Donnadieu, G.A., J. Rech. Cent. Natn. Rech. Scient., 51, p. 161, 1960.

100. Muchi, I., Ozaki, K., Kagami, T., and Yagi, S., Chem. Eng., Tokyo, 24, p. 70, 1960.

101. Fritz, J.C., "Heat Transfer Between Air and Solid Particles in Sixteen Inch Diameter Fluidized Beds," Ph.D. Thesis, University of Wisconsin, 1956.

102. Yeh, G.C., J. Chem. Eng. Data, 6, p. 526, 1961.

103. Holman, J.P., Moore, T.W., and Wong, V.M., "An Experimental Study of Particle-Fluid Heat Transfer in a Water Fluidized System," United States Atomic Energy Commission, Washington, D.C., NYO-10702, p. 125, 1963.

104. Moore, T.W., "Experimental Study of Particle-Fluid Heat Transfer in a Water Fluidized System," United States Atomic Energy Commission, Washington, D.D., TID-19477, 1963.

105. Solntsev, M.Ya., Bobe, L.S., and Korotaeva, G.K., Int. Chem. Eng. Process Ind., 3, p. 215, 1963.

106. Fujishige, H., J. Soc. Chem. Ind. Japan, 67, p. 1322, 1964.

107. Lindin, V.M. and Kazakova, E.A., Khim. Prom., 8, p. 604, 1965.

108. Rowe, P.M. and Claxton, K.T., Trans. Inst. Chem. Eng., 43, p. T321, 1965.

109. Chang, T.M. and Wen, C.Y., Chem. Eng. Prog. (Symp. Ser. No. 67), 62, p. 111, 1966.

110. Petrovic, L.J. and Thodos, G., Canadian J. Chem. Eng., 46, p. 114, 1968.

111. Fedorov, I.M., "Theory and Calculations of Drying Processes in the Suspended State," Dokt. Dissertation, Moskovskii Institut Khimi-Cheskogo Mashinostroeniya, Moscow, 1950.

112. Heertjes, P.M. and McKibbins, S.W., Chem. Eng. Sci., 5, p. 161, 1956.

113. Mann, R.S. and Feng, L.C.L., "Gas Solid Heat Transfer in Fluidized Beds," I&EC Prog. Des. & Dev., Vol. 7, p. 3, 1968.

114. Holman, J.P., Moore, T.W., and Wong, V.M., Ind. Eng. Chem. Fundam., 4, p. 21, 1965.

115. Balakrishnan, A.R. and Pei, D.C.T., Ind. Eng. Chem. Prog. Des. Dev., 13, p. 441, 1974.

116. Achenbach, E., "Forced Convective Heat Transfer and Pressure Drop of a Randomly Packed HTGR Cove," Proceedings of ANS/ASME, Int. Topical Meeting on Nuclear Reactor Thermal Hydraulics, New York, October 1980.

117. Eichhorn, J., and White, R.R., "Particle-to-Fluid Heat Transfer in Fixed and Fluidized Beds," Chem. Engng. Prog. Symp., Ser. 48, pp. 11-18 (1952).

118. Kunii, D. and Smith, J.M., "Heat Transfer Characteristics of Porous Rocks," A.I.Ch.E. Journal, 7, pp. 29-34 (1961).

119. Mimura, T., "Studies on Heat Transfer in Packed Beds," Graduate Thesis, Univ. of Tokyo (1963).

120. Suzuki, K., "Studies on Heat Transfer in Packed Beds," Graduate Thesis, Univ. of Tokyo (1964).

121. Tokutomi, T., "Heat Transfer Dynamics of Packed Beds," M.S. Thesis, Univ. of Tokyo (1966).

122. Donnadieu, G., "Transmission de la Chaleur dans les Milieux Granulaires," Revue Inst. Fr. Petrole 16, 1330 (1961).

123. Harada, H., "Studies on Axial Heat Transfer in Packed Beds," Graduate Thesis, Univ. of Tokyo (1965).

124. Sato, K., et al., paper presented at The Annual Meeting, Soc. Chem. Engrs., Japan, May (1950).

125. Yoshida, K., B.S. Thesis, Univ. of Tokyo, (1961).

126. Ferron, J.R., Ph.D. Thesis, Univ. of Wisconsin (1958).

127. Mitsumori, T., "Unsteady State Heat-Transfer in Packed Beds," Graduate Thesis, University of Tokyo (1966).